

UNCLASSIFIED

AD NUMBER
AD483690
NEW LIMITATION CHANGE
TO Approved for public release, distribution unlimited
FROM Distribution authorized to U.S. Gov't. agencies and their contractors; Administrative/Operational Use; JUL 1961. Other requests shall be referred to Aeronautical Systems Division, Attn: AFSC, Wright-Patterson AFB, OH 45433.
AUTHORITY
AFFDL ltr, 31 May 1973

THIS PAGE IS UNCLASSIFIED

CDIC 1168
Duplicate

CDIC 1168
Duplicate

483690

DDC FILE COPY

19 TR-
ASD TECHNICAL REPORT 61-104-Vol-1
VOLUME 1

6 APPLICATION AND EVALUATION OF
CERTAIN ADAPTIVE CONTROL TECHNIQUES
IN ADVANCED FLIGHT VEHICLES.

1
TR

Volume I.

C.E. SELF ADAPTIVE
FLIGHT CONTROL SYSTEM.

9 Technical rept's

10 John M. Schuler,
Charles R. Chalk
Arno E. Schelhorn.

Cornell Aeronautical Laboratory, Inc.

11 July 1961
12 158 p.
13

Flight Control Laboratory
Contract No. AF33(616)-7572
14 AF Project No. 76225
Task No. 02381
15

DDC
RECORDED
JUN 21 1966
B. J. J.

Aeronautical Systems Division
Air Force Systems Command
United States Air Force
Wright-Patterson Air Force Base, Ohio

(098 500)

**Best
Available
Copy**

NOTICES

When Government drawings, specifications, or other data are used for any purpose other than in connection with a definitely related Government procurement operation, the United States Government incurs no responsibility nor any obligation whatsoever; and the fact that the Government may have formulated, furnished, or in any way supplied the said drawings, specifications, or other data, is not to be regarded by implication or otherwise as in any manner licensing the holder or any other person or corporation, or conveying any rights or permission to manufacture, use, or sell any patented invention that may in any way be related thereto.

Qualified requesters may obtain copies of this report from the Armed Services Technical Information Agency (ASTIA), Arlington Hall Station, Arlington 12, Virginia.

Copies of ASD Technical Reports and Technical Notes should not be returned to the Aeronautical Systems Division unless return is required by security considerations, contractual obligations, or notice on a specific document.

SECTION NO.		
ASTIA	WHITE SECTION	<input type="checkbox"/>
	DIFF SECTION	<input type="checkbox"/>
CLASSIFICATION <i>per statement</i>		
<i>out doc</i>		
DISTRIBUTION/AVAILABILITY CODES		
DIST.	AVAIL.	SPECIAL
<i>2</i>		

ASD-TR-61-104, Vol. I
ASTIA
Arlington Hall Station
Arlington 12, Virginia

FOREWORD

This report was prepared for the United States Air Force by the Cornell Aeronautical Laboratory, Inc., Buffalo, New York as required by Contract AF33(616)-7572.

The work reported herein was performed by the Flight Research Department of Cornell Aeronautical Laboratory under the sponsorship of the Flight Control Laboratory of the Aeronautical Systems Division, Wright-Patterson Air Force Base, Dayton, Ohio, as Project No. 8225; Task No. 82181, to perform research into basic considerations of adaptive flight control systems. The project was administered by Lt. P. C. Gregory of the Flight Control Laboratory.

Work was performed on this project primarily by the following members of the staff of the Flight Research Department: C. R. Chalk, E. G. Ry-naski, A. E. Scheinhorn, and the project engineer J. M. Schuler. Consultants on this project were R. G. Buscher of the General Electric Company, D. O. Dommasch of DODCO, Inc., and G. W. Anderson of Aeronutronic.

ABSTRACT

The This report contains, in two volumes, the results of a study of the application and evaluation of certain adaptive control techniques ^{were studied} as applied to advanced vehicles of the X-15 and Dyna-Soar type. Volume I deals with those aspects of the study pertaining to the General Electric Self-Adaptive Flight Control System, Volume II deals with the DODCO, Inc., Optimum Limited-Information Adaptive Flight Control System.

Volume I: The general concept of adaptive control through the use of reference models is discussed, and particular models are evaluated based on the present status of airplane handling qualities research. The G.E. System is applied to the problem of controlling the longitudinal short-period motions of the X-15 airplane during re-entry. The first treatment of the problem is rather general, and uses essentially linear techniques to investigate the reference model concepts, selection of system parameters, responses to command inputs and gusts, effect of basic airplane static and dynamic instability, effect of sensor dynamics, and dynamics of the adaptive loop. Then a more detailed study is made of certain problem areas, including the response to inputs at the actuator valve, effect of actuator non-linearities, frequency sensor characteristics, and the effect of noise in the primary sensor, in this case a rate gyro.

PUBLICATION REVIEW

This report has been reviewed and is approved.

FOR THE COMMANDER:

GEORGE M. MANNING
Lieutenant Colonel, USAF
Chief, Flight Control Laboratory

TABLE OF CONTENTS

SECTION	PAGE
I INTRODUCTION	1
1.1 Philosophy	1
1.2 Purpose	4
1.3 Approach	4
II DEFINING THE CONTROL PROBLEM	8
2.1 General Considerations	8
2.2 High-Gain Control Schemes	9
2.3 Model Approach to Control System Design	14
2.4 Aircraft Model and Variables	17
III INITIAL STUDY AND APPLICATION OF G. E. SYSTEM	28
3.1 Introduction	28
3.2 General Analysis of the System	29
3.3 Application of the G. E. System to the X-15 Airplane	37
3.4 Adaptive Loop Characteristics	46
IV STUDY OF SPECIFIC PROBLEMS IN APPLICATION OF G. E. SYSTEM	50
4.1 Introduction	50
4.2 Response to Pilot Inputs at the Actuator Valve	51
4.3 Effect of Actuator Nonlinearities	54
4.4 Frequency Sensor Characteristics	59
4.5 Effect of Noise in the Rate Gyro Output	63
V CONCLUSION	67
REFERENCES	74
APPENDIX A - AIRPLANE EQUATIONS AND PARAMETERS USED IN THIS STUDY	140
APPENDIX B - ESIAC COMPUTER AND ROOT LOCUS COORDINATES	143
APPENDIX C - EASE ANALOG COMPUTER SCHEMATIC DIAGRAMS	149
APPENDIX D - REAC ANALOG COMPUTER SCHEMATIC DIAGRAMS	154

LIST OF FIGURES

FIGURE		PAGE
1	Block Diagram of Single-Input Single-Output Feedback System	10
2	Block Diagram of Dual-Input Single-Output Feedback System	11
3	The Model in the Prefilter	14
4	Inverse-Model in the Feedback	15
5	Combined Prefilter and Feedback Models	15
6	Block Diagram with Inverse $\dot{\theta}$ -Model in the Feedback	20
7	Block Diagram with Inverse $\dot{\theta}$ -Denominator in the Feedback and $\dot{\theta}$ -Numerator in the Prefilter	23
8	Block Diagrams of the G. E. System	82
9	Functional Diagram of the G. E. Frequency Sensor	83
10	Complex-Plane Plot of Short-Period Handling Qualities Data from References 14 and 15	83
11	Comparison of $\dot{\theta}$ and α Responses for the Uncontrolled Airplane, and the Controlled Airplane with Two Different $\dot{\theta}$ Models	84
12	Root Locus Plots Showing General Operation of G. E. System	85
13	Selection of Time Constant (τ_c) of Inverse-Model Feedback	86
14	Composite Root Loci for G. E. System and X-15 Airplane at Various Times During Re-entry	87
15	Analog Responses of G. E. System and X-15 Airplane at Various Times During Re-entry	88
16	Comparison of Gust Responses as Computed on the Analog	91
17	Effect of Destabilizing Airplane Statically (M_{α}) and Dynamically ($M_{\dot{q}}$ and $M_{\ddot{\alpha}}$)	92
18	Effect of Variations in Actuator Time Constant	98
19	Attempted Compensation for Variation in Actuator Time Constant	98
20	Effect of Variation in Rate Gyro Damping	99
21	Response of Adaptive Loop to Initial Gain Offset	100
22	Response of Adaptive Loop to Initial Negative Gain Offset Followed by a Positive Step Increase in Actuator Gain	105
23	Response of Airplane to Step Changes in Adaptive Gain	106

FIGURE		PAGE
24	Block Diagram of the G. E. System with Pilot Inputs at the Actuator Valve	108
25	Analog Responses of X-15 with G. E. System	111
26	Root Loci for X-15 with G. E. System	114
27	Gain (K_3) Required to Produce $\zeta = .02$ for the Actuator Pole for Two Actuator Time Constants	118
28	Frequency Response of G. E. Feedback	119
29	Frequency Response of Analog Second-Order Systems for Valve Servo and Rate Gyro	120
30	Rate of Change of Flow with Valve Displacement for Nonlinear Actuator Valve	121
31	REAC Function Generator for Nonlinear Actuator Valve	122
32	Block Diagram of REAC Simulation of Nonlinear Actuator	123
33	Frequency Response of Nonlinear Actuator	124
34	Transient Response of Nonlinear Actuator	125
35	Operation of Frequency Sensor with Linear Actuator	126
36	Operation of Frequency Sensor with Nonlinear Actuator	127
37	Function Generator Shape and Gate Output for Two Input Frequencies	129
38	Effect of Inj. Frequency and Function Generator on Steady-State Rate of Gain Servo	130
39	Steady-State Rate of Gain Servo for Several Input Frequencies to the Frequency Sensor	131
40	Effect of Noise in Rate Gyro Output on Operation of Frequency Sensor and Gain Servo	133
41	Response of Frequency Sensor and Gain Servo to Input Signal Composed of Two Sinusoids	136
42	Relative Amplitude of Two Sine Waves Resulting in No Gain Change	139
43	The Flight Research Department ESIAC	146
44	Root Locus Coordinates	147
45	Root Locus of the Function - $1=K \frac{(1-\frac{s}{0.5})(1-\frac{s}{1.0})}{(1-\frac{s}{0.22+0.20j})(1-\frac{s}{0.22-0.20j})}$	148
46	Analog Schematic - Aircraft	150
47	Analog Schematic - Control System	151
48	Analog Schematic - Frequency Sensor	152
49	Analog Schematic of the Frequency Sensor	155
50	Analog Schematic of Aircraft Equations	156
51	Analog Schematic of G. E. Feedback and Rate Gyro	157
52	Analog Schematic and Sketch of Valve Servo and Actuator	158

LIST OF TABLES

TABLE		PAGE
I	Flight Path Parameters for X-15 Re-entry	77
II	Numerical Data for X-15 Equations of Motion	77
III	Lumped Parameters for $\dot{\theta}/\delta_e$ and α/δ_e Transfer Functions for X-15	78
IV	Gain (K_3) and Frequency Data from ESIAC for Actuator Mode, $\zeta = 0$ and $\zeta = .2$	79
V	Gain (K_3) and Frequency Data from Analog for Actuator Mode, $\zeta = 0$	80
VI	Coefficient Potentiometer Settings for Analog Simulation of X-15	153

SYMBOLS AND DEFINITIONS

The symbols used in this report are defined below. Those which relate only to the immediate context in which they appear are defined when used.

Dimensional Units

- Distance - feet
- Time - seconds
- Angle - radians (unless otherwise stated)
- Force - pounds
- Moment - foot-pounds
- Mass - slugs

Aerodynamic Notation

- h altitude
- ρ air density
- q dynamic pressure, $\frac{1}{2} \rho V^2$
- S wing area
- c wing chord
- m mass
- g acceleration of gravity (i. e., 32.2 ft/sec^2)
- I_y airplane moment of inertia about y axis
- V airspeed
- M Mach number
- α angle of attack, angle between x axis and projection of relative wind in x-z plane
- $\dot{\varphi}$ pitching velocity
- γ flight path angle, positive up
- δ_e elevator angle, positive for trailing edge down
- x, y, z airplane body axes

- ψ heading angle, angle between reference azimuth (North) and the projection of the x axis in the horizontal plane
- Θ attitude angle, angle between x axis and the horizontal plane
- ϕ bank angle, angle between y axis and a horizontal line in the y - z plane
- a_z component of acceleration of cg along z axis
- n_z normal accelerometer reading in g units, positive in pull-up
- F_S stick force
- L lift, force in plane of symmetry and normal to relative wind, positive up
- M pitching moment about y axis, positive nose up
- C_L lift coefficient, $L/\frac{1}{2}\rho V^2 S$
- C_m pitching moment coefficient, $M/\frac{1}{2}\rho V^2 S c$

$$C_{L\alpha} = \frac{\partial C_L}{\partial \alpha}$$

$$C_{L\delta} = \frac{\partial C_L}{\partial \delta}$$

$$C_{m\alpha} = \frac{\partial C_m}{\partial \alpha}$$

$$C_{mq} = \frac{\partial C_m}{\partial \frac{qc}{2V}}$$

$$C_{m\dot{\alpha}} = \frac{\partial C_m}{\partial \frac{\dot{\alpha}c}{2V}}$$

$$C_{m\delta} = \frac{\partial C_m}{\partial \delta}$$

$$L_\alpha = \frac{\rho S V}{2m} C_{L\alpha}$$

$$L_\delta = \frac{\rho S V}{2m} C_{L\delta}$$

$$M_\alpha = \frac{\frac{1}{2}\rho V^2 S c}{I_y} C_{m\alpha}$$

$$M_\delta = \frac{\frac{1}{2}\rho V^2 S c}{I_y} C_{m\delta}$$

$$M_q = \frac{\frac{1}{2}\rho V^2 S c}{I_y} \frac{c}{2V} C_{mq}$$

$$M_{\dot{\alpha}} = \frac{\frac{1}{2}\rho V^2 S c}{I_y} \frac{c}{2V} C_{m\dot{\alpha}}$$

Control System and Transfer Function Notation

A transfer function is defined for an element or system as the ratio of the Laplace transforms of output to input. For a linear system, this represents the transform of the impulse response.

- t time
- $(\dot{\quad})$ time derivative, $\frac{d(\quad)}{dt}$
- s complex frequency $s = \sigma + j\omega$, Laplace transform variable
- $F(s)$ Laplace transform of $f(t)$, $F(s) = \mathcal{L}[f(t)] = \int_0^{\infty} f(t)e^{-st} dt$
- $G(s)$ forward loop transfer function
- $H(s)$ feedback loop transfer function
- $P(s)$ prefilter transfer function
- $N(s)$ numerator of transfer function
- $D(s)$ denominator of transfer function
- $M(s)$ reference model transfer function
- C command input
- R response output
- D disturbance input
- E error signal
- ω frequency, rad/sec
- ζ damping ratio
- ω_n undamped natural frequency
- τ time constant
- f frequency, cps
- T period

- K_1 integrator gain in G. E. system
- K_2 proportional feedback gain in G. E. system
- K_3 adaptively varied forward loop gain in G. E. system
- K_4 derivative feedback gain in G. E. system
- T_c canceller (of derivative feedback) time constant in G. E. system
- p value of s at a pole of a transfer function
- z value of s at a zero of a transfer function
- z actuator valve displacement, in.
- Q actuator hydraulic fluid flow rate, in.³/sec
- δ signal in control system

Subscripts

- ACT actuator
- A/C aircraft
- C command
- M model
- RG rate gyro
- VS valve servo

SECTION I INTRODUCTION

1.1 Philosophy

The automatic control specialist faces a serious problem when trying to design a flight control system for a modern, high-speed flight vehicle. Vehicle characteristics vary so much that it is extremely difficult to design a satisfactory constant parameter control system. The concept of using feedback in a control system was originally devised to overcome such changes in system characteristics. However, for supersonic and hypersonic vehicles, these variations are so extreme that the control system designer finds it impossible to devise satisfactory constant parameter control systems. He is forced to program the control system parameters as functions of the flight condition — for example, a feedback gain as a function of dynamic pressure. To successfully design such a control system, the designer usually requires extensive knowledge of the vehicle's characteristics, and often sufficient data is not available until after the vehicle is flight tested.

Recently, considerable attention has been focused on the "self-adaptive" control concept. Self-adaption implies measurement of the system's dynamic response, evaluation of this response by some criteria or by comparison with a desired response, and adjustment of the parameters of the control system to bring the measured response into agreement with the desired response. This is essentially the process used by the control system designer, but a self-adaptive system performs the process itself. Basically, an adaptive system is one in which the control system parameters are automatically adjusted to compensate for changing vehicle characteristics, either due to a changing environment or due to internal changes; a self-adaptive system is one in which this adjustment is made by internal measurement and evaluation of the dynamic response itself rather than by measurement of some environmental characteristic. An environmental characteristic is one which is only indirectly correlated with the response of the control system being considered. An internal process is

Manuscript released by author 31 July 1961 for publication as an ASD Technical Report.

one which is included in the control system directly, and internal changes are correlated with the response of the control system being considered. The terms "adaptive" and "self-adaptive" are conceptual in nature as is the term "feedback", and their implication is not on what quantity is measured but rather why it is measured and what is done with the measurement.

To see what adaptive control may have to offer, the problem must be formulated more precisely. The object is control the dynamic performance of a flight vehicle in some desired manner. The vehicle's characteristics change, and the change is so extreme that conventional feedback control techniques will not suffice to compensate adequately for this change. Accordingly, compensating changes could be programmed in the control system parameters as a function of the environmental condition that produces the change. The real difficulty lies in obtaining a sufficiently accurate description of the vehicle's characteristics as a function of the environment. What is needed are methods for simplifying the design problem by minimizing its dependence on information concerning the vehicle's characteristics. There are a number of possibilities. Part of the design task can be shifted to the control system. New techniques can be developed to measure the dynamic performance directly, and use this information to adjust the control system parameters without recourse to knowledge of the vehicle's characteristics. New types of control system elements - presumably nonlinear ones - can be developed which would be insensitive to changes in the vehicle's characteristics. More exotic concepts, such as thinking or self-organizing systems, implying drastic changes in control philosophy, can be readily conceived though their implementation represents a formidable task. However, practically speaking, it can be assumed that the basic tenets of feedback control theory will be retained, and that improvements in the design of flight control systems can be expected to result from the introduction of logical or decision-making elements, non-linear elements, direct measurements of dynamic performance, and other similar innovations. Clearly, the introduction of new techniques and the concepts of self-adaptive control offer methods for designing better flight control systems.

Reflection on the principal purpose for introducing adaptive control (and also simple feedback control) leads to a rather interesting and significant conclusion. The purpose is to provide for a wider latitude of vehicle or plant characteristics, or, to minimize the need for knowledge of these characteristics. Consider two extreme hypothetical cases: one, the case where the plant characteristics are known completely; two, the case where only the input and output quantities are known. Further, consider that a particular and explicitly defined response is desired, and that the sole basis for performance evaluation is the error between the achieved response and the desired response. To obtain the desired response in the first case requires only an open loop input - no feedback and no adaption - and in theory the error can be made identically zero. To obtain the desired response in the second case requires the ultimate in adaption - the response of the plant to the input must be measured, interpreted, and then used to modify the input (compensation), and this must be done continually. Because knowledge of the system can only be achieved after some finite response has been measured, and because the measurement, evaluation, and compensation process requires a finite time, there must necessarily always be a finite error. Thus in theory, the first system will always outperform the second system, because it is designed with complete a priori knowledge of the plant while the second system must make an identification of these dynamics. Generalizing leads to a rather significant conclusion. The use of an adaptive process leads to a degradation or slowing up of the control process; however, performance gains can be achieved through the indirect effects of adaption, that is, by making the system less sensitive to unknown or changing characteristics. This phenomenon is commonly demonstrated in digital computer programs, where it is well known that the addition of logical or decision steps slows the computing process. Thus, just because a system is adaptive does not mean it will perform better, and making a system adaptive where it is not required may be actually undesirable. Full advantage should be taken of all available knowledge of the components in designing any control system.

1.2 Purpose

A study of some basic considerations of adaptive flight control systems has been undertaken by the Flight Research Department of the Cornell Aeronautical Laboratory for the Flight Control Laboratory of the Aeronautical Systems Division, under the direction of Lt. Philip Gregory. Some of the earliest work in this field was performed by Campbell of the Cornell Aeronautical Laboratory (References 1 and 2), and interest in this work has continued since. The Flight Control Laboratory has sponsored considerable research on adaptive flight control systems, and gave impetus to much of the earlier work (Reference 3). The results have led to the formulation of a number of different schemes for adaption. During the course of the present project, three of these schemes - ones developed by General Electric, DODCO, and Aeronutronic - were evaluated with respect to their application to advanced flight vehicles of the X-15 and Dyna-Soar type. The intent of this study was not to determine which system would be best for the X-15 or Dyna-Soar; rather, the intent was to achieve a more thorough understanding of self-adaptive control systems - how do they behave? how can they be designed? what problems will be encountered? what kind of adaptive elements are most likely to solve these problems? The study was directed toward the problems associated with hypersonic flight vehicles, but the results are generally applicable to the control of any flight vehicle whose characteristics vary over a wide range.

1.3 Approach

The approach used in this study may be outlined briefly as follows. First, a detailed description and specification of the airframes and the adaptive systems was needed. Obtaining the airframe data was no problem since data for the X-15 and Dyna-Soar were already available in house. But for the adaptive control systems, not only was it necessary to obtain all the available published material, but it was also necessary, for a number of reasons, to contact the people responsible for the development work on each of the three systems, and to establish a working relationship with these people. None of the three systems was sufficiently well defined in the published literature, because the development work was very recent or still underway and because of the proprietary nature of

some of this work. Furthermore, it was desirable not only to obtain an accurate physical description of each of the three systems, but also to obtain a good understanding of the underlying design philosophy. If the evaluation of the capabilities of the three systems was to be meaningful, each would need the full benefit of the developer's work and the best thoughts and concepts concerning their application.

A general plan was used to study the various systems. First, the adaptive concepts were applied under idealized conditions - optimum conditions - to obtain a measure of the best performance that could be realized. Practical considerations were next introduced to see what degradation in performance occurred. Finally, the over-all scope of the work was broadened to include new considerations. It was not intended to expend equal effort on each of the three systems or the two vehicles being considered. The effort was expended where it could be expected to yield the most results, and the direction of this effort was re-oriented whenever it was deemed appropriate.

The airframe characteristics specifically studied were restricted to longitudinal motions. Speed was not included as a degree of freedom, but as an independent variable or a parameter. The equations of motion for the airframe were linearized. In application of the adaptive control systems, only pitch-rate signals were used for control, though other variables (flight path angle, angle of attack, etc.) were monitored. Sensor and actuator dynamics were included. Both linear and non-linear analysis techniques were used. The root locus technique was relied upon heavily for the linear analysis because an ESIAC computer was available (described in Appendix B). Analog computers were used for computing actual responses - for convenience in the linear case, of necessity in the non-linear one.

When the required data describing the three systems and the two airframes was in hand, a preliminary evaluation was made of the problems and difficulties associated with applying each of the systems to the two vehicles. This evaluation led to the following conclusions. The X-15 would be suitable for most of the work, since it represented a defined configuration, and embodies most of the longitudinal short period problems that would be encountered

in Dyna-Soar. The G.E. system was the best defined and its principle of operation the most easily understood of the three systems, and hence would be the first analyzed. The DODCO system, though not so well defined or as easily analyzed as the G.E. system, was still a complete concept and would be suitable as the second candidate for study. The Aeronutronic system was not a complete concept. Rather, it represented a developed concept for measurement of dynamic performance; the application of the measurement concept to adaptive control still required further research. In addition, actual hardware, in the form of a digital cross-correlator, would have to be used to obtain analog simulation. Thus, study of the Aeronutronic concept would best be deferred. A brief description of the concept of each system and how it was evaluated is given in the succeeding paragraphs.

The G.E. system (Reference 4) embodies a frequency sensor as the basic adaptive element and a reference model in the feedback. Conceptually, the frequency sensor maximizes loop gain while the reference model holds the response constant. These concepts were applied to synthesize a pitch-rate control system for the X-15, and root locus techniques and analog computers became the primary tools for system analysis and evaluation. Among subjects studied were the reference model concepts sensor dynamics, actuator dynamics and non-linearity, adaptive loop dynamics, and frequency sensor characteristics.

The DODCO System (References 5, 6, and 24) employs in the main control loop a dual-gain adaptive element - a gain switching device - which is controlled by functions of the error and error rate. Here the error is defined as the difference between the actual response as measured and the desired response as obtained from a reference model. The system is non-linear; though simple in mechanization, it presents the analyst with a formidable problem. The key concept lies in the switching logic which derives from asking the question: What is the optimum control policy for minimizing the error? The system as applied to pitch-rate control was mechanized on an analog computer, and the first task was to duplicate some of the results in Reference 5 which were obtained using a digital computer. Then system parameters were varied on the analog computer to evaluate performance and stability. Emphasis was placed

on determining the limitations of the system and on developing synthesis methods for use in design.

The Aeronutronic system (Reference 7) embodies the principle of using the impulse response of the vehicle, obtained from the cross-correlation of the output to a tailored white noise input, to adapt the flight control system. Study of the control concepts led to the following conclusions. Though Aeronutronic had demonstrated a technique for generating the impulse response and had conceived a method for controlling the damping ratio of a second order system, no satisfactory way of adapting a flight control system using the impulse response was readily available. It appeared that development of such an adaptive technique would be feasible and practical, but would require substantial effort. One limitation appeared to be clearly present: there is an important and fundamental time delay involved in the adaptive process; this time delay is the time it takes to obtain the impulse response, and must be at least as long as the time it takes for the impulse response to decay to sensibly zero. In view of the difficulties involved and the limited effort available, further study of the Aeronutronic concept was abandoned.

SECTION II

DEFINING THE CONTROL PROBLEM

2.1 General Considerations

The control problem for a hypersonic or re-entry vehicle is a multi-variable one, involving many modes of motion. The pilot or flight director must control the vehicle's attitude with respect to the flight path (α and β), its orientation in space (ψ , θ , and ϕ), and its flight path (h , γ , V and flight path azimuth). Control is normally obtained through four vehicle control inputs: the pitch, roll, and yaw controls either of the aerodynamic or reaction type, and the thrust. It is quite obvious that independent control of all the output variables is not possible. Usually, attitude control is associated with the rapid modes of motion; flight path dynamics, with the slow modes of motion. Accordingly, the control problem and control systems are broken up into two general groups, which, following Dommasch (Reference 5), may be labeled as:

1. The micro-control problem - associated with the fast modes of motion and what are often called the "inner" loops in the control system - and
2. The macro-control problem - associated with the slow modes of motion and what are often called the "outer" loops in the control problem.

The micro-control problem has two objectives: (1) to provide satisfactory dynamics for the fast modes of motion, and (2) to provide suitable responses of the fast motions for use in the macro-control problem. The second objective implies providing the proper statics and insuring that the fast modes of the micro-control problem are fast enough to avoid interaction with the slow modes of the macro-control problem. Of course, such interaction cannot always be avoided, but it can be minimized.

In the present study, we are concerned with only the micro-control problem and with only the longitudinal aspects of that problem. Thus the concern is to provide a proper longitudinal short-period response for the airplane - the micro-control problem - and insuring that the adaptive process is fast enough to account for the changes associated with flight condition - the macro-control problem. More severe requirements on the adaptive process may be posed by changes that occur rapidly - perhaps with angle of attack or due to some control system non-linearity such as backlash.

The general approach to the control problem may be listed in several steps:

1. Defining the vehicle's characteristics,
2. Defining a desired response,
3. Developing general control schemes which will produce the desired response,
4. Determining the problems associated with the control schemes and the adverse conditions that they will be subjected to,
5. Implementing the control schemes into concrete systems, and
6. Evaluating the efficacy of these systems under expected adverse conditions.

This study is primarily concerned with the last step, but from a theoretical standpoint rather than a hardware standpoint. However, all these steps are involved, though the vehicles and the control schemes, and even their implementation to some extent, are defined and are the starting point for this study.

2.2 High-Gain Control Schemes

The control schemes used in this study are based on those developed in feedback control theory, but modified to provide greater adaption to changes in the elements of the system.

The general single loop problem - one input and one output - can be reduced to the block diagram shown in Figure 1,

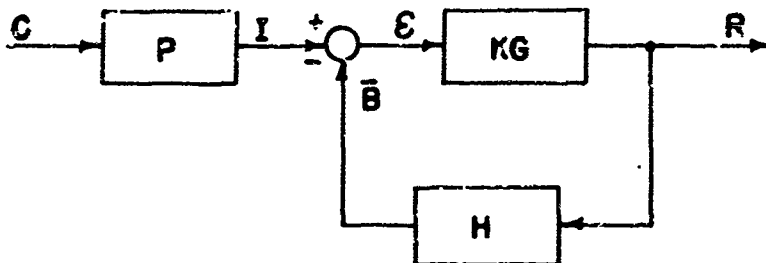


FIGURE 1 BLOCK DIAGRAM OF SINGLE-INPUT SINGLE-OUTPUT FEEDBACK SYSTEM

- C = command
- I = input to closed loop
- R = response
- B = feedback
- E = $I - B$, the error
- P = prefilter transfer function
- KG = forward loop transfer function
- H = feedback loop transfer function

The response to a command input is

$$\frac{R}{C} = \frac{P}{H} \left(\frac{KGH}{1 + KGH} \right) \quad (2.1)$$

and

$$\lim_{K \rightarrow \infty} \frac{R}{C} = \frac{P}{H} \quad (2.2)$$

If the gain K can be maintained at a high value, then the response of the system will be approximated by P/H . We have control over P and H , and hence the ability to tailor the response of the system. We may formalize this with the following equation:

$$\left(\frac{R}{C}\right)_{\text{DESIRED}} = \lim_{K \rightarrow \infty} \frac{P}{H} \left(\frac{KGH}{1+KGH}\right) \quad (2.3)$$

The difference between tailoring the response with a prefilter or with feedback control has two basic facets. The first is purely a practical one. With prefiltering only, and unity feedback

$$\left(\frac{R}{C}\right)_{\text{DESIRED}} = P \quad (2.4)$$

With feedback compensation only,

$$\left(\frac{R}{C}\right)_{\text{DESIRED}} = \frac{1}{H} \quad (2.5)$$

and H is the inverse of the desired response. In practice, it may be difficult to generate one of the two forms - most likely the inverse. The second difference between the two methods of compensation is a more fundamental one. Consider the case shown in Figure 2, where a disturbance enters the system at some interior point in the forward loop transfer function.

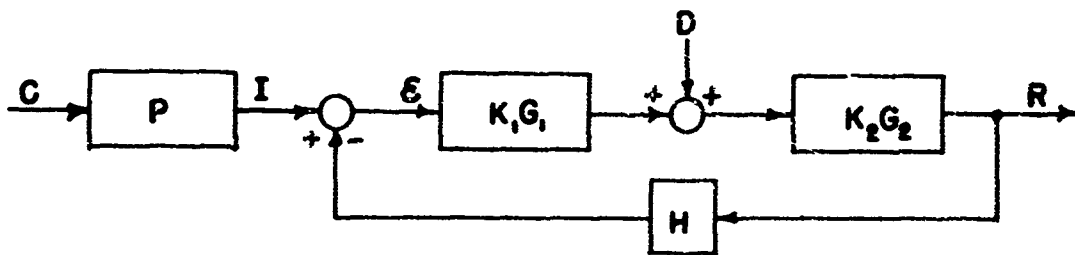


FIGURE 2 BLOCK DIAGRAM OF DUAL-INPUT SINGLE-OUTPUT FEEDBACK SYSTEM

$$KG = K_1 G_1 K_2 G_2$$

D = Disturbance Input

The response to command inputs is unchanged (Equation 2.1), but the response to a disturbance is given as

$$\frac{R}{D} \Big|_{c=0} = \frac{1}{K_1 G_1 H} \left(\frac{KGH}{1+KGH} \right) \quad (2.6)$$

For high loop gain,

$$\frac{R}{D} \approx \frac{1}{K_1 G_1 H} \quad (2.7)$$

If K_2 is finite and the high loop gain is obtained by making K_1 large, then

$$\lim_{K_1 \rightarrow \infty} \frac{R}{D} = 0 \quad (2.8)$$

Thus, the important difference between prefilter type compensation and feedback compensation lies in their different effect on the response to disturbance inputs. These disturbance inputs may be external as from gust inputs, or internal as from noise in electronic components; or they may represent cross-coupling inputs from other portions of the control system. In general, one attempts to minimize the response to disturbances. Thus, it may be advisable to tailor R/D with H , and $K_1 G_1$, while P is used to tailor R/C .

$$\left(\frac{R}{C} \right)_{\text{DESIRED}} = \frac{P}{H} \quad (2.9)$$

$$\left(\frac{R}{D} \right)_{\text{DESIRED}} = \frac{1}{K_1 G_1 H} \quad (2.10)$$

The role of $K_2 G_2$ is of significance, and can be illustrated by rewriting Equation 2.6 as

$$\frac{R}{D}\bigg|_{C=0} = \frac{K_2 G_2}{1 + KGH} \quad (2.11)$$

The disturbance response is proportional to K_2 . If $K_2 G_2$ is unity, then the disturbance effectively occurs directly in the output; and the higher the frequency content of the disturbance (beyond a certain frequency), the less will be the effect of the control system in minimizing the disturbance. For instance, a step in D will result initially in a step in R .

So far the concept of adaption, in the sense of adjustment, has not been introduced. However, adaption in the broader sense, i. e., ability to cope with changes in the controlled element in the forward loop, has been considered. The simple feedback systems of Figure 1 and 2 have been discussed from the adaptive point of view. That is, the open loop gain K has been assumed sufficiently high that the response has been formulated in terms of P and H , without regard to the specific value of K or the form of G . This is not a new approach (e. g., Reference 9, Chapter 6, p. 322), but it has not been applied in flight control systems for good reasons. The value of the loop gain K contains the elevator effectiveness which varies over a wide range (considering longitudinal control and just one of the varying parameters), and it is difficult to design a control system with a sufficiently high constant gain to accommodate the variations. The dilemma is sluggish, inadequate response at one end of the spectrum, instability at the other end. In practice, control systems have been designed with variable gains using air data parameters such as dynamic pressure for adjustment. The results have often been unimpressive, and have led to the quest for better concepts of adaption.

Applying the high-gain adaptive concept to feedback control in an optimum manner implies developing techniques for keeping the loop gain at the highest value compatible with stability. Most of the proposed adaptive control schemes approach

the problem in this manner. Some measurement of the response is made, interpreted in terms of stability, and then used to adjust the loop gain. Thus, an organized and clear understanding of the linear feedback control problem is a necessary prerequisite to the study of adaptive control systems.

2.3 Model Approach to Control System Design

The concept of using a reference model in flight control systems was probably first proposed by Campbell (Reference 1). The concept was suggested by studies, reported in References 10, 11 and 12, which showed that an "optimum" response for the longitudinal short-period mode could be specified in terms of a second-order model with constant characteristics. The concept is nothing more than the specification of the prefilter and the feedback compensation, depicted in Figure 1 of Section 2.2, in terms of this "optimum" model. As Campbell points out (Reference 2), these "optimum" characteristics do not peak sharply, and reasonable departures are allowable. Thus, the approach seems feasible.

The model concept as applied to a prefilter is illustrated in Figure 3.

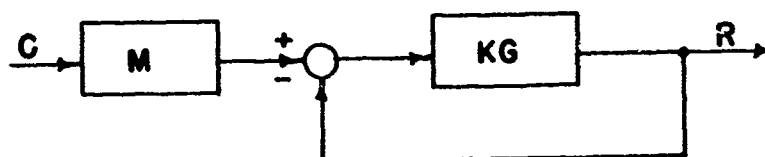


FIGURE 3 THE MODEL IN THE PREFILTER

The response is given as

$$\frac{R}{C} = M \left(\frac{KG}{1+KG} \right) \quad (2.12)$$

and if K is sufficiently high

$$\frac{R}{C} \cong M \quad (2.13)$$

The model concept as applied to feedback compensation is illustrated in Figure 4.

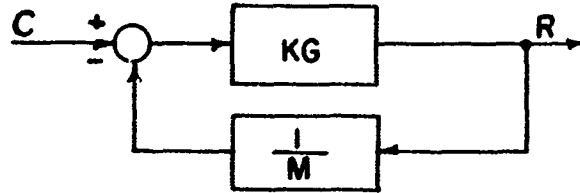


FIGURE 4 INVERSE-MODEL IN THE FEEDBACK

The response is given as

$$\frac{R}{C} = M \left(\frac{\frac{KG}{M}}{1 + \frac{KG}{M}} \right) \quad (2.14)$$

and if K is sufficiently high

$$\frac{R}{C} \cong M \quad (2.15)$$

Combinations of prefilter and feedback compensation can be used to independently control the response to commands and the response to disturbances - say gusts. If we designate M_p as the prefilter model, and M_H as the feedback model, then the scheme can be depicted as follows if the gust disturbance is considered to affect the response directly.

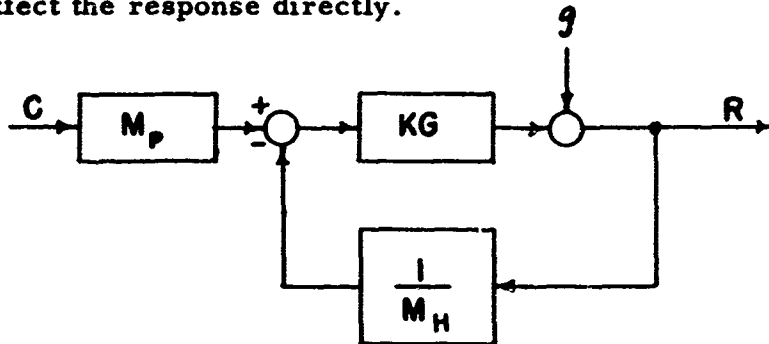


FIGURE 5 COMBINED PREFILTER AND FEEDBACK MODELS

The independent responses are given as

$$\frac{R}{C} = M_P M_H \left(\frac{\frac{KG}{M_H}}{1 + \frac{KG}{M_H}} \right) \quad (2.16)$$

and

$$\frac{R}{g} = \frac{M_H}{KG} \frac{\frac{KG}{M_H}}{1 + \frac{KG}{M_H}} \quad (2.17)$$

If K is sufficiently high

$$\frac{R}{C} \cong M_P M_H = M_c \quad (2.18)$$

$$\frac{R}{g} \cong \frac{M_H}{KG} = M_g \quad (2.19)$$

where M_c is the command model, and M_g is the gust (disturbance) model.

The problems associated with obtaining a desired gust response are manifest from Equations 2.18 and 2.19. The feedback model, M_H , and compensation in the forward loop, KG , provide the means for tailoring the gust response. In terms of frequency spectra, if R/g is to be minimized, then M_H/KG must be minimized over the expected frequency range of g . A high value of gain, K , will tend to minimize the effect of gust disturbances.

Thus, in theory, it is possible to obtain any desired response to a disturbance input (R/g) by means of compensation in the forward and feedback loops (M_H/KG) provided the loop gain is high. Similarly, in theory, it is possible to obtain any desired response to a command input (R/C) by means of compensation in the prefilter and the feedback loop ($M_P M_H$) provided the

loop gain is high. In practice, stability problems limit the value of gain that can be used; practical problems of mechanization limit the range of desired responses that can actually be realized.

Other reasons for combining prefilter and inverse-feedback model techniques arise from practical considerations. It may be convenient to generate part of the model in the feedback and the remainder in the prefilter. Or, the prefilter may be needed to cancel undesired feedback characteristics which are generated necessarily for purposes other than inverse-model generation. Using both types of compensation will generally allow more flexibility.

2.4 Aircraft Model and Variables

The longitudinal control problem was picked for study because difficulties have been encountered with longitudinal motions in the past (unstable airplane-pilot combinations have been encountered, commonly called pilot-induced oscillations). Also, the longitudinal short-period mode is one of the primary control modes and considerable research has been directed toward determining optimum response characteristics for this mode. A considerable portion of this research has been performed by the Cornell Aeronautical Laboratory and is reported in References 10 through 15. The earlier results are summarized in the Appendix of Reference 2; the later results are presented in References 14 and 15. The results of most of the research on longitudinal handling qualities done to date (including that done by NASA, various government agencies, research laboratories, and universities) are summarized in Reference 16, and a less comprehensive summary is found in Reference 17.

The data of Reference 14 define combinations of short-period undamped natural frequency and damping ratio which are acceptable to the pilot. The best tested area might be described as a "plateau" with gently sloping sides and no distinct "peaks" or optimum combinations of ω_n and ζ . In selecting a model however, consideration must be given to the relation of the model's speed of response or bandwidth with respect to the speed of response or bandwidth of

the closed-loop system incorporating the model. The bandwidth of the closed-loop system must be at least as large as that of the model. Particularly if the model is used as a prefilter and it is desired that the over-all response be that of the model, then the bandwidth of the closed loop following the model (see Figure 3 and discussion of Section 2.3) must be several times that of the model alone. Thus, it is obvious that the lower the bandwidth of the model, the less difficult will be the design of the system.

The short-period handling qualities data of References 14 and 15 are presented in Figure 10 in the form of a complex-plane plot. This figure presents the data for short-period configurations with complex roots in a straightforward and useful manner. For configurations with real roots, the plot degenerates to a single line, the real axis, and for this reason this representation was not used in References 14 or 15. However, for the purpose of selecting an adaptive system model, it is of some value, especially when root locus techniques are used for synthesis. Figure 10 shows that the point $\omega_n = 1.0$ cps and $\zeta = .9$ is in the "Best Tested" area and is acceptable from the pilot's point of view as a short-period model. However, the point $\omega_n = 0.5$ cps and $\zeta \approx .7$ is also in or on the boundary of the "Best Tested" area and, from the point of view of the adaptive control system designer, would be preferred because of its lower bandwidth.

The model or desired response that results from this research may be stated in transfer function form as:

$$\frac{\Delta n_z}{F_s} = \frac{K_{n_z}}{\left(\frac{s}{\omega_n}\right)^2 + \frac{2\zeta}{\omega_n}s + 1} \quad (2.20)$$

Δn_z = incremental normal acceleration, g
 F_s = stick force, lb
 ω_n = short-period frequency, rad/sec
 ζ = short-period damping ratio
 K_{n_z} = $1 / \left(\frac{F_s}{n_z}\right)_{ss}$, the inverse of the steady-state stick force per g.

The value of K_{n_z} depends on the configuration of both the aircraft and the pilot's control stick. For conventional fighter airplanes, with high maximum load factors (7 g maximum), typically good values of $(F_s/n_z)_{SS}$ lie between 4 and 8 lb/g. For conventional bombers, with low permissible load factors (4 g maximum), typically good values of F_s/n_z lie between 40 and 80 lb/g. It appears that a suitable value of $(F_s/n_z)_{SS}$ is obtained by matching the maximum normal acceleration capabilities of the airplane to the maximum control effort expected of the pilot.

The important aspects of the model defined by Equation 2.20 are listed for emphasis.

1. The model is a normal acceleration (n_z) one.
2. The frequency (ω_n) and damping (ζ) are specified constants invariant of the airplane configuration or flight condition. However, a winged vehicle is implied which derives its maneuvering capabilities from aerodynamic lift which is in turn controlled by the vehicle's angle of attack.
3. The numerator of the n_z/F_s transfer function - more generally $n_z/\text{pilot input}$ - involves no time constant or zeros.
4. The gain of the n_z/F_s transfer function is constant, though it may vary from one vehicle type to the next.

The results of the above described handling qualities research have received wide distribution. People working in the control system field, particularly adaptive control, have applied these results to the model-reference concept. The particular characteristics for the n_z/F_s transfer function have been applied to all manners of control system - pitch rate and roll rate command systems, pitch attitude and roll attitude command systems, etc - see Reference 3 for examples. This indiscriminate use of the n_z/F_s model - while not objectionable when used purely for illustrative purposes - becomes objectionable and damaging when it occurs in actual flight control systems. Misuse of the n_z/F_s model has occurred in several cases where it has been

applied to the design of adaptive pitch rate command systems - $\dot{\theta}/F_s$ systems. When evaluation pilots have flown these systems, they have complained of sluggish response, and that the response was not invariant with flight condition. One answer to complaints of sluggish response has been to reduce the damping ratio, to as low as $\zeta = .2$ or $.3$, leading to the conclusion that the desirable values determined by the handling qualities research are in error. The following development gives a better appreciation of what is involved, and why care must be used in selecting the reference model.

Three responses of the X-15 airplane to step inputs are compared in Figure 11: one is for the uncontrolled airplane; the other two are for the airplane with a high-gain control system which employs a model to tailor the response. The model in both cases is the n_z model of Equation 2.20 with $\omega_n = .5$ cps and $\zeta = .7$; but in one case it is used as a $\dot{\theta}$ model, in the other case as an α model (equivalent to an n_z model if L_S is small and the pilot is near the center of gravity). It is clear that in both controlled cases the design response has been obtained; in one case the model response is duplicated by $\dot{\theta}$, in the other by α . However, to one familiar with handling qualities requirements, the response with the $\dot{\theta}$ model is clearly objectionable while that with the α model is highly desirable. The objectionable quality in the one response is the very sluggish response in α , characterized by the very long time constant apparent in α .

The situation, as illustrated in Figure 11, can be clarified by examining the pertinent block diagrams and equations. First consider the " $\dot{\theta}$ model" case.

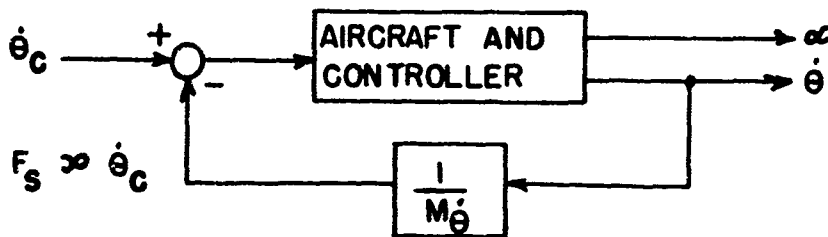


FIGURE 6 BLOCK DIAGRAM WITH INVERSE $\dot{\theta}$ -MODEL IN THE FEEDBACK

$\dot{\theta}$ Response (Figure 6):

For high loop gain

$$\frac{\dot{\theta}(s)}{\dot{\theta}_c(s)} \approx M_{\dot{\theta}} = \frac{1}{\frac{s^2}{\omega_n^2} + \frac{2\zeta}{\omega_n}s + 1} \quad (2.21)$$

where $\omega_n = .5$ cps
 $\zeta = .7$

α Response (Figure 6):

$$\frac{\alpha(s)}{\dot{\theta}_c(s)} = \frac{\frac{\alpha(s)}{\delta_c(s)}}{\frac{\dot{\theta}(s)}{\delta_c(s)}} \times \frac{\dot{\theta}(s)}{\dot{\theta}_c(s)} \quad (2.22)$$

Substituting the airplane transfer functions, given by Equations A-2 and A-3 of Appendix A, into Equation (2.22), yields

$$\frac{\alpha(s)}{\dot{\theta}_c(s)} = \frac{K_{\alpha} (\tau_{\alpha} s + 1)}{K_{\dot{\theta}} (\tau_{\dot{\theta}} s + 1)} \frac{\dot{\theta}(s)}{\dot{\theta}_c(s)} \quad (2.23)$$

Substituting the expressions for $K_{\dot{\theta}}$ and K_{α} , given by Equations A-12 and A-13 of Appendix A, into Equation 2.23, yields

$$\frac{\alpha(s)}{\dot{\theta}_c(s)} = \left(\frac{M_{\delta} + M_q L_{\delta}}{M_{\delta} L_{\alpha} - M_{\alpha} L_{\delta}} \right) \frac{(\tau_{\alpha} s + 1)}{(\tau_{\dot{\theta}} s + 1)} \frac{\dot{\theta}(s)}{\dot{\theta}_c(s)} \quad (2.24)$$

where $\tau_{\dot{\theta}}$ and τ_{α} are given by the following expressions (Equations A-14 and A-15 from Appendix A).

$$\tau_{\alpha} = \frac{-L_{\delta}}{M_{\delta} + M_q L_{\delta}} \quad (2.25)$$

$$\tau_{\dot{\theta}} = \frac{M_{\delta} - L_{\delta} M_{\alpha}}{M_{\delta} L_{\alpha} - M_{\alpha} L_{\delta}} \quad (2.26)$$

The relations may be simplified by neglecting the often small effect of elevator lift, L_S , to obtain the following approximation.

$$\frac{\alpha(s)}{\dot{\theta}_c(s)} \cong \left(\frac{1}{L_\alpha} \right) \frac{1}{\left(\frac{s}{L_\alpha} + 1 \right)} \frac{\dot{\theta}(s)}{\dot{\theta}_c(s)} \quad (2.27)$$

Now introducing the approximation given by Equation 2.21, yields

$$\frac{\alpha(s)}{\dot{\theta}_c(s)} \cong \frac{1}{s + L_\alpha} M \dot{\theta} \quad (2.28)$$

It is apparent from Equation 2.28 that the α response will be dominated by a long time constant approximately equal to $1/L_\alpha$. Also, since L_α changes with flight condition, it is apparent that the α or n_z response will not be invariant with flight condition. Furthermore, the " α -model" responses of Figure 11 show that a pilot does desire a large initial overshoot in $\dot{\theta}$, as this is necessary in order to give the desired α and θ response. If the pilot were faced with the response given using the n_z -model (Equation 2.20) as a $\dot{\theta}$ -model, then he would perhaps settle for a lower damping ratio than $\zeta \cong .7$ in order to obtain this initial $\dot{\theta}$ overshoot. The complaints of the evaluation pilots, referred to earlier, are thus explained and can be attributed to improper application of the data obtained from the handling qualities research.

Next consider the " α -model" case. The model, in this case, is formed by adding a prefilter to the arrangement of Figure 6. The purpose of the prefilter is to add a zero or a numerator time constant in $\dot{\theta}(s)/\dot{\theta}_c(s)$ so as to cause the proper initial overshoot in the $\dot{\theta}$ response to a step command input.

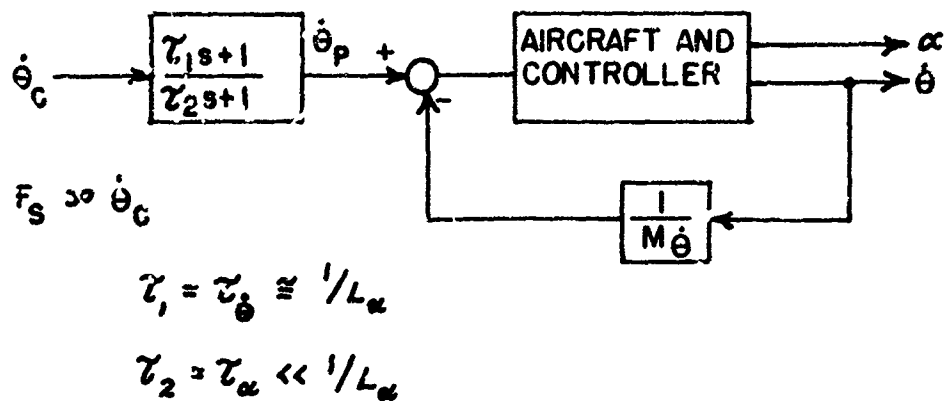


FIGURE 7 BLOCK DIAGRAM WITH INVERSE $\dot{\theta}$ -DENOMINATOR IN THE FEEDBACK AND $\dot{\theta}$ -NUMERATOR IN THE PREFILTER

$\dot{\theta}$ Response (Figure 7):

$$\frac{\dot{\theta}(s)}{\dot{\theta}_c(s)} = \frac{\dot{\theta}(s)}{\dot{\theta}_p(s)} \frac{\dot{\theta}_p(s)}{\dot{\theta}_c(s)} = \frac{(\tau_1 s + 1)}{(\tau_2 s + 1)} \frac{\dot{\theta}(s)}{\dot{\theta}_p(s)} \quad (2.29)$$

For high loop gain, $\dot{\theta}/\dot{\theta}_p$ is given by Equation 2.21, and if the assigned values for τ_1 and τ_2 are introduced, then Equation 2.29 becomes

$$\frac{\dot{\theta}(s)}{\dot{\theta}_c(s)} \approx \frac{(\tau_{\dot{\theta}} s + 1)}{(\tau_{\alpha} s + 1)} M \dot{\theta} \quad (2.30)$$

Again simplifying by neglecting $L_{\dot{\theta}}$ and the small time constant τ_2 , the following expression is obtained

$$\frac{\dot{\theta}(s)}{\dot{\theta}_c(s)} \approx \left(\frac{s}{L_{\alpha}} + 1 \right) M \dot{\theta} \quad (2.31)$$

α Response (Figure 7):

The α response can be written from Equations 2.23 and 2.29 as

$$\frac{\alpha(s)}{\dot{\theta}_c(s)} = \frac{K_\alpha (T_1 s + 1)(T_\alpha s + 1)}{K_{\dot{\theta}} (T_2 s + 1)(T_\theta s + 1)} \frac{\dot{\theta}(s)}{\dot{\theta}_p(s)} \quad (2.32)$$

If the assigned values for τ_1 and τ_2 are introduced, then Equation 2.32 becomes

$$\frac{\alpha(s)}{\dot{\theta}_c(s)} = \frac{K_\alpha}{K_{\dot{\theta}}} \frac{\dot{\theta}(s)}{\dot{\theta}_p(s)} \quad (2.33)$$

For high gain $\dot{\theta}/\dot{\theta}_p$ is given by Equation 2.21, and if L_s is again neglected, Equation 2.33 becomes

$$\frac{\alpha(s)}{\dot{\theta}_c(s)} \approx \left(\frac{1}{L_\alpha} \right) M_{\dot{\theta}} \quad (2.34)$$

It is apparent from Equations 2.31 and 2.34 that the desired results are achieved by the arrangement depicted in Figure 7. The proper $\dot{\theta}$ -model numerator (Equation 2.31) is provided to give the proper α -model (Equation 2.34) and hence the desired n_z -model (Equation 2.20). Proper control gearing is presumed, and the desired response will be realized only if the loop gain is sufficiently high.

In summary, both systems depicted in Figures 6 and 7 are pitch rate command systems, but essentially different reference models are used. The two models may be expressed, without gain specification, as:

$$M_{\dot{\theta}} = \frac{1}{\left(\frac{s}{\omega_n}\right)^2 + \frac{2\zeta}{\omega_n} s + 1} \quad \text{UNDESIRABLE} \quad (2.35)$$

$$M_{\dot{\theta}_1} = \frac{T_1 s + 1}{\left(\frac{s}{\omega_n}\right)^2 + \frac{2\zeta}{\omega_n} s + 1} \quad \text{DESIRABLE} \quad (2.36)$$

$\omega_n = .5 \text{ cps}, \quad \zeta = .7, \quad T_1 = T_\theta \approx 1/\omega_n \text{ sec}$

The desirability of the two models is evaluated on the basis that the input comes from the pilot, as from a control stick, and that the pilot is controlling the aircraft's primary motions - specifically the longitudinal short-period motions. Another way to state this is that the pilot is directly in the micro-control loop. For other inputs, say from an automatic macro-controller or autopilot, a different model might be desirable.

The above results may be related more closely to the data obtained from the handling qualities research, and the story made complete by considering the steady-state (gain) relations.

$$\frac{n_z}{F_s} = \frac{n_z}{\delta} \frac{\dot{\gamma}/\delta_e}{\dot{\theta}/\delta_e} \frac{\dot{\theta}}{\dot{\theta}_c} \frac{\dot{\theta}_c}{F_s} \quad (2.37)$$

Introducing the steady-state values for $\dot{\theta}/\delta_e$, $\dot{\gamma}/\delta_e$, and n_z/δ from Equations A-7, A-9, and A-10 of Appendix A, and for n_z/F_s from Equation 2.20, and letting $\dot{\theta}/\dot{\theta}_c = 1$, then the recommended gearing (gain) is found to be

$$\frac{\dot{\theta}_c}{F_s} = \frac{g}{V} K_{n_z} \quad (2.38)$$

where K_{n_z} , the inverse of the steady-state stick force per g, is an appropriately selected constant as discussed earlier.

The foregoing analysis has all been based on the assumption that the desired response for $\dot{\theta}$ can be achieved (i. e., that the aircraft's response will duplicate that of the reference model). Even with this assumption, it is necessary to program the control gearing ($\dot{\theta}_c/F_s$) with speed (V), and the numerator time constant of the model (τ_i) with flight condition on the following basis.

$$\tau_i = \tau_{\dot{\theta}} \cong \frac{L}{L_{\alpha}} = \frac{\rho V S C_{L_{\alpha}}}{2 m} \quad (2.39)$$

The gearing can be programmed with speed rather easily, and accuracy is not important. But programming the time constant in the manner indicated is difficult and objectionable (particularly if the approximation of τ_{θ} by $1/L_{\alpha}$ cannot be allowed). Furthermore, in practical applications the ideal response (model response) for $\dot{\theta}$ will not usually be achieved due to gain limitations, and the required values for the time constant (τ_i) may thereby be affected. (For example, a specific case where this occurs is dealt with in Section 3.3, where the G.E. System is applied to the X-15.) Accordingly, a better method for obtaining the desired α or n_z response may be to use α or n_z feedback directly in the control system. This is an appropriate subject for further study.

The control problem, for the longitudinal short-period motions, can be formulated in rather general fashion. One can categorize the types of command inputs, the variables that are suitable for sensing, the variables that need to be controlled in some satisfactory or desired manner, the suitable control quantities, and the tasks or objectives.

- I Types of Command Inputs
 - a. Pilot control
 - 1. Force
 - 2. Position
 - b. Automatic Control
 - c. Monitored Control
- II Suitable Responses for Sensing
 - a. Angle of attack, α
 - b. Normal acceleration, n_z
 - c. Pitch rate, q
 - d. Derivatives of (a), (b), and (c)
 - e. Integrals of (a), (b), and (c)
- III Controlled Responses
 - a. Angle of attack, α
 - b. Normal acceleration, n_z

- c. Pitch rate, q
 - d. Flight path curvature, $\dot{\gamma}$
 - e. Attitude angle, θ
 - f. Flight path angle, γ
 - g. Altitude, h
- IV Suitable Control Quantities
- a. Elevator angle, δ_e
 - b. Reaction control
- V Task or Objective - Vehicle Control During:
- a. Boost
 - b. Glide or Enroute Flight
 - c. Re-entry
 - d. Approach
 - e. Landing

Only one control input is available for the control problem under consideration, so that only one possible form of response is available during any particular time interval for all of the variables listed in Item III. Thus, the control synthesis problem can be reduced to the following steps: select a suitable model for the response of any one variable (listed in III) to the given type of command input (listed in I); sense one or more of the variables listed in II; finally, develop a control system which links the sensor (II) and the input to the airframe controller (elevator and/or reaction control), and use the model as the reference for the desired response. The task or objectives are influential in the process of selecting the model, the specific application governs what sensors are used, while the controller configuration is dictated primarily by the performance required of the system.

SECTION III
INITIAL STUDY AND APPLICATION OF G. E. SYSTEM

3.1 Introduction

The analysis of the G. E. system was conducted in two separate phases. The phase reported in this section (Section III) was a general study of the system and its application. This study used linear analysis techniques based principally on the root locus method. An ESIAC computer was used to obtain the root locus plots. This computer and the form of the root locus plots are described in Appendix B. The system also was simulated on an analog computer. The analog computer used to simulate the system in the first study was a small EASE computer. Simulation of the airplane, the actuator, the reference model, and the frequency sensor used its full capacity and few components were available for simulating any additional elements or nonlinearities.

The second phase of the analysis was directed at specific problems in application of the G. E. system. The results of this study are reported in Section IV. The ESIAC computer was again used in the analysis and the system was simulated on a larger REAC analog computer which permitted simulation of actuator nonlinearities.

The X-15 was the study vehicle in both phases. The G. E. system was applied to the problem of controlling the X-15 short-period dynamics during re-entry. The equations used to represent the airplane are contained in Appendix A.

During the first study using the ESIAC and EASE analog computer the following problem areas were examined.

1. General Analysis of the System
 - a. Block diagrams
 - b. Model concept
 - c. Root locus analysis
2. Application of the G. E. system to the X-15
 - a. Selection of system parameters
 - b. Response to step command inputs
 - c. Response to gusts
 - d. Modification of basic airplane characteristics - particularly unstable configurations

e. Sensor and actuator dynamics

3. Adaptive loop characteristics.

During the second study using the ESIAC and the REAC analog computer the following specific problems were examined.

1. The response of the system to inputs at the actuator valve
2. The effect of actuator nonlinearities
3. Characteristics of the frequency sensor
4. The effect of "noise" in the rate gyro output

3.2 General Analysis of the System

The General Electric Self-Adaptive Flight Control System (GESAC) - referred to in this study as the G.E. System - involves the following general concepts:

1. Inverse model in the feedback,
2. Rate gyro sensing device,
3. Invariant $\dot{\theta}$ response with flight condition,
4. Adaptive control of the primary or forward loop gain employing a frequency sensor, and
5. No inserted test signal, per se.

Two block diagrams of the system, applied as a pitch rate control system, are presented in Figure 8. One shows the system as actually mechanized, the other shows the system as it would appear with the model transfer function explicitly in the feedback. The purpose of the K_1/s block in the forward loop is to provide a zero error system, so the gain of the closed-loop system will be invariant of the aircraft gain.

The equations for the model, in terms of the parameters of the physical system depicted in Figure 8, are

$$\frac{\dot{\theta}_M}{\dot{\theta}_{RG}} = \frac{s^2 \left[\frac{K_4 T_c + K_2 T_c}{K_1} \right] + s \left[\frac{K_1 T_c + K_2}{K_1} \right] + 1}{s T_c + 1} \quad (3.1)$$

$$(\omega_n^2)_M = \frac{K_1}{T_c (K_4 + K_2)} \quad (3.2)$$

$$\left(\frac{Z}{\omega_n}\right)_M = \frac{K_1 T_c + K_2}{K_1} \quad (3.3)$$

There are four parameters available (K_1 , K_2 , K_4 , and T_c), so that in theory, K_1 , T_c , $(\omega_n)_M$, and $(Z)_M$ can all be set independently - actually there are practical limits.

The general concept of how the system works is based on the explanation given in Section 2.3; the gain K_3 is kept high enough so that the system response approximates that of the model; the function of the frequency sensor is to maintain the gain at an optimum value - as high as possible without causing instability. The specific operation of the system can best be described using the root locus technique. Two root locus plots are presented in Figure 12, one for a second-order actuator, the other for a first-order actuator. To illustrate the general concept only the actuator, airplane, and model zeros and poles need be included.

Consider first the case with the second-order actuator as depicted in Figure 12. As the loop gain of the system is increased, the aircraft poles approach the feedback zeros (the poles of the model), the integrator pole at the origin approaches the airplane zero (at $-1/T_0$), the feedback pole (at $-1/T_c$) goes out the negative real axis, and the actuator poles approach the imaginary axis and eventually go into the right-half plane - unstable. The limiting value of the loop gain is determined by the actuator poles, and some value less than that for instability represents the optimum value of the gain.

In order to see how the system works and understand the design philosophy, it is necessary to consider the equations which define the open-loop and closed-loop response in terms of the zeros and poles of the root locus plot (Figure 12, also refer to Figure 8).

Forward Loop:

$$\frac{\dot{\theta}(s)}{\delta(s)} = K_F G_F(s) = K_F \frac{N_F(s)}{D_F(s)} \quad (3.4)$$

$$K_F = K_1 K_3 K_{ACT} K_{A/C} \quad (3.5)$$

$$N_F(s) = \left(1 + \frac{s}{1/T_0} \right) \quad (3.6)$$

$$D_F(s) = s \left(\frac{s^2}{\omega_n^2} + \frac{2\zeta}{\omega_n} s + 1 \right)_{ACT} \left(\frac{s^2}{\omega_n^2} + \frac{2\zeta}{\omega_n} s + 1 \right)_{A/C} \quad (3.7)$$

Feedback Loop:

$$\frac{\dot{\theta}_M(s)}{\dot{\theta}(s)} = K_H G_H(s) = \frac{N_H(s)}{D_H(s)} \quad (3.8)$$

$$K_H = 1 \quad (3.9)$$

$$N_H(s) = \left(\frac{s^2}{\omega_n^2} + \frac{2\zeta}{\omega_n} s + 1 \right)_{MODEL} \quad (3.10)$$

$$D_H(s) = \left(1 + \frac{s}{1/T_c} \right) \quad (3.11)$$

Closed Loop:

$$\frac{\dot{\theta}(s)}{\dot{\theta}_e(s)} = KG(s) = K \frac{N(s)}{D(s)} \quad (3.12)$$

$$\frac{\dot{\theta}(s)}{\dot{\theta}_e(s)} = \frac{K_F G_F(s)}{1 + K_F G_F(s) K_H G_H(s)} = \frac{K_F N_F(s) D_H(s)}{D_H(s) D_F(s) + K_F N_F(s) N_H(s)} \quad (3.13)$$

The root locus plot determines the zeros of $D(s)$ which are the poles of $G(s)$. The zeros of $G(s)$ are given directly by the zeros of $N_F(s)$ and $D_H(s)$. The closed-loop gain is obtained easily from the zero frequency value of the closed-loop response:

$$K = \lim_{s \rightarrow 0} \frac{\dot{\Theta}(s)}{\dot{\Theta}_c(s)} \quad (3.14)$$

Thus the following closed-loop characteristics are obtained:

$$K = \lim_{s \rightarrow 0} \frac{K_F N_F(s) D_H(s)}{D_H(s) D_F(s) + K_F N_F(s) N_H(s)} = \lim_{s \rightarrow 0} \frac{K_F}{s + K_F} \quad (3.15)$$

$$K = 1 \quad (3.16)$$

$$N(s) = \left(1 + \frac{s}{T_c}\right) \left(1 + \frac{s}{T_c}\right) \quad (3.17)$$

$$D(s) = \left(1 + \frac{s}{p_0}\right) \left(\frac{s^2}{\omega_{nA}^2} + \frac{2\zeta_A}{\omega_{nA}} s + 1\right) \left(\frac{s^2}{\omega_{nB}^2} + \frac{2\zeta_B}{\omega_{nB}} s + 1\right) \left(1 + \frac{s}{p_1}\right) \quad (3.18)$$

- $-p_0$ = pole in region D
- ω_{nA} = magnitude of the pole in Area A
- ζ_A = measure of the angle of the pole in Area A
- ω_{nB} = magnitude of pole in Area B
- ζ_B = measure of the angle of the pole in Area B
- $-p_1$ = pole along the real axis emanating from $-1/T_c$

The design approach assumes that the poles emanating from the actuator can be maintained in Area B by appropriately adjusting the loop gain, and that correspondingly the following conditions will be obtained:

$$p_0 \approx 1/T_0 \quad (3.19)$$

$$p_1 \gg \omega_{nc} \quad (3.20)$$

$$\omega_{nB} \gg \omega_{nc} \quad (3.21)$$

so that

$$\frac{\dot{\theta}}{\dot{\theta}_c} \approx \frac{T_c s + 1}{\frac{s^2}{\omega_{nc}^2} + \frac{2\zeta_c}{\omega_{nc}} s + 1} \quad (3.22)$$

The desired response is that given by Equation 3.22, and the question is, how stringently must Equations 3.19 - 3.21 hold in order to achieve this? Truxal (Reference 9, p. 43) gives the criteria that if p_1 is to have negligible effect on the response, then

$$p_1 > 6 \zeta_c \omega_{nc} \quad (3.23)$$

Using the same reasoning, we may say that

$$\omega_{nB} > 6 \omega_{nc} \quad (3.24)$$

The criteria on p_0 poses a much more significant problem. Since this pole is near the origin, it could dominate the response if it were not close enough to the zero at $-1/T_0$, and thereby make the adaptive system ineffective. It is necessary to evaluate the residue at this pole in order to determine its effect. The residue for a unit step response is

$$R_{-p_0} = \left[(s + p_0)^{-1} G(s) \right]_{s = -p_0} \quad (3.25)$$

The factors in $G(s)$ associated with the poles and zeros that are far from the origin will contribute negligibly to R_{-p_D} .

$$R_{-p_D} = \left[\frac{p_D \left(1 + \frac{s}{1/T_\theta}\right) \left(1 + \frac{s}{1/T_c}\right)}{s \left(\frac{s^2}{\omega_{nc}^2} + \frac{2\zeta_c}{\omega_{nc}} s + 1\right)} \right]_{s=-p_D} \quad (3.26)$$

$$R_{-p_D} = \left(\frac{p_D}{1/T_\theta} - 1\right) \left(\frac{1 - T_c p_D}{\frac{p_D^2}{\omega_{nc}^2} - \frac{2\zeta_c}{\omega_{nc}} p_D + 1}\right) \quad (3.27)$$

To obtain some feel for the numerical values, consider a case where $p_D \cdot 1/T_\theta$ and T_c are numerically small so that

$$R_{-p_D} \cong \frac{p_D}{1/T_\theta} - 1 = \frac{p_D - \frac{1}{T_\theta}}{1/T_\theta} \quad (3.28)$$

Since that part of the amplitude of the step response associated with the pole p_D is just R_{-p_D} , then if $p_D < 1/2(1/T_\theta)$, the step response will be dominated by the pole at p_D . If $T_\theta \gg \frac{2\zeta_c}{\omega_{nc}}$, then perhaps p_D should not differ from $1/T_\theta$ by more than 10 or 20%. As T_c decreases, then this percentage difference should be even less. Thus, it is very important that the pole at $-p_D$ should be near the zero at $-1/T_\theta$. Hence Equation 3.19 is a strong requirement.

The response of the closed-loop system is characterized by:

1. Short-period mode defined by the roots found in area C.
2. Actuator mode defined by the roots found in area B.
3. A numerator time constant, T_c -- which actually turns out to be quite small and of negligible effect.
4. A pole and a zero in region D.

5. Unity closed-loop gain. If the feedback gain, K_H , is not unity, then the closed-loop gain would be $1/K_H$.

The function of the adaptive device, the frequency sensor, is to maintain the gain at the optimum value - in area B. The frequency sensor measures the response of the closed-loop actuator mode, compares it with a reference frequency ω_0 , and changes the loop gain so as to null the difference in the two frequencies. This can be expressed symbolically as follows:

$$\frac{dk_g}{dt} = f(\omega_i - \omega_0) \quad (3.29)$$

where ω_i is the frequency of the input signal to the frequency sensor. If the input frequency is too high, the gain decreases; if the input frequency is too low, the gain increases. The value of the frequency is picked so that the damping of the actuator mode will be within the limits

$$.2 < \zeta < .3 \quad (3.30)$$

The actuator mode is not supposed to go unstable, but on the other hand, a definite oscillation is required in order to sense the frequency. The details of the frequency sensor mechanization are discussed in Sections 3.4 and 4.4.

The significance of the four areas in Figure 12 is as follows:

- Area "A": This is the envelope of the aircraft's short-period roots throughout the flight spectrum.
- Area "B": This is the envelope in which the closed-loop actuator mode is maintained by the frequency sensor. Changes in frequency are associated with noise and frequency sensor resolution. Changes in damping are associated

with changes in the actuator locus caused by changes in the aircraft poles or other poles and zeros.

Area "C": This is the envelope for the short-period roots of the controlled airplane. This envelope, then, represents the actual adaptive capabilities of the system. The feedback zeros may be thought of as the model generators rather than the true model. The system is designed so that the desired model roots fall in area C, and if area C can be made small then the system provides invariant response.

Region "D": This is the region or range for the pole-zero combination. This pole-zero combination can have a significant effect on the closed-loop transient response if they do not cancel. How well they cancel depends on the maximum gain achieved. This pole-zero combination is of particular significance if a prefilter is used to shape the response as described in Section 2.4.

The second case presented in Figure 12 employs a first order power actuator and a second order servo to control the power actuator - similar to the X-15 control system. Modes of higher frequency than the actuator need to be included in this case in order to cause the "actuator modes" to go unstable - a representation of rate gyro dynamics would have served equally well.

The two cases illustrated in Figure 12 have substantially different types of root loci and the comparison points out some of the design problems. Clearly, the general form of the root loci must be known, and the locus of the "actuator mode" in the vicinity of the operation point must be carefully established and stabilized (not allowed to move much). The operation of the frequency

sensor depends on having a sufficient gradient of frequency with loop gain in the vicinity of the operating point. That is, $d\omega_i/dK$ must be large, where ω_i is the closed-loop actuator mode and K is the open-loop gain. The root locus approach, as described here, sheds little light on the dynamic characteristics associated with the adaptive loop itself, the loop through the frequency sensor. This subject is considered in Sections 3.4 and Sections 4.4 and 4.5.

3.3 Application of the G.E. System to the X-15 Airplane

3.3.1 Selection of Parameters

The first problem considered, in applying the G.E. System to controlling the longitudinal short-period motions of the X-15 airplane, was the synthesis of a control system of the form shown in the block diagram of Figure 8. The following transfer functions were assumed in the various blocks.

$$\text{Aircraft: } \frac{\dot{\theta}}{\delta_e} = \frac{K_{\dot{\theta}}(\tau_{\dot{\theta}}s+1)}{\left(\frac{s}{\omega_n}\right)^2 + \frac{2\zeta}{\omega_n}s+1} \quad (\text{A-7})$$

Parameters listed in Table III.

$$\text{Actuator: } \frac{\delta_e}{\delta_{ACT}} = \frac{K_{ACT}}{\left(\frac{s}{\omega_n}\right)^2 + \frac{2\zeta}{\omega_n}s+1} \quad (3.31)$$

$$\text{Rate Gyro: } \frac{\dot{\theta}_{RG}}{\dot{\theta}} = 1$$

The feedback gains and time constants were selected to give the following equivalent model in the feedback.

$$\text{Model: } \begin{pmatrix} \dot{\theta} \\ \theta_c \end{pmatrix}_M = \frac{sT_c + 1}{\left(\frac{s}{\omega_n}\right)^2 + \frac{2\zeta}{\omega_n}s + 1} \quad (3.32)$$

$$(\omega_n)_M = .5 \text{ cps} = 3.14 \text{ rad/sec}, \zeta_M = .7$$

Feedback Gains and Time Constants:

$$K_1 = 1$$

$$K_2 = K_1 \left[\left(\frac{2\zeta}{\omega_n}\right)_M - T_c \right] \quad \text{from Equation 3.3} \quad (3.33)$$

$$K_4 = \frac{K_1}{T_c (\omega_n^2)_M} - K_2 \quad \text{from Equation 3.2} \quad (3.34)$$

$$K_3 = \text{Variable Gain}$$

To establish some idea of the possible values of T_c , the parameters for the X-15 at $t = 90$ sec in the re-entry (see Tables I, II, and III) were selected, and a root locus plot was made for the closed-loop system with various values of T_c , shown in Figure 13. The coordinates of Figure 13 are those used by the ESIAC computer, and are described in Appendix B. The results, when interpreted with the adaptive concept in mind, show that the possible values of T_c are restricted. Particularly, note the case for $T_c = .5$ and the locus for the actuator pole. As discussed in Section 3.2, the closed-loop actuator pole must lie in the region

$$.2 < \zeta < .3$$

and in this region, the actuator frequency must increase with gain ($d\omega_i/dK \gg 0$). This is not the case for $T_c = .5$. In fact, there are two possible values of gain

($K_3 = 1.5$ and $K_3 < 1$) for the proper reference frequency $\omega_0 \approx 26$ rad/sec. Furthermore, the aircraft pole is far from the model zero even at $K_3 = 2.5$. Clearly T_c must not be too large - the pole at $-1/T_c$ should lie to the right (in EASAC coordinates) of the actuator poles, or $\frac{1}{T_c} > (\omega_n)_{ACT}$.

Based on the foregoing results, the following values of control system constants were selected for use with the second-order actuator.

$$\begin{aligned} T_c &= .025 \text{ sec} \\ K_1 &= 1 \\ K_2 &= .413 \\ K_4 &= 3.39 \end{aligned}$$

3.3.2 Response to Step Commands

The performance of the control system, from the linear standpoint, is shown by the root locus plots in Figure 14 for the full gamut of the X-15's flight range. The dynamic pressure, q_c , ranges from 20 psf at the apex of the altitude run to a 1000 psf maximum, giving a 200:1 gain change requirement. The range for the roots of the short-period mode of the controlled airplane is found to be $.35 \text{ cps} < \omega_n < .65 \text{ cps}$, and $.4 < \zeta < .5$.

The response realized with the control system configuration of Figure 8 is shown in Figure 11, the " $\dot{\theta}$ -model" case. The various model concepts have been discussed in Section 2.4 and need no elaboration. An attempt was made to set $T_c = \tau_\theta$ in order to produce the response labeled " α -model", but with no success. (T_c must be used to shape the locus of the high frequency modes as discussed previously). Also a lead-lag filter $\left(\frac{1 + \tau_2 s}{1 + \tau_1 s} \right)$ was considered for the feedback, but the necessary separation between τ_1 and τ_2 caused an intolerable gain loss when used in this manner. Accordingly, a prefilter was inserted (as suggested in Section 2.4, Figure 7 and Equation 2.29) ahead of the input summing point.

$$\frac{\dot{\theta}_p(s)}{\theta_c(s)} = \frac{\tau_1 s + 1}{\tau_2 s + 1} \quad (3.35)$$

The time constant T_1 was first selected on the basis of Equation 2.30, and T_2 was made small. The response for the X-15 at $t = 90$ sec was computed on the analog using the following prefilter time constants.

$$T_1 = T_{\dot{\theta}} = 4.4 \text{ sec}$$

$$T_2 = .01 T_{\dot{\theta}} = .04 \text{ sec}$$

Surprisingly, the α response, though improved, still exhibited the long time constant. Analysis of the situation showed that it was the pole-zero combination (in Region D of the root locus plot of Figure 12) in the $\dot{\theta}/\dot{\theta}_c$ transfer function that was the culprit - the two were not cancelling. To show the effect, the complete transfer function for $\dot{\theta}$ must be used and not just the model equation. Continuing with the notation of Figure 7, the $\dot{\theta}$ response can be expressed for the bandwidth of interest using Equations 3.13 and 3.14 as

$$\frac{\dot{\theta}(s)}{\dot{\theta}_p(s)} = \frac{(T_{\dot{\theta}} s + 1)}{\left(\frac{s^2}{\omega_{nc}^2} + \frac{2\zeta_{\dot{\theta}}}{\omega_{nc}} s + 1 \right) \left(1 + \frac{s}{p_0} \right)} \quad (3.36)$$

and repeating Equation 2.32, but neglecting the small time constants T_2 and T_{α} :

$$\frac{\alpha(s)}{\dot{\theta}_c(s)} = \frac{K_{\alpha} (T_1 s + 1)}{K_{\dot{\theta}} (T_{\dot{\theta}} s + 1)} \frac{\dot{\theta}(s)}{\dot{\theta}_p(s)} \quad (3.37)$$

Now when Equations 3.36 and 3.37 are combined, we see that the pole at $-1/T_{\dot{\theta}}$ (in Equation 3.37) is cancelled, leaving the pole at p_0 as the only pole in the vicinity.

$$\frac{\alpha(s)}{\dot{\theta}_c(s)} = \frac{K_{\alpha} (T_1 s + 1)}{h_{\dot{\theta}} \left(1 + \frac{s}{p_0} \right) \left(\frac{s^2}{\omega_{nc}^2} + \frac{2\zeta_{\dot{\theta}}}{\omega_{nc}} s + 1 \right)} \quad (3.38)$$

Clearly, the desired α response can be achieved only if

$$\frac{1}{\tau_1} \approx p_0 \quad (3.39)$$

The situation is illustrated in the root locus plot of Figure 17, part a, where the poles corresponding to the appropriate gain (K_3) for $\zeta_B = .2$ is indicated. For this case, the X-15 at $t = 90$ sec,

$$p_0 = .1$$

$$1/\tau_0 = .23$$

and if τ_1 is set equal to τ_0 , then $p_0 < \frac{1}{2}(1/\tau_1)$ and (based on the approximate relation of Equation 3.28) more than half the magnitude of the α response will be comprised of the sluggish response yielded by p_0 . Thus, in the practical situation illustrated in Figure 17, part a, and also for the α -model case of Figure 11, the prefilter time constant was made $\tau_1 = 10$ sec rather than $\tau_1 = \tau_0 = 4.5$ sec as it would have been had the loop gain been very high. An idea of the error involved by making $\tau_1 = \tau_0$ can be obtained by looking at the response in Figure 15: for $t = 60$ sec. For this condition $\tau_1 = 10$ sec was used and $\tau_0 = 11$ sec. It is seen that there is a substantial "tail" in α . Thus, in order to achieve the desired response for α and $\dot{\theta}$, it is necessary to adapt τ_1 according to Equation 3.39. Since p_0 is a function not only of τ_0 but also of the variable gain K_3 , this becomes an even more difficult task than adapting τ_1 equal to $\tau_0 \approx 1/L\alpha$.

Responses are shown in Figure 15, comparing the open-loop airplane with the controlled airplane, for all the selected re-entry times. The prefilter time constants were selected to give the desired response for the X-15 at $t = 90$ sec.

$$\tau_1 = 10 \text{ sec}$$

$$\tau_2 = 0.1 \text{ sec}$$

The prefilter (τ_1 and τ_2) was not varied for two reasons: one, to evaluate what the effect of a constant rather than an adapted prefilter would be; two, so that the capabilities of the system to maintain invariant $\dot{\theta}$ response could be evaluated. The responses shown in Figure 15 correspond to the root loci of Figure 14. The variations in the $\dot{\theta}$ response are small; a long α response time appears for the higher altitudes, but the prefilter is effective to a certain extent even without adapting the time constant.

3.3.3 Response to Gusts

The gust response of the airplane with the G. E. System is compared in Figure 16 with that of the uncontrolled airplane, and with that for a control system employing just high-gain pitch-rate feedback. The difference between the two types of feedback was discussed in Sections 2.2 and 2.3, and they were shown to differ principally in the response to disturbances. For gust inputs of the type shown in Figure 16, there seems to be little difference in the response for the two types of control systems.

3.3.4 Modification of Basic Airplane Characteristics - Particularly Unstable Configurations

Configurations suitable for hypersonic flight tend to have unstable pitching moment curves (positive $C_{M\alpha}$), particularly at low speeds and at high angles of attack. Accordingly, the X-15 equations were modified by arbitrarily changing M_{α} in the direction of static instability, and both root locus plots and analog responses were obtained for these conditions. To complete the picture, $M_{\dot{\theta}}$ and $M_{\ddot{\theta}}$ were also varied to produce dynamic instability. The results are presented in Figure 17 and show that the control system stabilized the response in all cases. The $\dot{\theta}$ response was kept invariant, qualitatively, but the initial $\dot{\theta}$ overshoot increased for $M_{\alpha} = 0$ or $M_{\alpha} > 0$. The root locus plots show that the pole-zero configuration changes substantially for $M_{\alpha} > 0$ and therefore, the prefilter zero at $-1/\tau = -0.1$ does not cancel the real pole that is approaching $-1/\tau_{\dot{\theta}}$, but now from the high frequency side. This accounts for the increase in the initial $\dot{\theta}$ overshoot and the attendant overshoot in α .

3.3.5 Sensor and Actuator Dynamics

The results discussed in the preceding paragraphs of Section 3.3 were all obtained with the second-order actuator (Equation 3.31) and no sensor dynamics. The effect of incorporating an actuator of the X-15 type and rate gyro dynamics were studied on the ESIAC.

Actuator:
$$\frac{S_e}{S_{SERVO}} = \left(\frac{K_{ACT}}{T_{ACT} s + 1} \right) \left(\frac{K_{SERVO}}{\left(\frac{s}{\omega_n}\right)^2 + \frac{2\zeta}{\omega_n} s + 1} \right) \quad (3.40)$$

power actuator actuator servo

$$K_{ACT} K_{SERVO} = 1$$

$$\omega_{nSERVO} = 200 \text{ rad/sec} = 32 \text{ cps}$$

$$\zeta_{SERVO} = .4$$

$$.5 \text{ sec} > T_{ACT} > .1 \text{ sec}$$

The change in the actuator time constant is produced by nonlinearity in the control system: $T_{ACT} = .5$ for small deflections, $T_{ACT} = .1$ for large deflections. This nonlinearity was simulated in the REAC analog studies and is discussed in Section 4.3.

Rate Gyro:
$$\frac{\dot{\theta}_{RG}}{\theta} = \frac{K_{RS}}{\left(\frac{s}{\omega_n}\right)^2 + \frac{2\zeta}{\omega_n} s + 1} \quad (3.41)$$

$$K_{RG} = 1$$

$$\omega_{nRG} = 100 \text{ rad/sec} = 16 \text{ cps}$$

$$\zeta_{RG} = .5$$

The effect of incorporating the above actuator and sensor characteristics into the system is shown in the root locus plots of Figure 18. One important observation is that it is now the poles at $1/T_{ACT}$ and $1/T_c$ that combine and go unstable, and it is the frequency of this mode that must now be detected by the frequency sensor, and used to adjust the system gain. The two root loci

for $\tau_{ACT} = .5$ and $.1$ sec are compared in Figure 18 and show that a problem is presented. The variation in τ_{ACT} causes the root locus of the detected mode to vary, and no satisfactory reference frequency (ω_0) can be picked. If the reference frequency ω_0 is picked on the basis of the $\tau_{ACT} = 0.5$ sec locus ($\omega_0 \cong 40$ rad/sec), then the frequency sensor will attempt to provide the following gains.

$$\left. \begin{aligned} K_3 &\cong 20 \text{ for } \tau_{ACT} = .5 \\ K_3 &\cong 4 \text{ for } \tau_{ACT} = .1 \end{aligned} \right\} \quad (3.42)$$

The aircraft poles are close to the model zeros for $K_3 = 20$ but not so close for $K_3 = 4$. The given situation is marginal, but if the τ_{ACT} variation were larger (say $.5 < \tau_{ACT} < .05$) then the aircraft response would be hardly adapted at all for the low gain case.

An attempt was made to compensate for the τ_{ACT} changes by inserting lead-lag compensation (of the form $\frac{T_3 s + 1}{T_4 s + 1}$) in the control system, and the results are presented in Figure 19. The lead zero was centered in the range of the actuator pole ($1/\tau_{ACT}$) so as to attract it. The lag pole was placed to the left (ESIAC coordinates) of the feedback pole ($1/T_c$) to attract it. The purpose was to stabilize the locus of the mode detected by the frequency sensor. Figure 19 shows that stabilization was accomplished in a sense - the two loci are much closer together than in Figure 21. Now, however, the shape of the loci of the detected mode is poor since the frequency variation with gain ($d\omega_0/dK$) is small; but this could be cured by introducing an extremely fast rate gyro - say one with $\omega_n \cong 400$ rad/sec.

However, another problem exists (demonstrated in both Figures 18 and 19) which may impose a serious limitation. Consider Figure 18 and the conditions imposed (Equations 3.42) by selecting $\omega_0 = 40$ rad/sec. Assume that the system is operating at small amplitudes (no pilot input, and only noise is exciting the system) so that it would be operating on the locus for $\tau_{ACT} = .5$ sec

and the gain would be stabilized at $K_3 \cong 20$. Now, if a large input occurs (pilot command input) the system will "jump" to the locus for $\tau_{ACT} = .1$, and with the gain at $K_3 \cong 20$ the system will be unstable ($\zeta \cong -0.3$ for the actuator or detected mode). To avoid this instability the frequency sensor will have to decrease K_3 very rapidly - as fast as the large input increases the gain. In a "nut-shell", where nonlinearities in the control system cause changes in the locus of the mode being used to adapt the system (the mode whose frequency is the input to the frequency sensor), then the adaptive loop must be able to respond (change the gain) fast enough to accommodate the changes in allowable gain which result from the locus shift. This applies even if the shift is just one of gain and not of position in the s-plane. For the example case, the adaptive loop must be able to respond at least as fast as the airplane short period and perhaps faster. Conclusions based on the foregoing linear analysis are verified by the analysis of Section 4.3 which properly includes the nonlinearities and the adaptive loop dynamics.

The damping of rate gyros tends to vary with temperature, even for "temperature compensated" rate gyros. A typically modest variation for such a rate gyro was selected, $.2 < \zeta_{ro} < .7$, and its effect is evaluated in Figure 20. The root locus variations are extreme, and the situation presented in Figure 20 is clearly unsuitable for application of the G. E. frequency sensor. The variation of the gyro poles causes far too extreme a variation in the locus of the mode that goes unstable and would not be detected by the frequency sensor. Figure 20 is a good illustration of one of the basic problems involved in applying the G. E. frequency sensing technique to adaptive control. The root locus of the detected mode must be well defined and stabilized (fixed in the s-place). This means knowing many of the control system characteristics quite accurately, especially those with natural frequencies near the frequency to be detected by the frequency sensor. Furthermore, the characteristics of such control system elements must be relatively invariant. If elements in the control system have varying characteristics, these variations must be considered, just as are the variations in airplane characteristics.

3.4 Adaptive Loop Characteristics

Study of the adaptive loop characteristics requires introducing the specific characteristics of the frequency sensor. The frequency sensor has been simulated on both the EASE analog computer and the REAC analog computer. A description of the G.E. frequency sensor is given in the following paragraphs.

A functional diagram of the analog set-up for the frequency sensor is given in Figure 9. The complete EASE analog schematic is given in Figure 48, Appendix C and the REAC analog schematic is given in Figure 49 of Appendix D. These analog circuits are similar to that used by G.E. in their analog analysis of the system. The frequency sensor operation is explained using the functional diagram Figure 9. The input to the frequency sensor, δ_1 , is obtained from a signal available in the closed-loop system that contains the frequency f_i which is to be stabilized at the chosen reference frequency, f_0 . A satisfactory signal can be obtained before or after the variable gain potentiometer, K_3 in Figure 8, or from the output of the canceller. The input signal δ_1 goes through a relatively broad bandpass filter $\left[\frac{s^2}{(1 + \tau s)^4} \right]$ where τ is chosen so that the peak amplitude of the filter is approximately at the reference frequency f_0 . This filter produces a 12 db/octave rise and 12 db/octave decay around this peak frequency. The purpose of the filter is to isolate the frequency of the mode being detected by the frequency sensor, from either lower frequency modes such as the airplane short period, or from higher frequency modes such as structural modes or rate gyro modes. The signal at δ_2 then, is largely composed of frequencies around the reference frequency f_0 . On the block diagram, the first half period of the signal at δ_2 is designated as being equal to T_i , where $T_i = \frac{1}{2f_i}$ and f_i can be larger or smaller than f_0 . The sinusoidal signal δ_2 is converted to a square wave. The zero crossings of this square wave signal become the controlling quantities for the gain changer operation. The square wave is now converted to a pulse signal of approximately .02 seconds duration at the time of each zero crossing. This pulsed signal provides the control inputs for the elements in the lower blocks of Figure 9.

The integrator, at the lower left of Figure 9, has an adjustable input, called T_0 adjust, which controls the rate at which the input IN sweeps along the function programmed into the function generator. This adjustment sets

the frequency f_0 . If f_0 is present in δ_2 , no change is produced in the gain. Any deviation from f_0 in δ_2 will result in an increase or decrease in gain. The integration starts approximately at the end of each gate pulse and continues through the next pulse. The integrator is reset by the pulse (integrator reset signal) derived from the RC network and diode as indicated on the functional diagram. The output of the function generator (OUT) thus depends on the sweep rate provided by the integrator and the time each pulse occurs in the integrator reset signal. The gate allows only the last .02 seconds of the output (OUT) signal to pass (for any one integration cycle). The output (OUT) of the function generator that passes through the gate will be zero if the pulse occurs at the set time ($T_i = T_0$), positive (+) if it occurs sooner ($T_i < T_0$), or negative (-) if it occurs later. The specific input T_i shown in Figure 9 occurs before T_0 indicating that the frequency at δ_2 is too high. Small deviations from the reference frequency produce a linear output. Large deviations, however, are weighted less as governed by the function generator.

When each pulse occurs, the gate is opened and the output (OUT) of the function generator is integrated for the duration of the pulse. The gain control servo positions a potentiometer, a variable voltage divider, which is the variable forward-loop gain of the closed-loop system. The polarity of the output signal from the gate determines whether the gain increases, decreases, or remains constant. The maximum increment of gain change that can occur for each pulse duration is determined by the peaks of the function generator. This increment, which can be adjusted, determines the speed of adaptation. Since the integrator only operates during the time of the pulse, the servo moves in steps. These steps can be filtered by slowing down the response of the servo; however, this filtering also will decrease the speed of adaptation. These aspects of the frequency sensor are discussed further in Section IV.

Dynamic responses for the controlled airplane were obtained on the analog with the frequency sensor in the system. Aircraft (X-15), actuator (second order), and control system characteristics used were those given in Section 3.3, and the flight condition studied corresponded to $t = 90$ sec in the re-entry. The prefilter, for obtaining the desirable α response, was included in the input. The analog responses obtained are presented in this section, along with brief commentary. No extensive analysis was performed on the data.

To interpret the time histories of the system gain, it is necessary to explain how this gain was mechanized on the analog computer. Two stages were used. The first stage was a potentiometer, or attenuator, controlled by the gain changer servo, which varied the input to a fixed gain amplifier.

The variable gain can be described by the following equations (Refer to Figure 8):

$$K_3 = K_x K_F \quad (3.43)$$

$$K_x = K_{x_0} + \Delta K_x \quad (3.44)$$

$$K_x = K_{x_0} + \frac{e_3}{1 + \tau_x S} \quad (3.45)$$

$$K_3 = \left[K_{x_0} + \frac{e_3}{1 + \tau_x S} \right] K_F \quad (3.46)$$

- where
- K_x is potentiometer setting
 - K_{x_0} is trimmed or initial potentiometer setting
 - ΔK_x is change of the potentiometer from K_{x_0}
 - K_F is gain of amplifier
 - e_3 is output of frequency sensor integrator
 - τ_x is time constant. This can be thought of as a filter time constant for e_3 , or as the time constant of the servo which moves the potentiometer.

From these equations, it is seen that a "unit" change in the output of the frequency sensor integrator (e_3) causes a "unit" change in the potentiometer setting, ΔK_x . If K_{x_0} is large, that is, if the potentiometer setting is near 1.0, a "unit" change in e_3 or ΔK_x will cause a small percentage change in K_x or K_3 . However, if K_{x_0} is small, the "unit" change in e_3 or ΔK_x causes a large percentage change in K_x or K_3 .

The analog records of Figures 21 through 23 demonstrate this situation. Also, these analog records contain data on the effect of varying the time constant, T_x . The analog records presented in Figure 21a show how the speed of adaption is affected by T_x when the gain is too high initially, and the desired gain is such that K_{x0} is large. The same effect is shown in Figure 21b when the desired gain is such that K_{x0} is small. Figure 21c shows the case when the desired gain is very low, near zero. Finally, Figure 22 shows both the case of initially too high, and initially too low K_x . In all of these figures, step command inputs are inserted to show the effect of adaptive gain dynamics on the airplane response. Also shown are the effects of pulses forced into the gain changer servo. In general, the responses show good characteristics at high K_{x0} , and poor ones at low K_{x0} . At low K_{x0} , the system is noisy and changes in ϵ_3 cause severe disturbances in the airplane's response. A comparison of Figures 23a and 23b shows most clearly the effect of changes in ΔK_x or ϵ_3 . The following equation for the error signals in the system helps interpret the results (see Figure 8).

$$\delta_{ACT} = K_3 \epsilon_2 = K_F K_1 \frac{\epsilon}{s} (K_{x0} + \Delta K_x) \quad (3.47)$$

A change in K_x , that is, a ΔK_x , has the same effect as the change in ϵ_2 (the integral of the error).

The inputs from ΔK_x could be made more tolerable if the integration were performed after the gain changer rather than before. In this case K_3 would be operating on the error (ϵ) and not the integral of the error ($\epsilon_2 = \frac{1}{s} \epsilon$). The error is usually small, but the integral of the error usually has a large value required to trim the aircraft. Thus the "gain" for a ΔK_x input would be much smaller, in fact, zero except during transient responses, if the integration followed the gain changer. This would require modification of the method of mechanizing the feedback loops of the control system.

Another method for improving the performance of the adaptive loop would be to mechanize the variable gain, K_g , such that a "unit" change in ϵ_3 or ΔK_x would result in a constant percentage change in the existing gain.

SECTION IV
STUDY OF SPECIFIC PROBLEMS IN APPLICATION OF
G. E. SYSTEM

4.1 Introduction

The analysis of the G. E. System discussed in Section III used linear analysis techniques based principally on the root locus method, and simulation of the system on an analog computer. The X-15 was the study vehicle, and the equations and parameters used are described in Appendix A.

The problems examined in the analysis of Section III may be listed as follows:

1. Model concepts
2. Selection of system parameters
3. Responses to step pitch rate commands
4. Response to gusts
5. Modification of the basic airplane characteristics - particularly unstable configurations
6. Sensor and actuator dynamics
7. Dynamics of the adaptive loop.

The analog computer used in the above studies was a small EASE computer, and simulation of the airplane, the actuator, the reference model and the frequency sensor used it to full capacity. Few components were available for simulation of any additional elements or nonlinearities. Since the results of the root locus studies had indicated that actuator non-linearities could be a very important problem area for the G. E. System, it was decided to remechanize the problem on a larger REAC computer so that actuator nonlinearities could be studied. This was done and the following problems were examined using this machine.

1. The response of the system to inputs at the actuator valve
2. The effect of actuator nonlinearities

3. Characteristics of the frequency sensor
4. The effect of "noise" in the rate gyro output

The analog schematics of the problem as it was mechanized on the REAC analog computer are contained in Appendix D.

4.2 Response to Pilot Inputs at the Actuator Valve

The method, illustrated in Figure 52, by which the valve servo displacements and pilot commands from the mechanical system can be mixed and applied to the power actuator valve in the X-15, suggested that it might be of interest to determine the response of the system to pilot inputs through the mechanical system to the power actuator valve.

The block diagram of Figure 24 illustrates the situation in a manner suitable for analysis. The elevator command signal can be moved to the left of the summing point by multiplying by the inverse of the transfer functions of the boxes between the summing point and the power actuator. From this diagram, it can be observed that a step command will now result in a step pitch angle response rather than a step pitch rate response. Also, the response amplitude will now be dependent on the value of K_3 , i. e., a larger K_3 value will result in a smaller pitch response for a given elevator command. In equation form:

$$\frac{\theta}{(\delta_e)_c} = \frac{\dot{\theta}_c}{(\delta_e)_c} \frac{\dot{\theta}}{\dot{\theta}_c} \frac{\theta}{\dot{\theta}} \quad (4.1)$$

where

$$\frac{\dot{\theta}}{\dot{\theta}_c} \approx \left[\frac{T_c S + 1}{\frac{s^2}{\omega_n^2} + \frac{2\zeta}{\omega_n} S + 1} \right] \text{MODEL}$$

$$\frac{\theta}{(\delta_e)_c} \approx \frac{s}{K_1 K_3 (KG)_{vs}} \frac{T_c S + 1}{\frac{s^2}{\omega_n^2} + \frac{2\zeta}{\omega_n} S + 1} \frac{1}{s} \quad (4.2)$$

$$\frac{\theta}{(\delta_e)_c} \approx \frac{T_c S + 1}{K_1 K_3 \left(\frac{S^2}{\omega_n^2} + \frac{2\zeta}{\omega_n} S + 1 \right)} \quad (4.3)$$

ignoring the high frequency zeros due to the valve servo.

Similarly, the angle of attack response can be written:

$$\frac{\alpha}{(\delta_e)_c} = \frac{\dot{\theta}_c}{(\delta_e)_c} \frac{\dot{\theta}}{\dot{\theta}_c} \frac{\alpha}{\theta} \quad (4.4)$$

$$\approx \frac{S}{K_1 K_3 (KG)_{vs}} \frac{T_c S + 1}{\frac{S^2}{\omega_n^2} + \frac{2\zeta}{\omega_n} S + 1} \frac{K_\alpha (\tau_\alpha S + 1)}{K_\theta (\tau_\theta S + 1)} \quad (4.5)$$

The angle of attack response to an elevator command will consist of a fast rise and then a decay to zero at a rate dependent on the value of τ_θ . However, for the flight conditions where the dynamic pressure is very low, the value of τ_θ is very large. This in effect puts the pole ($1/\tau_\theta$) at the origin and cancels the zero due to the (S) in the numerator. Under these conditions, τ_α would be very small and could be ignored along with the zeros due to the valve servo. The response would be

$$\frac{\alpha}{(\delta_e)_c} \approx \frac{K_\alpha}{K_\theta} \frac{T_c S + 1}{K_1 K_3 \left(\frac{S^2}{\omega_n^2} + \frac{2\zeta}{\omega_n} S + 1 \right)} \quad (4.6)$$

Thus one would expect a steady-state angle of attack in response to a step elevator command for the high altitude low q flight conditions.

The analog records of Figure 25 support the above conclusions. Responses of the open-loop airplane to elevator steps are shown in Figure 25a for flight conditions of $t = 0, 40,$ and 90 seconds in the re-entry. The records of Figure 25b are responses of the X-15 with the G.E. system to pitch rate

commands for flight conditions of $t = 40$ and 90 seconds, and finally, in Figure 25c are responses with the G.E. System to elevator commands for flight conditions of $t = 0, 40,$ and 90 seconds. The effect of the value of $\tau_{\dot{\theta}}$ on the response to elevator commands can be seen in Figure 25c by comparing the responses for $t = 90$ with those for $t = 0$ and 40 . The effect of K_3 on the amplitude can be seen by comparing two responses at the same flight condition. Unfortunately, the same recording scales were not used in all of the above records, and this tends to mask the effect of K_3 on the response amplitude in some of the records.

The two responses in Figure 25b to pitch rate commands at $t = 90$ flight condition for two gain values, $K_3 = 2$ and 4 , illustrate the effect on the $\dot{\theta}$ response of not having the gain high enough to drive the integrator pole to the airplane zero at $1/\tau_{\dot{\theta}}$ as was discussed in Section III, the effect being that the response is more like a third-order system than the second-order model. The response to pitch rate commands for the flight condition of $t = 40$ in Figure 25b illustrates the extremely slow angle of attack response obtained when $\tau_{\dot{\theta}}$ is large. The pulse inputs to the forward loop in Figure 25b illustrate the damping of the actuator mode for the two gain levels.

In summary, it was found that the effect of applying pilot commands through the mechanical stick to the elevator actuator valve rather than as pitch rate commands was to change the system from a pitch rate command system to a pitch attitude command system with the amplitude of the response being an inverse function of the K_3 gain.

After the analog study reported here had been completed, References 22 and 23 were obtained. It is interesting to note that, in the X-15 simulator study of the G.E. System reported in these references, the pilot input to the system was a combination of the normal mechanical input to the actuator valve and an electrical pitch rate command. This input can be expressed as follows:

$$\dot{\theta}_c = \delta_s \left[K_{\text{ELECT. TRANSDUCER}} + K_{\text{GEAR RATIO}} \frac{S}{K_1 K_3 (K_G)_{VS}} \right] \quad (4.7)$$

Thus, by moving the stick, the pilot commanded a combination of pitch rate and pitch attitude with the pitch attitude command inversely proportional to the gain.

4.3 Effect of Actuator Nonlinearities

4.3.1 Root Locus Studies

The root locus studies of Section III indicated that a nonlinearity which caused the actuator time constant to change with amplitude would result in changes in the root locus of the actuator mode that could have serious consequences on the operation of the G. E. frequency sensor and gain changer.

Further root locus studies were made using the ESIAC root locus plotter to establish gain levels and frequencies of the actuator mode for various flight conditions and two actuator time constant, $\tau_{ACT} = .5$ and $.1$ seconds. The results of these studies are illustrated in Figure 26a through d. It was noted for a flight condition of $t = 74$ and the slow actuator that the root locus plotter was undecided as to the locus path of the airplane poles and the actuator locus at certain gains. The frequency of the airplane short-period poles was increased and more root locus plots were made. It was found that a locus shift would occur with the result that the aircraft poles would go unstable and the actuator locus would go to the model zeros as shown in Figure 26d. However, there was no significant change in the frequency at which the loop became unstable. The values of K_j gain and actuator mode frequency for $\zeta = 0$ and $.2$ obtained from the ESIAC studies are tabulated in Table IV. Similar data for $\zeta = 0$ were obtained from the analog computer by pulsing the forward loop at various values of K_j until the value of K_j was reached where the transient response had zero damping. The frequency of the oscillation could be read from the time history. This data is tabulated in Table V. The agreement is fairly good for flight conditions of $t = 60, 74,$ and 90 seconds, but for the low dynamic pressure conditions of $t = 0, 20,$ and 40 seconds, the agreement with the ESIAC results is not so good. It is thought that this is due to inaccuracies in the analog solutions. The problem was scaled for the high dynamic pressure flight conditions and at the low q_i conditions, the analog voltages were too low for

accurate solutions. It is of interest to note that during the checkout of the analog set-up, in two instances, changes in the mechanization (to pick up gain or addition of a small capacitor in an amplifier feedback to reduce noise) introduced unwanted poles in the frequency band of interest. The result was that the root loci were shifted and the gain and frequency limits for stability were changed. This is reported as an example of the difficulties that practical considerations can introduce. It emphasizes the point that in applying the G. E. System to a control problem, it is necessary that all poles and zeros in the frequency band that might affect the root loci be known.

The K_y gain (ESIAC data) required to maintain the actuator mode damping at $\zeta = .2$ for each of the two actuator time constants is plotted in Figure 27.

4.3.2 Analog Simulation of Components

As part of the analog check-out, and to obtain accurate information for the ESIAC studies, frequency response measurements were made on the networks used to represent the rate gyro and valve servo together with the G. E. feedback network. The results of these tests are illustrated in Figures 28 and 29. The rate gyro was represented by a second-order system with a natural frequency of 13.2 cps and a damping ratio of $\zeta = .68$. The valve servo was represented by a second-order system with a natural frequency of 35 cps and a damping ratio of $\zeta = .43$. The frequency of this servo is probably higher than the servo actually installed in the X-15, but this is not thought to be very critical to the studies made. The main reason for using these servo dynamics was that the pad had been built up for another program and was available.

4.3.3 Nonlinear Actuator

Information available concerning the X-15 longitudinal control system indicated that its response rate was a function of amplitude and frequency, i. e., $\tau_{ACT} \approx .5$ seconds for low amplitude and $\tau_{ACT} \approx .1$ seconds for large amplitudes. This nonlinearity was considered to be primarily due to the flow characteristics of the actuator control valve. Additional nonlinearities that could be included were actuator rate and displacement limits and slop or backlash in the control linkages. In the studies, all of these nonlinearities except backlash were simulated.

A curve of rate of change of flow with valve displacement which contained the nonlinear characteristics to be simulated was found in Reference 18 and is considered to be representative. This curve is replotted in Figure 30. The scales were normalized and the curve was reshaped at the bottom to give a maximum value of $\partial Q/\partial q = 10$ and minimum value of $\partial Q/\partial q = 2$. These values of $\partial Q/\partial q$ correspond to actuator time constant of $\tau_{act} = .1$ and $.5$, respectively.

The curve of $\partial Q/\partial q$ in Figure 30 was numerically integrated to obtain data which was replotted as flow, Q , vs. valve displacement, q , in Figure 31. A function generator was built to produce this relation as indicated in the block diagram of the nonlinear actuator, Figure 32. By proper adjustment of the limiters on the output of amplifier 1B, limits are imposed on the actuator rate and by adjustment of the limiters on the output of the integrator 5P, limits are imposed on the actuator displacement. A detailed circuit schematic is contained in Appendix D. The position limits used were $\delta_e = 15^\circ$ and -35° , the rate limits were varied from a nominal value of $\dot{\delta}_e = 20^\circ/\text{sec}$. The frequency response and transient responses of Figures 33 and 34 illustrate the nonlinear response of the power actuator with valve displacement amplitude obtained in the analog simulation.

4.3.4 Analog Records of X-15 with G.E. System Including Nonlinear Actuator

The purpose of the analog studies was to explore and to demonstrate the possible effects of nonlinearities on the operation of the G.E. frequency sensor and gain changer. From the linear analysis based on the root locus techniques, it was found that the possibility existed that during conditions when small actuator valve displacements were required, the gain changer would select a gain level consistent with the root locus for the slow actuator. If then a large maneuvering command were inserted or a gust encountered, the system would "jump" to the locus for the fast actuator and the gain would be too high by a factor of about 2.5, and the system would go unstable. Since the gain would be too high by a considerable factor, the damping ratio of the unstable mode would be a large negative value and the instability would be expected to be nearly explosive. However, the actuator rate limits prevent this from happening and the result is a fixed amplitude

limit cycle, the amplitude of which is a function of the system loop gain. Thus, the rate limit has a beneficial effect in that it restricts the amplitude of unstable oscillations. Another phenomenon characteristic of limit cycles which has special significance for the operation of the G. E. frequency sensor is that the frequency of the limit cycle decreases with increasing gain. Thus, the possibility exists that the valve flow nonlinearity could cause the gain to be driven too high resulting in an unstable oscillation which would be converted into a limited amplitude limit cycle at a frequency lower than the free oscillation. If the frequency of this limit cycle falls below the reference frequency of the G. E. frequency sensor, the gain changer would drive the gain to even higher levels and a divergent situation would result. The above described operation has been demonstrated on the analog computer and is illustrated by the sample records reproduced in Figures 35, 36a, and 36b.

In Figure 35, the operation of the system with a linear actuator ($\tau_{ACT} = 0.1$ sec) at flight condition $t = 90$ is illustrated. In these records, the input to the frequency sensor was taken from the output of the "canceller" or washout portion of the G. E. feedback. In the absence of "pilot" inputs to the elevator, the frequency sensor had a tendency to drive the gain up. This could have been the result of low frequency noise or the integrator of the frequency sensor may have had a bias. In any event, the gain would increase until a disturbance excited the actuator mode and then the frequency sensor would reduce the gain and the process would tend to repeat. The amplitude of the oscillations was small ($\delta_0 < \pm .25^\circ$) and the rate limits were not exceeded. If continuous small amplitude elevator disturbances were applied by the "pilot", the system would tend to maintain a more constant gain level. For the record of Figure 35, the reference frequency was set at $\omega_0 = 5$ cps.

In Figure 36a the effects of the nonlinear actuator valve, the actuator rate limits, and the setting of the reference frequency of the frequency sensor are demonstrated. At the beginning of the record, in the absence of gusts or pilot inputs, the gain changer increased the gain as permitted by the slow actuator time constant, $\tau_{ACT} = .5$, which is stable for gains of $K_y = 18$. When the gain had increased to $K_y \approx 17$, however, the system became disturbed and

developed valve displacements large enough to decrease the actuator time constant to near $\tau_{act} = .1$ for which the maximum stable gain is only $K_g = 4.4$. Thus the system became suddenly very unstable and went into a limit cycle, which in this case had a frequency slightly higher than the reference frequency of $\omega_0 \approx 5.1$ cps and the gain was driven down. Close inspection of this record indicates a change in the amplitude of the signal from the frequency sensor gate amplifiers, and a corresponding change in the rate at which the gain decreased. Initially as the free oscillation was developing, it had a considerably higher frequency than the reference frequency, and the gate opened when the output of the function generator had nearly its maximum value. As the limit cycle developed, the frequency of the oscillation decreased and the gate then opened when the output of the function generator was lower or near the zero crossing and the gain changer slowed down. The result was that it took more than ten seconds for the system to recover. The recorder was then stopped and the reference frequency was increased to approximately $\omega_0 = 5.2$ cps. Again, the gain was increased by the frequency sensor until a disturbance set off the instability. However, this time the frequency of the fully developed limit cycle was lower than the reference frequency and the gain changer increased the gain to the maximum permitted by the servo. The actuator rate limits were set to approximately $\dot{\delta}_0 = \pm 20^\circ/\text{sec}$ for these records. The unstable gain changer operation could be made to occur with $\omega_0 = 5$ cps by reducing the rate limit to about $\pm 10^\circ/\text{sec}$, but the most critical parameter is the frequency sensor reference frequency setting.

Figure 35b illustrates the operation of the system for a flight condition of $t = 40$. For this record, the maximum K_g for the slow actuator was determined and the feedback potentiometer of the K_g amplifier was adjusted to permit this gain ($K_g = 175$) when the servo driven attenuator was at the high end. The actuator rate limits were set at approximately $\pm 25^\circ/\text{sec}$ and the reference frequency was set at $\omega_0 = 5.3$ cps. As before, the gain increased until a disturbance caused the oscillation to develop. The first two times, a disturbance occurred when the gain was not too high and the system recovered. However, the third time the disturbance did not occur until the gain had exceeded the critical value that caused the limit cycle frequency to be lower than the reference frequency and the frequency sensor caused the gain to increase to the limit.

In summary, it has been demonstrated that although the G. E. System with its frequency sensor and gain changer is capable of keeping the closed-loop performance nearly constant, independent of airplane characteristics and flight condition, the system can encounter real difficulties if the actuator has nonlinearities or changes its operation in such a manner as to cause the root locus of the mode which becomes unstable to shift. In the case of the system studied here, the critical parameters are the actuator time constant, τ_{ACT} , the canceller time constant, τ_C , and the rate gyro dynamics. A change in any of these parameters with environment or time can cause changes in the root loci such that the frequency sensor and gain changer may not operate properly. Thus, as pointed out in Reference 20, the adaptive control system does not require specific information on the exact configuration or flight condition other than the over-all range of the variables. However, the behavior of the system is often quite strongly dependent on the actuator characteristics. This situation has the advantage that the required system adjustment can probably be determined on the ground prior to the flight.

4.4 Frequency Sensor Characteristics

Some insight into the characteristics of the G. E. frequency sensor has been acquired through the process of mechanization, check-out and operation of the device on the analog computer. A description of the G. E. frequency sensor and the essence of how it works was included in Section III. Figure 9 is a functional block diagram of the frequency sensor. The REAC analog schematic is contained in Appendix D. Certain characteristics of the system are discussed in the following paragraphs.

First, the characteristics of the bandpass filter will be considered. The purpose of this filter is to isolate the frequency component of the input signal that is due to the mode being detected by the frequency sensor from lower frequency components due to pilot inputs or airplane short-period oscillations and higher frequency components that may be due to structural modes or rate gyro noise. In practice, the filter does indeed function in this manner provided there is a component of the input signal that is due to the actuator mode. However, if the gain is low and the actuator mode has relatively high damping or if there

are no inputs to the control system to excite the actuator mode, then there will not be any component in the frequency sensor input signal due to the actuator mode. In this situation, the frequency sensor will be triggered by any noise that causes a zero crossing of δ_2 in Figure 9. Obviously, zero crossings of δ_2 will depend on the relative amplitudes, weighted by the bandpass filter, of the various harmonic components of the input signal δ_1 . Data were taken during the analog computer studies to illustrate this characteristic and the results are discussed in Section 4.5.

The frequency sensor gates are opened by zero crossings of the signal δ_2 and remain open for a fixed length of time, and then close. The length of time that the frequency sensor gate is held open is somewhat arbitrary and so, for most of this study, the gate-open time was taken as .02 seconds because this was the value G. E. used in their flight tests and analog studies. It is interesting to note that in the drawings used to illustrate the function of the system in Reference 20, the gate is drawn as about 5% of the half period of the reference frequency, whereas actually, .02 seconds is nearer to 20% of the half period of the reference frequency. Thus, for $\omega_0 \approx 30$ rad/sec, the gate is open about 20% of the time. The limits on gate-open time are related to the shape of the function generator curve and the precision with which the gates can be made to open and close. The frequency sensor was first mechanized with a gate-open time of about 5% of the reference frequency half period, but it was found that this resulted in unsymmetrical outputs from the two gates due to tolerance on the gate width and any small bias due to diode characteristics. Thus, it appears better to use a wide gate to minimize these effects. The maximum gate width is dependent to some extent on the shape of the function generator curve. This is illustrated in Figure 37. It is obvious from this figure that if the gate is held open too long, then the significance of the shape of the function generator is lost. That is, presumably, the function generator is shaped in a particular manner so as to weight different frequency errors differently and if the gate-open time is made too long, the effect of the function shape will be compromised. Also in the limit, the half period of the input frequency will become less than the gate width and the gates will be open continuously.

The gate-open time also has an effect on the rate at which the gain changer servo runs. This is because the gate outputs are roughly trains of pulses and obviously, if the pulses are made wider, the integral of the pulse train for a given period of time will be larger. The servo rate can, of course, be controlled by other gains in the system so the effect of pulse width on gain servo rate is, for the most part, incidental.

The role of the frequency sensor function generator is to weight the frequency errors such that small errors ± 1 cps from the reference frequency will result in large error signals to the gain changer servo while very large frequency errors will be weighted less by the function generator to prevent random noise inputs from driving the gain servo. For random noise inputs, the result is as described, but if the noise is not random, but is due to a periodic source such as a vibration mode or electrical pick-up, then the frequency sensor output, i. e., the rate of change of the gain servo, becomes not only a function of the shape of the function generator curve, but also a strong function of the frequency of the input. This situation is illustrated in Figures 37 and 38. In Figure 37, the pulse trains are drawn for input frequencies of $\omega_i = 8.6$ cps and $\omega_i = 3.5$ cps. In both cases, the gate opens on the function generator tails and so the pulse heights and widths are the same. However, at $\omega_i = 8.6$ cps the pulses are much closer together than they are at $\omega_i = 3.5$ cps, and so the integral of these pulses will drive the gain changer servo at a higher rate. Figure 38 is a plot of the time required for the gain servo to run full scale in response to various input frequencies. This plot shows the effect of input frequency, the effect of the function generator shape, and the effect of having the input half period equal to or less than the gate width. This data was obtained from analog records similar to those of Figure 39. The analog traces of Figure 39 also illustrate the effect of input frequency on the gain servo rate. Two sets of traces are included in Figure 39, one set where the gate outputs are summed and then integrated and another set where the gate outputs are summed and lagged by a filter with a one-second time constant and then integrated. In both cases, the gate outputs are in steady-state when the integrator is turned on so that the gain servo rate obtained is the steady state rate and does not contain the transient that would be caused by the lag network. This effect will be illustrated

by records in Section 4.5. The records of Figure 39 illustrate the following: the effect of the input frequency on the servo steady-state rate, the effect of the function generator peaks on the servo steady-state rate, the effect of the lag network in smoothing the gate outputs, and the fact that the lag network has no effect on the steady-state rate of the gain servo.

The lag network was placed ahead of the integrator to permit easier control of the servo rate and to keep voltage levels within the limits of the amplifiers. See Figure 49 of Appendix D.

The maximum rate of change of the gain servo for small frequency errors, i. e., on one peak of a function generator, was set up to be approximately 40°/sec, where this rate refers to degrees of potentiometer travel on a 350° potentiometer. Thus, the servo could run from maximum gain to minimum gain in approximately 8 - 9 seconds.

Another observation of interest is that a bias or amplifier drift introduced after the gates will result in a tendency for the gain servo to drive in one direction. If the bias drives the servo toward high gain, the actuator mode will become lightly damped and will become excited, producing an input to the frequency sensor which will cause the gain to be corrected. This effect is illustrated in Figure 35. If the bias or drift is toward low gain, the system characteristics approach those of the open-loop airplane and there may be no component of the input to the frequency sensor that is near ω_0 . In this situation, the gain changer will operate on frequencies outside the center band of the bandpass filter and the center portion of the function generator. The result may well be that the frequency sensor will not recover the gain to the proper value and the system response will not be that of the model at all.

In summary, the G. E. frequency sensor operates on zero crossings of the input signal after its various harmonics have been weighted by the bandpass filter. These zero crossings open the gates and permit signal pulses to be emitted which have their amplitude weighted by the function generator. The gain changer servo is driven by a signal proportional to the integral of the pulse train from

the frequency sensor gates and its rate is therefore a function not only of the pulse amplitudes, but also of their frequency of occurrence. These characteristics are of significance in determining the response of the frequency sensor to periodic noise in its input signal.

4.5 Effect of Noise in the Rate Gyro Output

The characteristics of the G.E. frequency sensor described in the preceding section suggest the possibility that periodic noise in the input signal to the frequency sensor might result in unsatisfactory operation of the gain changer.

To investigate the effects of periodic noise on the operation of the frequency sensor, it was assumed that the rate gyro was mounted such that it could respond to structural vibrations, engine vibration or any other mechanical or electrical oscillation with a frequency in the band from zero to 30 cps. Analog records were taken of the system operation with an oscillatory signal injected into the output of the amplifier used to simulate the rate gyro. The input to the frequency sensor was taken from the washout network or canceller part of the G.E. feedback system. The amplitude of the oscillatory input was adjusted to equal $\pm 0.05^\circ/\text{sec}$ of pitch rate and records were taken at various frequencies from 3.5 to 30 cps. This data was used to obtain the plot of Figure 38. The sample analog record of Figure 40a, for flight condition $t = 90$ and the linear actuator with $\tau_{AGT} = 0.1$ sec, illustrates the operation of the system when the noise frequency was lower than the reference frequency. The gain servo was driven to high gain by the noise. The actuator mode became lightly damped and started to oscillate, causing an input to the frequency sensor with a frequency in the center range of the bandpass filter. The bandpass filter amplified the actuator mode frequency and attenuated the noise input so that the zero crossings of S_g on Figure 9 were due to the actuator mode and the function generator output was such that the gain was reduced. As the gain decreased, the damping of the actuator mode increased and the oscillation due to the actuator mode decayed. The rate gyro noise then again became predominant and the gain was increased to start another cycle. The period of this cycle of events was about 11 seconds.

Figure 40 illustrates the operation of the system when the noise frequency

was higher than the reference frequency. In this record, the noise amplitude was reduced by a factor of 10 to $\pm 0.005^\circ/\text{sec}$ of pitch rate at 8.5 cps. The amplitude of this noise input was too low to appear on the pitch rate trace except on the most sensitive scale, and then is barely perceptible.

If no other frequencies were present in the input to the frequency sensor, the 8.5 cps noise signal would cause the gain to be driven to the minimum permitted by the servo stop. By simulating pilot inputs to the elevator, it was possible to work or "jack" the gain back up to a high value, but each time the pilot inputs were stopped, the gain would immediately be driven to the minimum value by the noise input. An elevator step input then results in a δ response closer to the open-loop airplane than to the model.

Figure 40c illustrates the effect of short bursts of noise on the frequency sensor and gain changer. The problem was started and after about 14 seconds, a step elevator input was inserted. The response transient in the band-passed signal indicated that the actuator mode had a damping ratio of about $\zeta = .3 - .4$ and in the following 23 seconds, the gain gradually increased. At this point, the $\pm 0.005^\circ/\text{sec}$, 8.5 cps noise signal was switched into the rate gyro for about 4 seconds, and the gain was immediately reduced toward the minimum. This procedure was repeated two more times on the remainder of the record.

The recording of the summed and filtered gate outputs on channel 2 of Figure 40c illustrates the exponential rise of the filter time constant when the noise signal is switched into the circuit. This lag is also evident in the response of the gain servo, δ_y , on channel 3.

In order to illustrate the weighting effect of the bandpass filter, the function generator, and the gate frequency on noise inputs, a series of analog records was run with two oscillators feeding the frequency sensor, one at relatively high frequency and one at relatively low frequency. The procedure used was to set the low frequency oscillatory at a certain frequency (.66 cps or 3.5 cps) with an amplitude of 1.1 volts peak to peak and to set the second oscillator at a higher frequency (8.3, 20 and 35 cps) and adjust its amplitude until

the gain servo had essentially no mean displacement. This amounts to superimposing the two oscillatory signals with the proper relative amplitude such that the zero crossing time intervals of δ_g in the frequency sensor are spaced so that the gate output pulses due to closely spaced zero crossings integrate to a value that cancels the integral of the gate output pulses due to zero crossings that are far apart and therefore of the opposite sign.

Three sample records are contained in Figures 41a, b, and c. In Figure 41a, the low frequency oscillator was set at 3.5 cps and 1.1 volts double amplitude, and the high frequency oscillator was set at 8.3 cps and 1.6 volts double amplitude. This combination of frequencies and amplitudes, when weighted and operated on by the various components of the frequency sensor, results in essentially no steady state change in the gain servo position. The recorder paper was run at two speeds to better show the various frequencies in the traces. The trace of the summed and lagged gate outputs is a complex waveform which is, however, fairly repetitive or periodic with a high frequency component of about 2.3 cps and a low frequency component with a period of about 6.3 seconds. Due to the fact that the frequency of one oscillator signal was about as far above the center of the bandpass filter as the other was below it, the attenuation of the two signals was nearly the same and the output from the bandpass filter looks nearly the same as the input to it.

In Figure 41b, however, the high frequency (20 cps) input was attenuated much more than the low frequency (3.5 cps) input and the bandpass filter has exerted a powerful effect in determining the zero crossings of the signal δ_g . Again, the summed and lagged gate outputs appear to be periodic.

In Figure 41c, the high frequency (20 cps) input and the low frequency (.66 cps) input are both far from the center frequency of the bandpass filter and both are greatly attenuated. However, the very small amplitude signal remaining is sufficient to operate the frequency sensor in the absence of other inputs.

Figure 42 is a summary plot of the above described data. In this plot,

the ratio of the amplitude of the high frequency input to the amplitude of the low frequency input is plotted against the frequency of the low frequency input with the frequency of the high frequency input as a parameter.

From such a plot, it can be determined whether the gain will increase or decrease when there are two noise sources present of different frequency and different amplitude. For example, if there were two noise sources present, one at 2.0 cps and one at 8.3 cps, and the amplitude of the high frequency input was equal to the amplitude of the low frequency input, one would expect the gain to be reduced by the frequency sensor.

This study indicates that periodic noise in the input signal to the frequency sensor can result in the gain being driven to one extreme or the other. This emphasizes the importance of knowledge of structural modes, gyro mount location and any other source of periodic noise that may find its way into the frequency sensor input signal. The study also suggests the possibility of using other filters than the simple bandpass filter in the frequency sensor input signal. It is of interest to note that filters in the frequency sensor input signal line do not affect the system root locus plots. Improvement in the performance of the frequency sensor in the presence of noise might also result from a differently shaped function generator. The present configuration results in high frequency inputs being more effective in changing the gain than low frequency inputs, as illustrated in Figure 38. It is suggested that this curve may be reshaped to advantage.

Other possible ways to control the effect of noise on the frequency sensor which have occurred to the writer, but which have not been investigated, would be to insert a very small D.C. signal in \mathcal{S}_2 to hold the gate closed unless the oscillatory part of \mathcal{S}_2 was sufficient to cause zero crossing. Another way would be to insert an oscillator signal into \mathcal{S}_2 of a frequency equal to ω_0 . This would dominate small amplitude noise signals and not result in any gain change. However, such an input would have to be very stable relative to ω_0 and would depend on precise gate-open times for it not to affect the gain servo.

SECTION V
CONCLUSION

The intent of this study was to achieve a more thorough understanding of the characteristics and behavior of self-adaptive flight control systems and the problems that will be encountered in designing such systems for new aircraft, particularly high speed ones. Three self-adaptive concepts, those of General Electric, DODCO, and Aeronutronic, were evaluated for application to re-entry vehicles using the X-15 airplane for the example. The G. E. system was studied in considerable depth and the results are presented in this report. The DODCO system, essentially a concept for a nonlinear gain element employing switching logic, was also studied in depth though its purely conceptual status did not permit the detailed type of examination given the G. E. system. The study of the DODCO system is the subject of Volume II of this report*. The principal conclusion for this system is that although the nonlinear switching technique can produce effectively higher gain and hence smaller system errors than in the equivalent linear system, the improvement is insufficient to warrant the added complexity and difficulties attendant with the gain switching except in very special circumstances. Specifically, serious problems with stability are encountered in high order systems, for example, a flexible airframe with sensor dynamics. The Aeronutronic system was examined only briefly because its development was incomplete and significant examination would have required effort beyond the scope intended for this project. The Aeronutronic system concept involves the determination of the system impulse response, for which a digital cross-correlator has been successfully developed, and the use of the impulse response to adjust the system gains. The general method, though powerful, has a serious fundamental disadvantage - a long adaption time - that is likely to preclude its application to self-adaptive flight control systems.

*An abbreviated version of ASD-TR-61-104, Volume II can be found in: Rynaski, E., and Schuler J., "The DODCO Optimal Control System - A Critical Evaluation", 1967 Joint Automatic Control Conference, Paper 12-3.

The conclusions concerning the subject matter of this report (Volume I) fall into three categories: (1) the use of models in high-gain adaptive flight control systems, (2) the evaluation of the G.E. system as a high-gain self-adaptive system, and (3) the evaluation of the G.E. frequency sensing technique for gain adaption. Though most of the study was concerned with control of the longitudinal short-period motions of the airplane using pitch-rate feedback, the results are generally applicable to control of motion about all three airplane axes and a variety of feedback sensors. Though control system and sensor dynamics were generally considered, aircraft flexibility was not.

High-Gain Adaptive Approach

1. Reference models can be used in closed-loop flight control systems to tailor the response of the aircraft so that it follows the model, provided a high enough system gain can be realized. Either prefilter models or inverse models in the feedback paths can be used to achieve the desired response to command inputs. Since disturbances affect only the closed-loop portion of the system, the response to disturbances can be tailored only by inverse models in the feedback paths. Thus the response to both commands and disturbances can be tailored, within practical limits, by a combination of prefilter and feedback models.
2. Handling qualities data must be used with care in defining models for control system design. In the past this data has been misused. Specifically, CAL's longitudinal data has been inappropriately applied to the design of pitch-rate adaptive systems by using the normal-acceleration model as a pitch-rate model. Unsatisfactory control systems have resulted. The airplane dynamicist generating the handling qualities data should be more careful to point out the significance and the limitations of the data. The control engineer, in turn, must become more familiar with airplane dynamics. It is not enough just to work from the airplane transfer functions.
3. Considerable caution must be exercised in the design of high-gain systems to ensure that higher order dynamics (of order higher than normally associated with the uncontrolled airplane) introduced by the

control system are properly taken into account. For example, unless properly compensated for, an integrator in the forward loop, introduced to eliminate steady-state errors, can dominate the system response or result in an inappropriate response and so produce an inadequate system. The effect of higher order dynamics can be subtle and may not be obvious in some airplane response variables, so all important response variables should be examined to ensure that a proper system has been realized.

4. The high-gain approach to adaptive flight control systems is fundamentally a single-input single-output approach (even though multiple loops are often involved) and allows the use of relatively simple concepts of self-adaption to set the system gains. In principle, the high-gain feedback is used to eliminate the normal airplane characteristics and desensitize the closed-loop system to changes in airplane parameters; then the desired response is achieved by the introduction of a model. This approach, though feasible, requires high feedback gains and makes it difficult to maintain stability and minimize noise. The low-gain approach, traditional in stability augmentation systems, employs only the minimum gain required to achieve the desired response since the feedback is used directly to modify the airplane parameters. This approach has the disadvantage that the closed loop is sensitive to changes in airplane parameters and the gains must be set precisely, so sophisticated concepts of self-adaption are required. However, all the benefits realizable with respect to stability and noise from the use of the low-gain approach demand that work be continued on this type of self-adaptive system until useable techniques are developed. The high-gain adaptive systems should be considered as interim or sub-optimal solutions to the problem of adaptive flight control system design.

G. E. System

1. The G. E. system, which for longitudinal control employs a pitch-rate feedback loop with an inverse second-order model, can produce a relatively invariant pitch-rate response for the longitudinal short-period motions

for wide variations in airplane flight conditions and aerodynamic parameters. However, the response so produced is not the response desired for good handling qualities and the pilot will not find the response invariant. The pilot desires essentially an invariant second-order response in normal acceleration and not in pitch rate. To achieve the proper response with the modeled pitch-rate feedback, a prefilter incorporating a variable gain and a variable lead time constant i. e., $[K_p (1 + \tau_p s)]$ must be inserted between the pilot's control and the input to the closed-loop system. The variable gain (K_p) must provide an approximately constant stick force per normal acceleration (F_s/n_z), so the gain must vary inversely with airspeed (V). The prefilter lead time constant (τ_p) must be equal to the time constant produced by the integrator in the forward loop, and the required programming is complicated since it is not only a function of flight condition but also the level of the adaptive gain. Because of the difficulties in programming the prefilter for a pitch-rate system, it is recommended that the use of normal acceleration (n_z) or angle of attack (α) feedback be considered for the G.E. longitudinal system. Normal acceleration feedback would require no programming. Angle of attack feedback would require only gain programming with dynamic pressure (or indicated airspeed).

2. In the present mechanization, the adaptive gain is located between the forward loop integrator and the elevator actuator. This location causes serious difficulty, in the form of spurious transients, whenever the adaptive gain changes rapidly and there is a significant value of trim elevator. It would be advisable to mechanize the inverse model so that the adaptive gain precedes the integrator so as to avoid the spurious transients that are likely to occur either in maneuvering or in low-speed flight.
3. The effect of applying pilot command inputs to the elevator actuator valve rather than as pitch-rate commands was found to change the basic response of the system from a pitch-rate command system to a

pitch-attitude command system, with the response amplitude being inversely proportional to the adaptive gain. Such a system would probably be more acceptable to the pilot during a re-entry than a pitch-rate command system. Also, the initial transient response of the pitch-attitude command system is similar to the desired short-period response. This change is a step in the right direction, so this variant of the G. E. system should be examined to see if the proper system response can be realized through further modification.

4. The presence of a test signal is fundamental to self-adaptive systems. Unless a response is excited, no information exists on which to base the adaptive process. It has been hypothesized that changes in characteristics, such as changes in transfer function parameters or poles, will in themselves excite the adaptive process. Careful reflection shows this hypothesis to be false. If no explicit test signal, per se, is generated, then either some implicit signal generator such as a limit cycle or noise is required, or the pilot must continually generate inputs of sufficient magnitude to maintain the adaptive process. The lack of a test signal in the G. E. system appears to be an undesirable feature, and consideration should be given to providing some means for maintaining the adaptive process. One possible method is to provide a small bias to continually drive the gain up. Another one is to provide a monitor which would insert a test signal whenever there had been no appropriate excitation of the adaptive loop for some given period of time.
5. Though the G. E. system can handle changes in aircraft aerodynamic parameters with ease, the system is sensitive to changes in the control system characteristics. Basically, the frequency and damping of the mode detected by the frequency sensor should have a unique, well defined, and accurately known relation to the adaptive gain. The gradient of the detected mode frequency with gain must be large for the adaptive process to work properly. These requirements mean that many of the control system characteristics must be known quite accurately,

especially those which have their natural frequencies nearest to the frequency of the detected mode. Also, these control system elements must have relatively invariant characteristics. In the example application to the X-15, the nonlinear character of the actuator caused the adaptive process to misbehave seriously. An instability was encountered which resulted in a large-amplitude elevator limit cycle with the actuator driving the elevator at its maximum rate, first one way and then the other. As another example, reasonable values for the variation of the damping of the rate gyro were assumed, and these variations were found to be intolerable for proper operation of the adaptive loop. The G. E. system essentially uses the frequency of the detected mode to set its damping ratio by means of the adaptive gain. If a damping ratio sensor for the detected mode were used instead, then the system would not be as sensitive to changes and nonlinearities in the control system.

6. The method of mechanizing the variable gain is important. In the system studied, the gain was a linear potentiometer driven by an integrating servo. Thus, a given incremental signal from the adaptive loop caused a fixed incremental change in the adaptive gain, irrespective of the value of that gain. This arrangement caused difficulty because, when the gain was low, a small increment in the adaptive loop signal caused a large percentage change in the gain, resulting in a noisy system. The adaptive gain should be a nonlinear function of the adaptive gain changer input so that approximately equal percentage gain changes are realized irrespective of the gain level. The nonlinear function must be selected with care since its form affects the rate of adaption.
7. The required rate or speed of the adaptive process will not generally be determined by the rapidity of changes in aircraft flight condition. Nonlinearities in the control system, nonlinearities in airplane dynamics and changes in airplane parameters with rapid motion variables such as angle of attack, and accommodation of the transients excited by large abrupt inputs or noise will generally impose the most severe conditions and determine the required speed of the adaptive process.

G. E. Frequency Sensor

1. The frequency sensor operates on zero crossings of the input signal after its various harmonics have been weighted by the band pass filter. Its output, which drives the gain changer, is weighted by the function generator. In the absence of a signal from the detected mode, the frequency sensor will operate on signals from lower and higher frequency modes. If the rate gyro picks up higher frequency modes, such as structural modes, the gain can easily be driven too low. Once this occurs there is no mechanism in the system for restoring the gain. If low frequency modes are present, such as low frequency structural modes or autopilot modes, then the gain can be driven too high. However, in this case, the detected mode becomes unstable and the resulting oscillation will tend to drive the gain back down toward its proper value. In the presence of continued low frequency signals, the gain settles into a nonlinear oscillation or limit cycle, accompanied by periodic bursts of the detected mode.
2. It has been shown that improper operation of the frequency sensor and gain changer is likely if either noise is present in the system or the control system, particularly the control actuator, is nonlinear. The improper operation can manifest itself as a slow limit cycle of the gain, or in severe cases, the gain can migrate to either its upper or lower stop. Migration to the lower stop could probably be prevented by adding a bias to the frequency sensor output which would continually drive the gain up. However, this bias would probably result in a continual limit cycle of the gain. The over-all operation of the adaptive loop, and particular its sensitivity to noise, could be improved by the addition of a test signal to continually excite the detected mode. Malfunction of the frequency sensor due to control system nonlinearity can be prevented by eliminating the nonlinearity or its effect on the detected mode. If the effect of the nonlinearity is not eliminated, then extreme caution must be exercised in the system design to insure that the nonlinearity will not cause the gain changer to malfunction. These conclusions emphasize the importance of knowledge of control system characteristics and nonlinearities, structural modes, gyro mount location, and any sources of periodic noise.

REFERENCES

1. Campbell, G.: Proposal for Research to Determine the Feasibility of the Use of an Adaptive Servo to Improve Airplane Flight Characteristics. Cornell Aeronautical Laboratory Flight Research Department Memorandum, dated March 1955 (Re-issued 17 June 1955).
2. Campbell, G.: Use of an Adaptive Servo to Obtain Optimum Airplane Responses. Cornell Aeronautical Laboratory Report No. 84, February 1957.
3. Lt. P.C. Gregory, Editor: Proceedings of the Self Adaptive Flight Control Systems Symposium. WADC Technical Report 59-49, March 1959.
4. Buscher, R.G.: General Electric Self-Adaptive Flight Control System Description. Armament and Control Advance Engineering, Light Military Electronics Department, General Electric Company, Schenectady, New York, memorandum dated April 12, 1960.
5. Dommasch, D.O. and R.L. Barron: The Theory and Application of Optimum Limited-Information Adaptive Flight Control Techniques. WADC TR 59-468, October 1959.
6. Ball, J.N.: Outline of DODCO, Inc. Adaptive Servo Principle. Cornell Aeronautical Laboratory Flight Research Memorandum dated 13 January 1960.
7. A Study to Determine the Feasibility of a Self-Optimizing Automatic-Flight Control System. Aeronutronic, a Division of Ford Motor Company. WADD TR 60-201, June 1960.

8. X-15 Aerodynamic Derivative Data for NT-33 Program. Air Force Flight Test Center Memorandum, dated 11 April 1960. (CONFIDENTIAL).
9. Truxal, J.G.: Automatic Feedback Control System Synthesis. McGraw-Hill Book Company, Inc., 1955.
10. Newell, F. and G. Campbell: Evaluation of Elevator Force Gradients and Types of Force Feel in a B-26. Cornell Aeronautical Laboratory Report No. TB-757-F-10, WADC TR 54-442, November 1954.
11. Newell, F. and Campbell, G.: Flight Evaluations of Variable Short Period and Phugoid Characteristics. Cornell Aeronautical Laboratory Report No. TB-757-F-11, WADC TR 54-594, December 1954.
12. Harper, R.P.: Flight Evaluations of Various Longitudinal Handling Qualities in a Variable-Stability Jet Fighter. Cornell Aeronautical Laboratory Report No. TB-757-F-12, WADC TR 55-299, July 1955.
13. Chalk, C.R.: Additional Flight Evaluations of Various Longitudinal Handling Qualities in a Variable Stability Jet Fighter - Part I. Cornell Aeronautical Laboratory Report No. TB-1141-F-1, WADC TR 57-719, Part I, March 1958.
14. Chalk, C.R.: Additional Flight Evaluations of Various Longitudinal Handling Qualities in a Variable Stability Jet Fighter - Part II. Cornell Aeronautical Laboratory Report No. TB-1141-F-2, WADC TR 57-719, Part II, July 1958.
15. Bull, G.: Minimum Flyable Longitudinal Handling Qualities of Airplanes. Cornell Aeronautical Laboratory Report No. TB-1313-F-1, December 1959.

16. Breuhaus, W.O.; P.A. Reynolds, and E.A. Kidd: Handling Qualities Requirements for Hyper-Velocity Aircraft. Cornell Aeronautical Laboratory Report No. TC-1332-F-1, September 30, 1959 (Revised January 29, 1960) (CONFIDENTIAL).
17. Westbrook, C.B. and D.T. McRuer: Handling Qualities and Pilot Dynamics. Aero/Space Engineering, May 1959.
18. Necker, D.: Calculated Data for Primary Control Systems of the X-15 Airplane. North American Aviation, Inc. Report No. NA57-506. 4 June 1957.
19. Schuler, J.M.; A.E. Schelhorn; C.R. Chalk; G.A. Wardly: Application and Evaluation of Certain Adaptive Control Techniques in Advanced Flight Vehicles. Second Quarterly Progress Report, Cornell Aeronautical Laboratory Report No. ID-1471-F-1, January 1961.
20. General Electric Co.: Navy Self-Adaptive Control Flight Test Evaluation. Final Report, 31 December 1960. Armament and Control Section, Light Military Electronics Department, General Electric.
21. Chalk, C. and Schuler, J.: Application and Evaluation of Certain Adaptive Control Techniques in Advanced Flight Vehicles. Third Quarterly Progress Report. Cornell Aeronautical Laboratory Report No. ID-1471-F-2, 30 April 1961.
22. General Electric Company: Self-Adaptive Control System Evaluation on X-15 Simulator.
23. Farr, J.E.; Hoffman, D.P.; Cooper, N.R.: Evaluation of the G.E. Self-Adaptive Control System on the X-15 Flight Control Simulator. WADD TR 61-81 North American Aviation
24. Dommasch, D. and Landeman: Background to Astronautical Systems Engineering. Chapter 10. DODCO Technical Report 100 (August 1961) to be published as an ASD Technical Report).

TABLE I
FLIGHT PATH PARAMETERS FOR X-15 RE-ENTRY

t sec	h 1000 ft	M	$\sqrt{q_i}$	α deg	n_z g	V ft/sec
0	226	5.6	4.7	0	0	5690
20	211	5.3	5.1	0	0	5690
40	147	5.5	9.6	15	.4	5940
60	102	5.9	26.0	15	2.6	5930
74	80	5.4	32.3	12.6	5.0	5200
90	77	4.8	29.3	3	1.1	4700

$$q_i = 1/2 \rho V^2$$

The data were obtained from a typical design-altitude re-entry mission flown on the North American Aviation flight simulator (Reference 8)

TABLE II
NUMERICAL DATA FOR X-15 EQUATIONS OF MOTION

t sec	M_q	$M_{\dot{\alpha}}$	$M_{\dot{\alpha}^2}$	M_{δ}	L_{α}	L_{δ}
0	-.0011	-.0004	-0.1569	-.1131	.0016	.0002
20	-.002	-.0007	-0.3173	-0.2317	.0034	.0004
40	-.0078	-.0027	-1.5083	-1.1664	.0114	.0022
60	-.0595	-.0208	-11.11	-8.51	.112	.0172
74	-.1541	-.0539	-26.41	-17.5	.2795	.0417
90	-.1322	-.0463	-17.1	-12.2	.2767	.0372

These data correspond to those of Table I.

TABLE III
LUMPED PARAMETERS FOR $\dot{\theta}/\delta_e$ AND α/δ_e
TRANSFER FUNCTIONS FOR X-15

t sec	ω_R rad/sec	ζ	$K_{\dot{\theta}}$ sec ⁻¹	$\tau_{\dot{\theta}}$ sec
0	0.396	.00391	-.000949	755
20	0.563	.00542	-.0021	360
40	1.229	.0101	-.00894	86.6
60	3.33	.0289	-.0684	11.2
74	5.14	.0475	-.1435	4.6
90	4.13	.0551	-.160	4.45

t sec	K_{α}	τ_{α} sec
0	-.721	.0018
20	-.730	.0017
40	-.773	.0019
60	-.766	.0020
74	-.662	.0024
90	-.712	.0031

These data correspond to those of Table I and result from numerical substitutions in Equations (2.4), (2.5), and (2.8) to (2.10).

TABLE IV
 GAIN (K_3) AND FREQUENCY DATA FROM ESIAC
 FOR ACTUATOR MODE, $\zeta = 0$ AND $\zeta = .2$

t	$\tau = .5 \sim \text{sec}$				$\tau = .1 \sim \text{sec}$			
	$\zeta = 0$		$\zeta = .2$		$\zeta = 0$		$\zeta = .2$	
	K_3	$\omega \sim \frac{\text{rad}}{\text{SEC}}$	K_3	$\omega \sim \frac{\text{rad}}{\text{SEC}}$	K_3	$\omega \sim \frac{\text{rad}}{\text{SEC}}$	K_3	$\omega \sim \frac{\text{rad}}{\text{SEC}}$
0	1700- 1950	37- 38.5	1100	30.5	475	44	220- 230	36.5
20	1100- 1300	37- 40.5	620- 730	29.7- 31.5	265- 295	43.5- 44.5	155- 170	36.5- 37.5
40	273- 332	36- 39.5	170- 193	29.5- 31.5	75- 83	43.5- 46	42- 46	36- 38
60	25.5- 37.5	35.5- 39	16- 18	29- 30.5	7.2- 7.5	43.5	4.0- 4.3	36- 37
74	12- 14	36- 38.5	7.3- 7.6	29- 29.5	3.0- 3.6	42- 44.5	1.7- 1.9	35.5- 36
90	20	36.5- 37	12	29	5.1	43.5	2.75- 3.0	35- 37.5

TABLE V
 GAIN (K_3) AND FREQUENCY DATA FROM ANALOG
 FCR ACTUATOR MODE AT $\zeta = 0$

Flight Condition t sec	Linear Actuator			
	$\tau = 0.1 \text{ sec}$		$\tau = 0.5 \text{ sec}$	
	K_3	$\omega_n \sim \frac{\text{rad}}{\text{sec}}$	K_3	$\omega_n \sim \frac{\text{rad}}{\text{sec}}$
0	357	5.0	1070	4.5
20	160	5.0	450	4.5
40	44	5.7	175	5.0
60	6	5.9	24	5.1
74	3	5.9	13	5.0
90	4.4	6.0	18	5.1

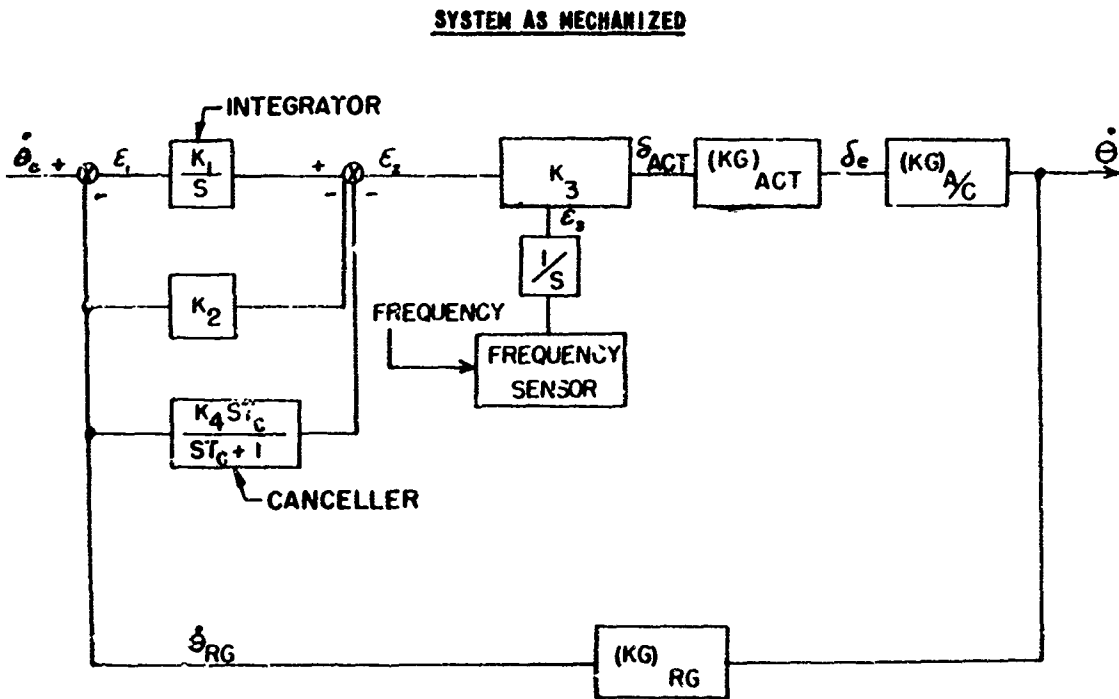
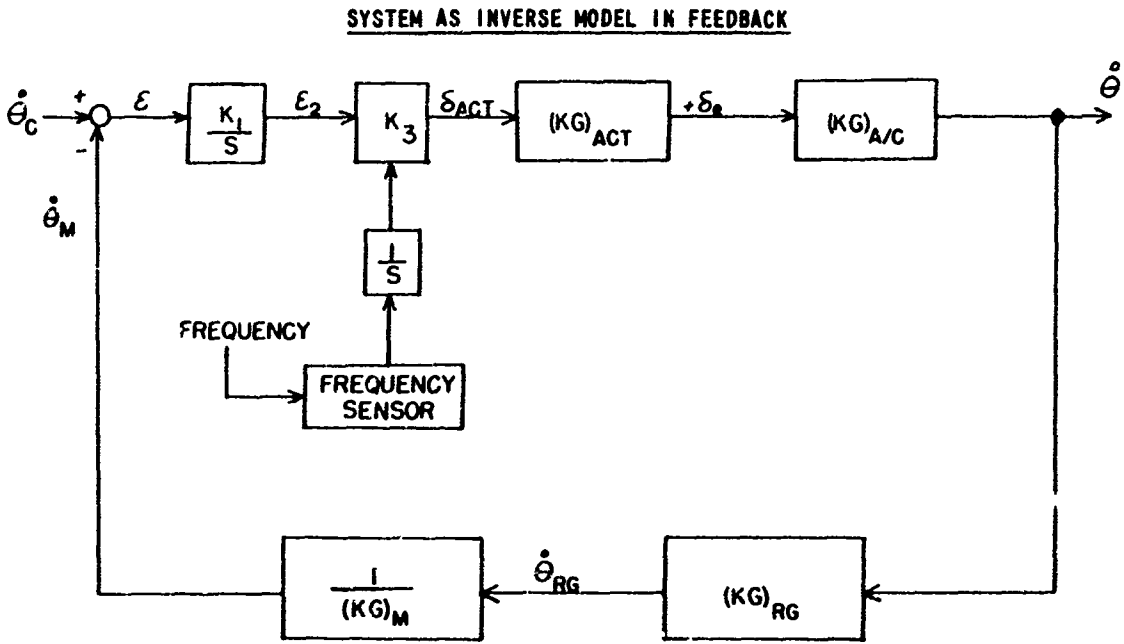


Figure 8 BLOCK DIAGRAMS OF THE G.E. SYSTEM

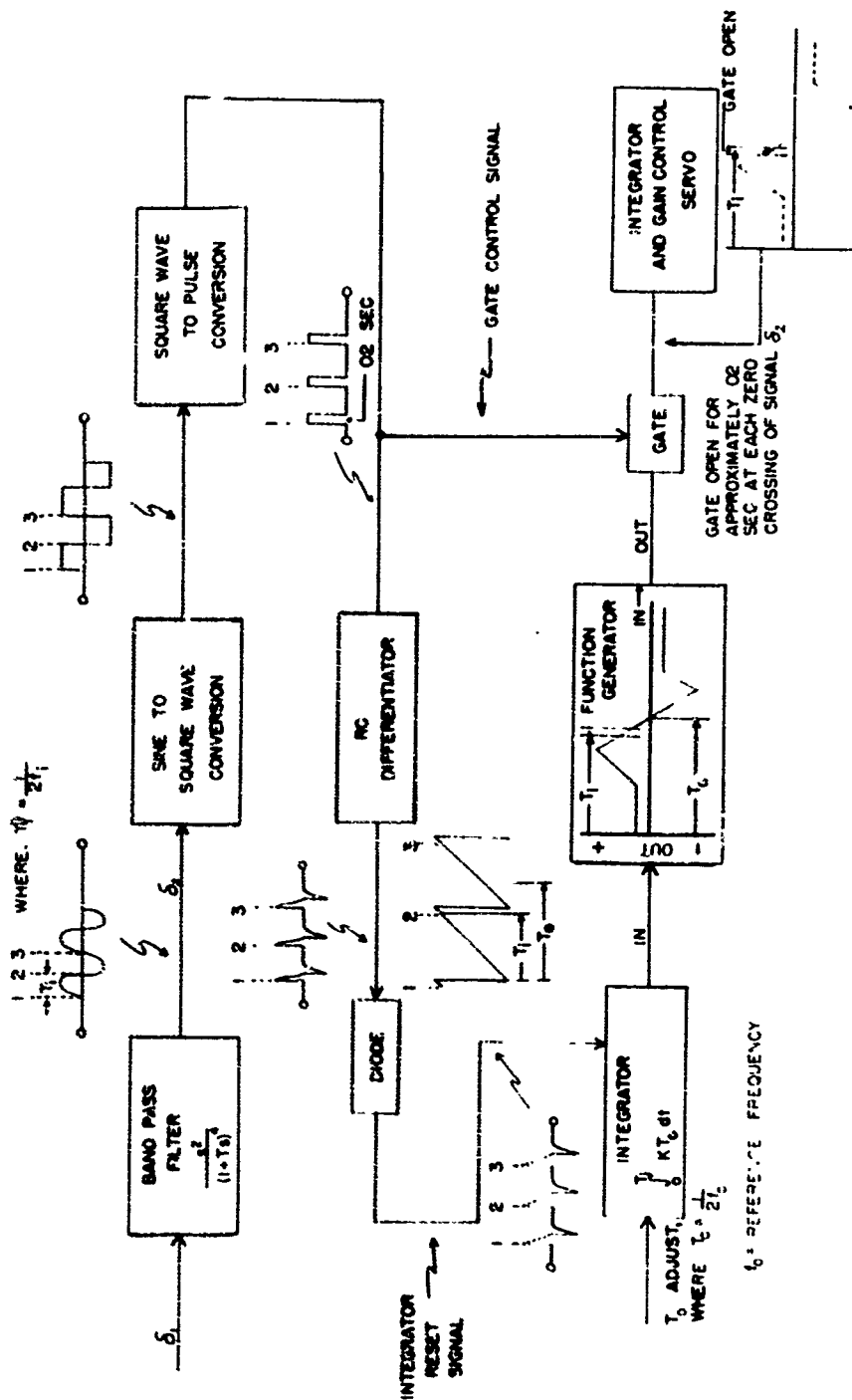


Figure 9 FUNCTIONAL DIAGRAM OF THE G.E. FREQUENCY SENSOR

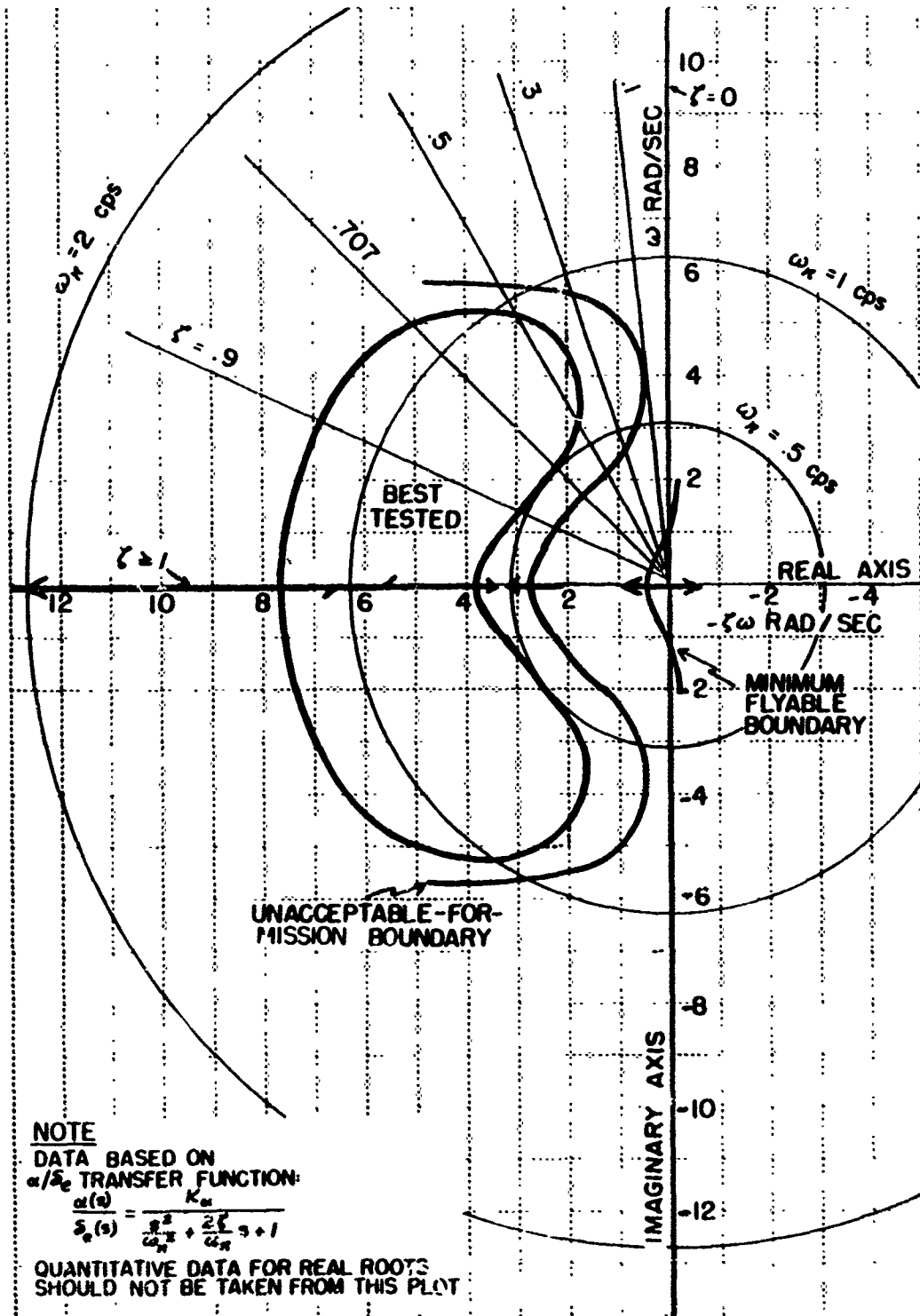


Figure 10 COMPLEX-PLANE PLOT OF SHORT-PERIOD HANDLING QUALITIES DATA FROM REFERENCES 14 AND 15

X-15 AIRPLANE $\tau = 80$ sec STEP COMMAND INPUT

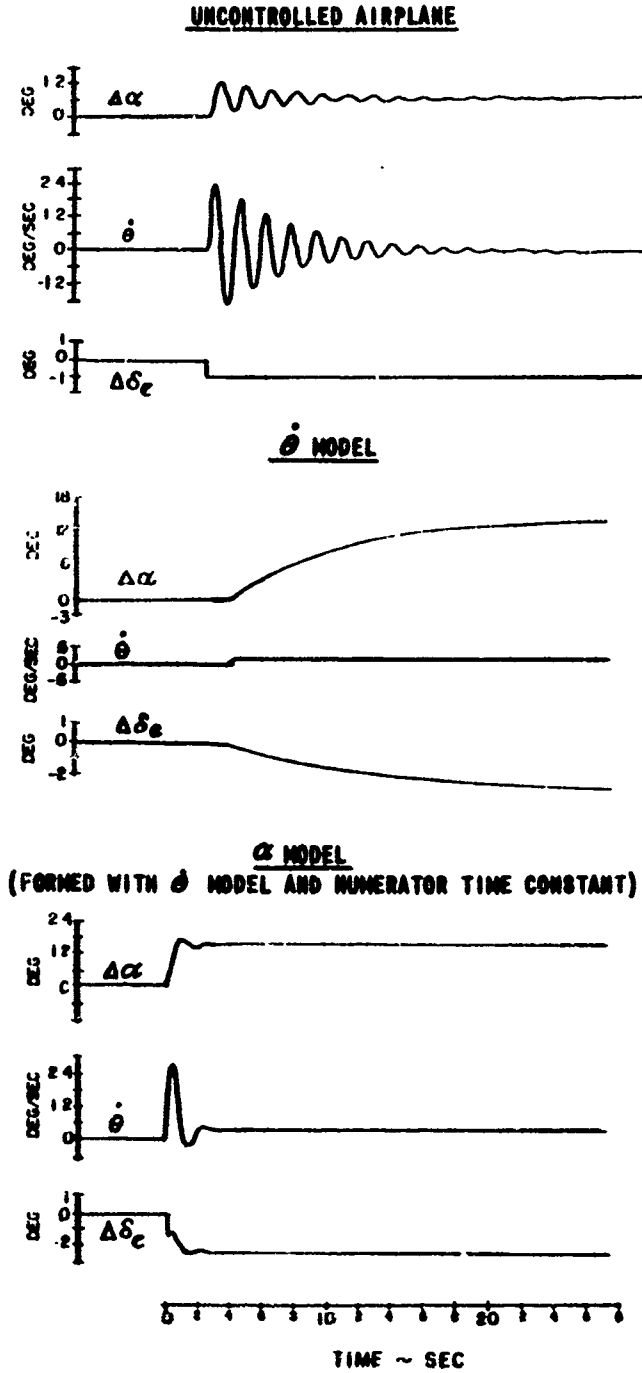


Figure 11 COMPARISON OF $\dot{\theta}$ AND α RESPONSES FOR THE UNCONTROLLED AIRPLANE, AND THE CONTROLLED AIRPLANE WITH TWO DIFFERENT $\dot{\theta}$ MODELS

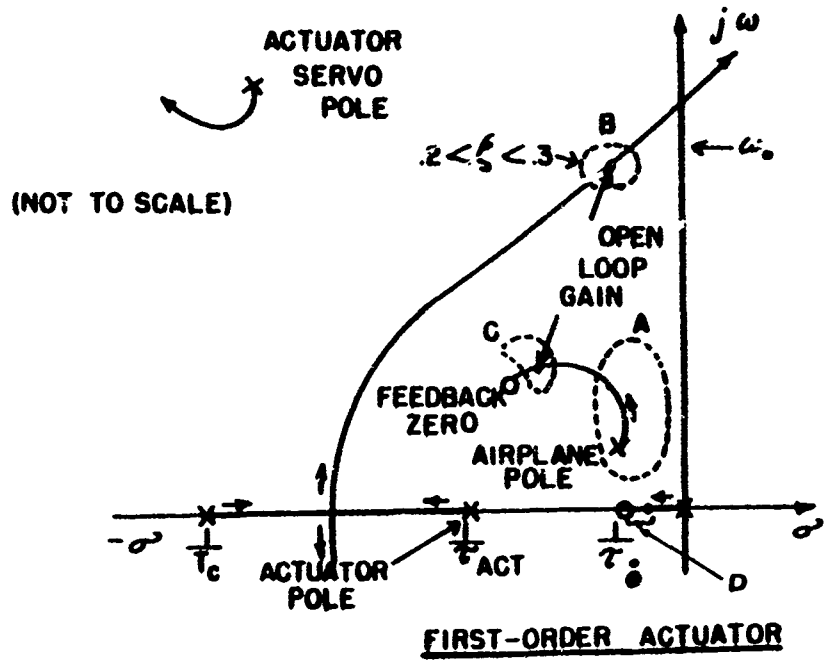
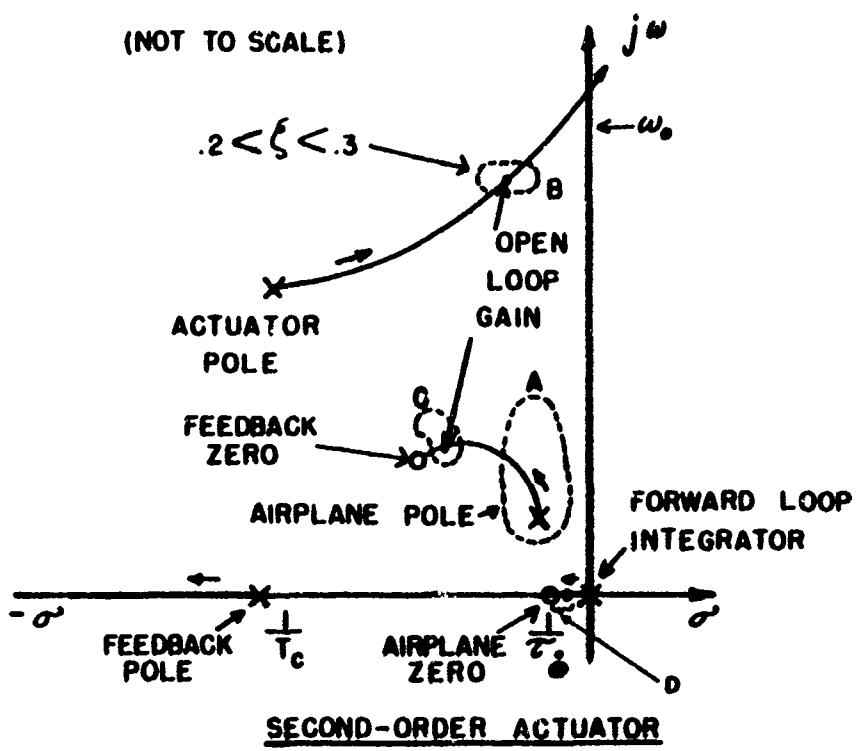


Figure 12 ROOT LOCUS PLOTS SHOWING GENERAL OPERATION OF G.E. SYSTEM

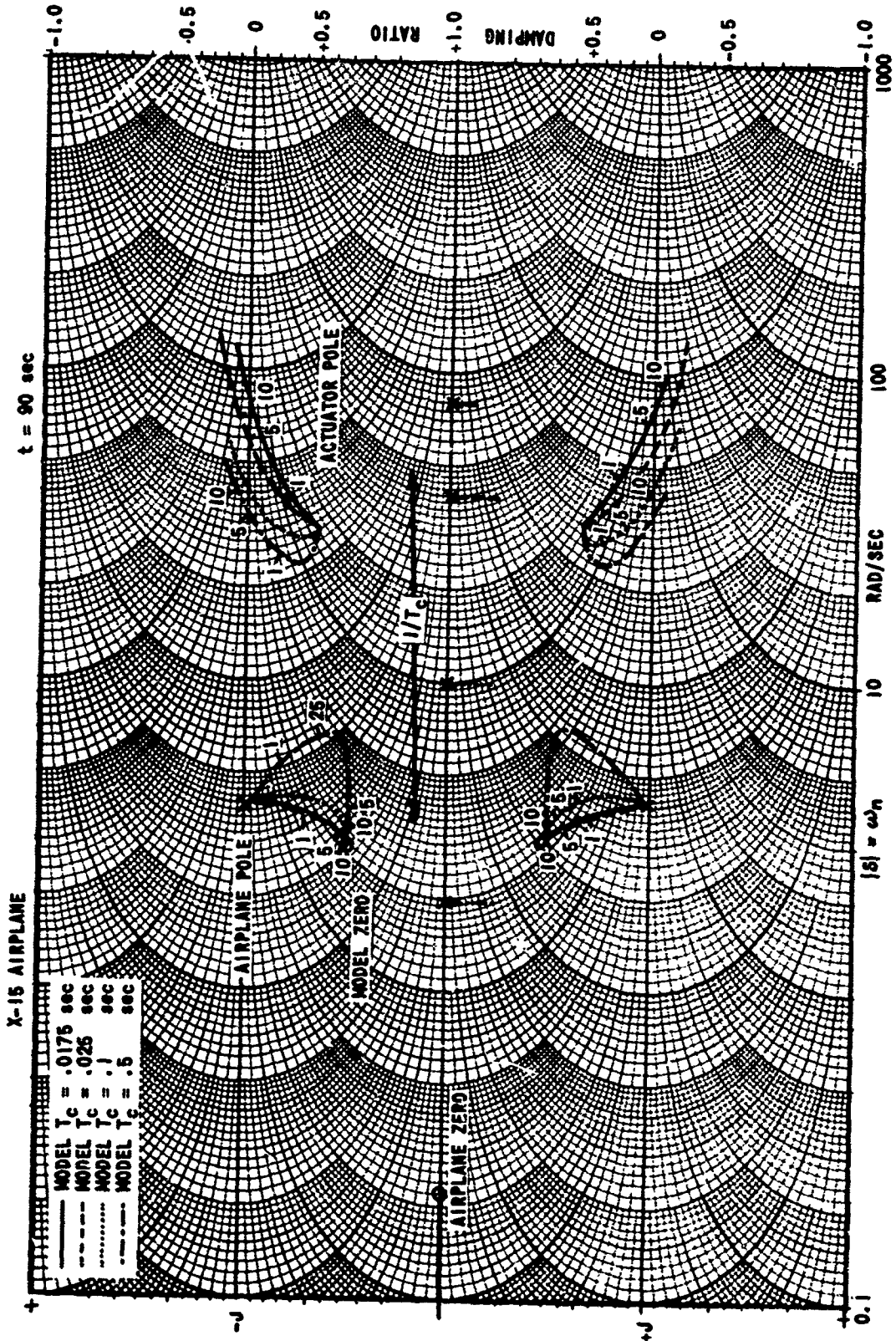


Figure 13 SELECTION OF TIME CONSTANT (T_c) OF INVERSE-MODEL FEEDBACK

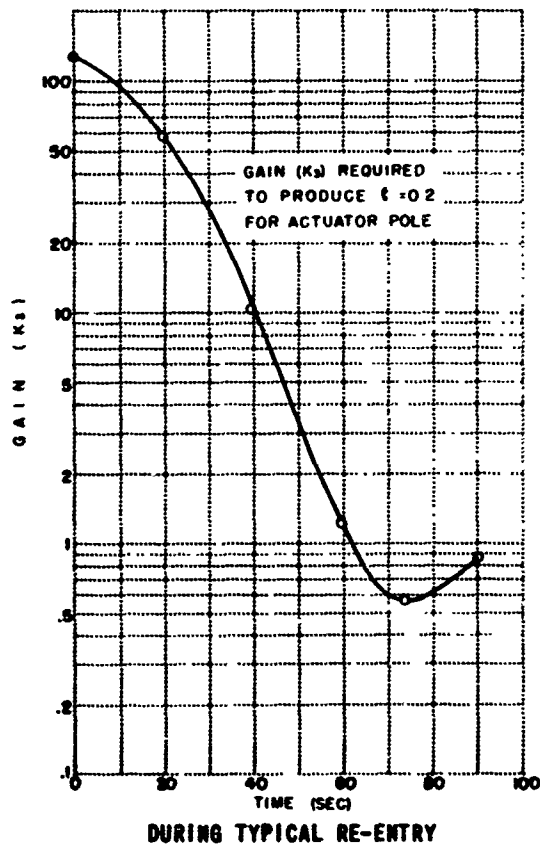
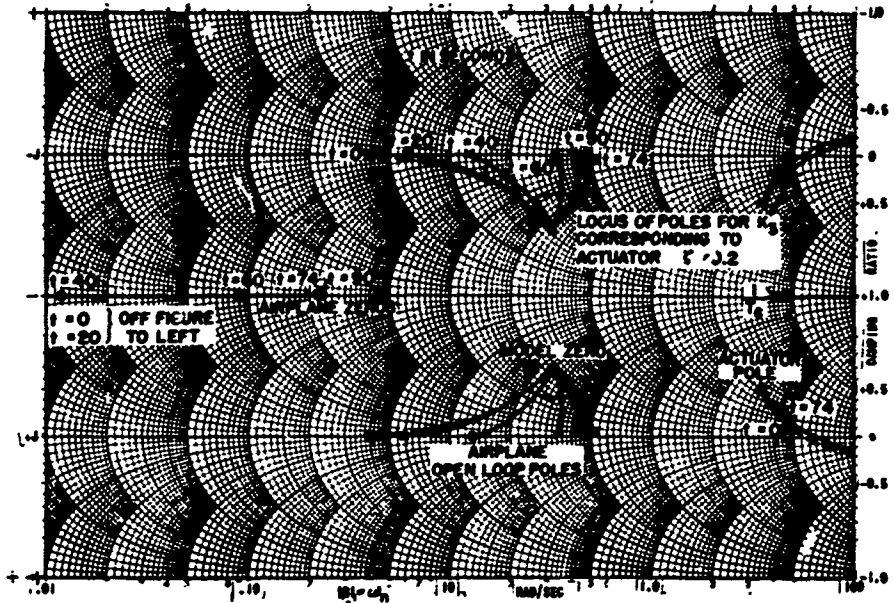


Figure 14 COMPOSITE ROOT LOCI FOR G.E. SYSTEM AND X-15 AIRPLANE AT VARIOUS TIMES DURING RE-ENTRY

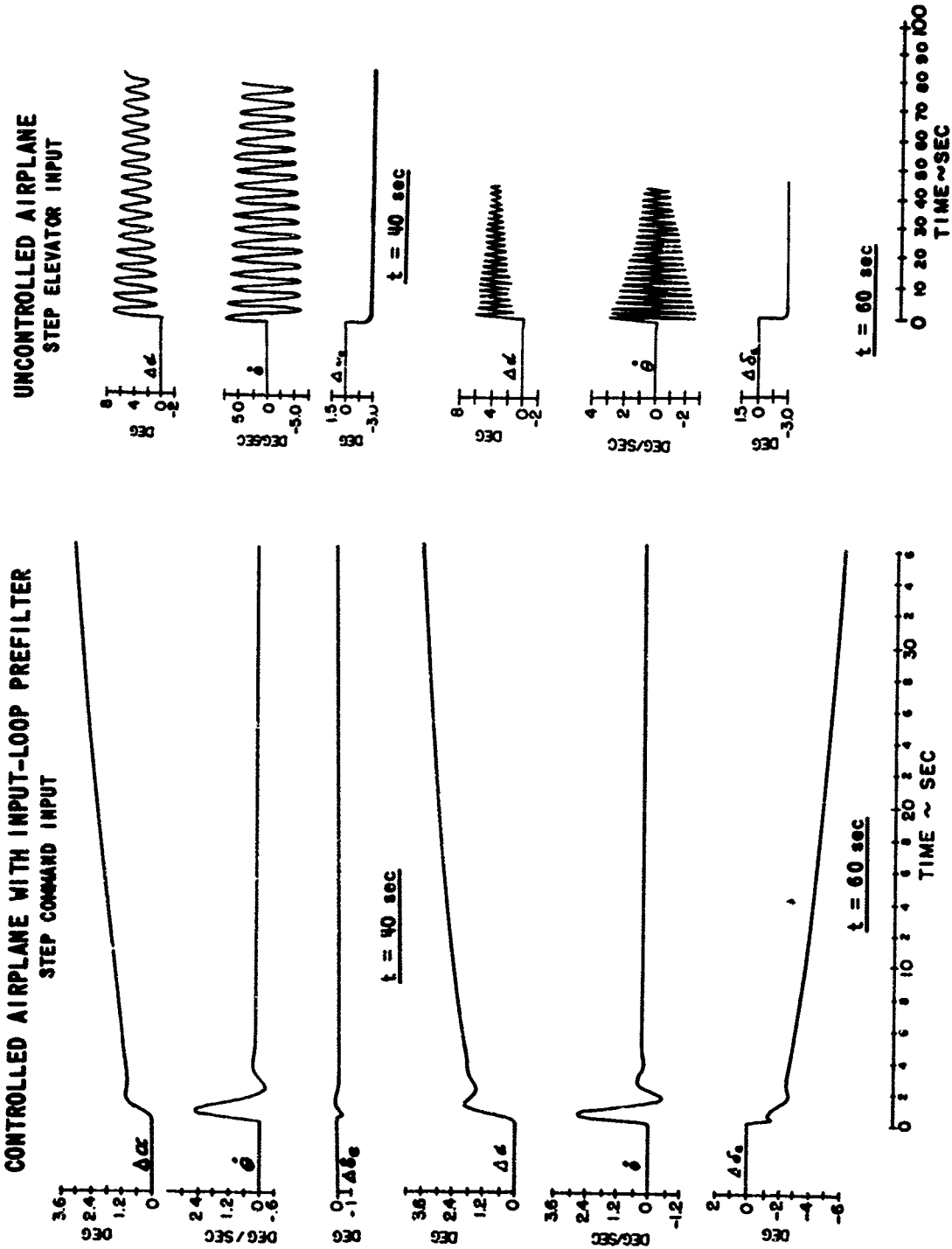


Figure 15 ANALOG RESPONSES OF G.E. SYSTEM AND X-15 AIRPLANE AT VARIOUS TIMES DURING RE-ENTRY (PART b)

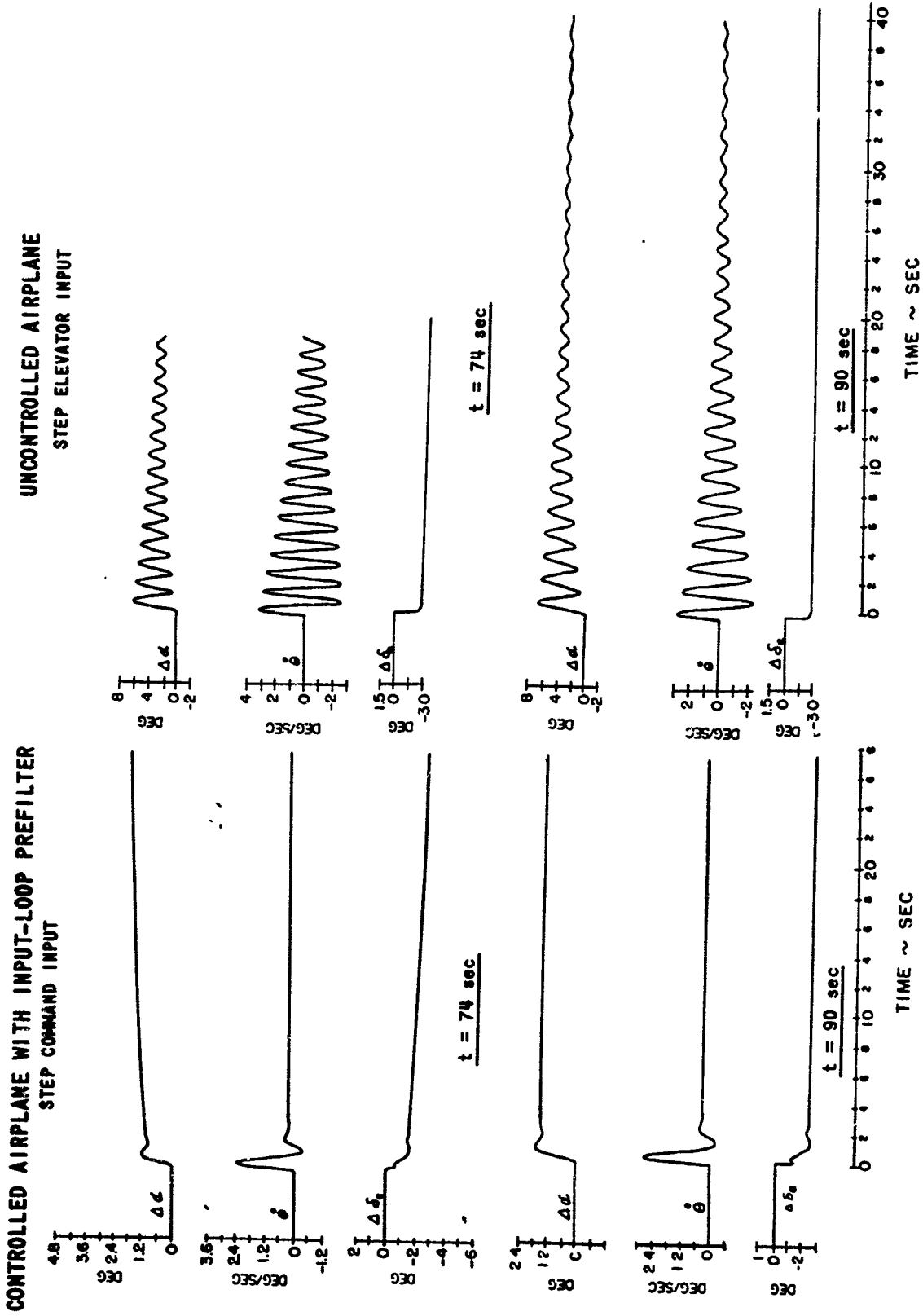
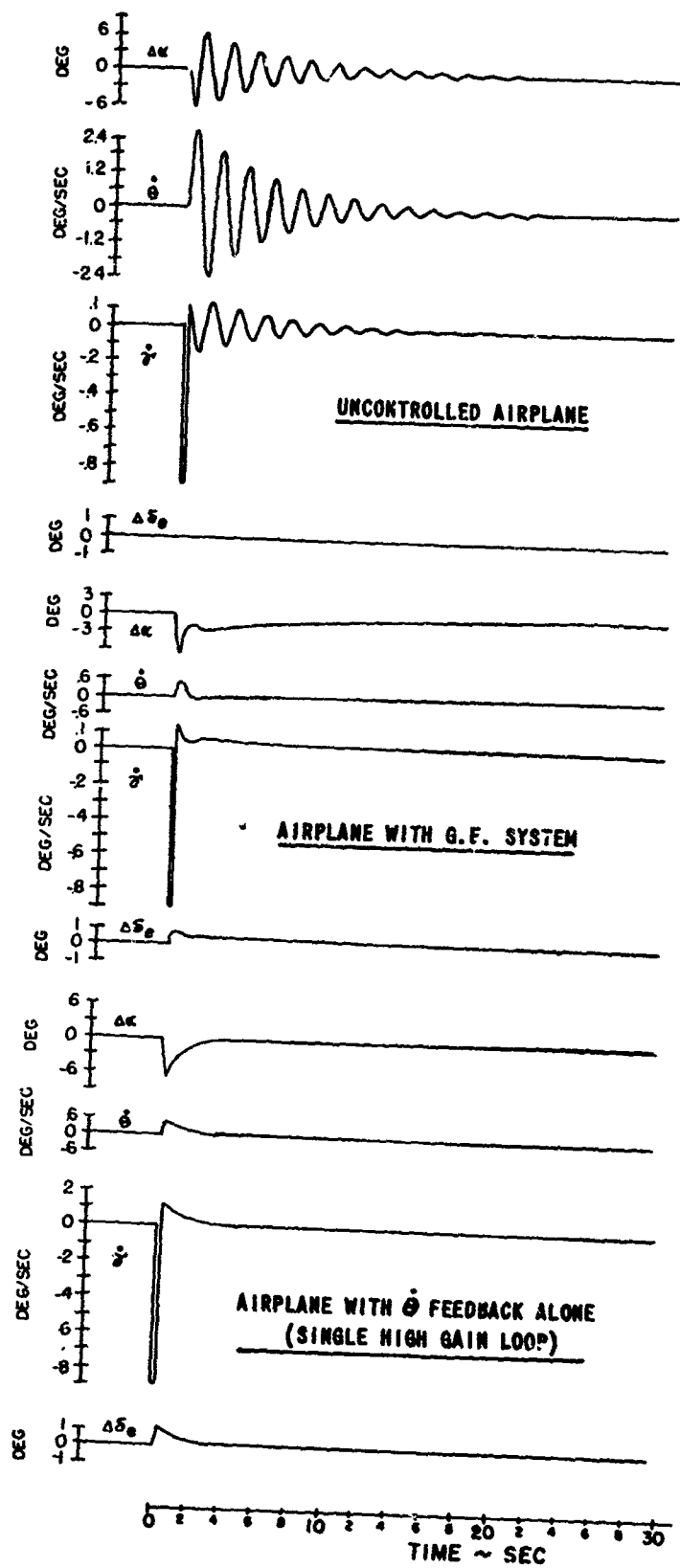


Figure 15 ANALOG RESPONSES OF G.E. SYSTEM AND X-15 AIRPLANE AT VARIOUS TIMES DURING RE-ENTRY (PART c)



X-15 Airplane
t = 90 sec

Gust Input - Sharp Edged
Pulse in α of Short Time
Duration

(NOTE: length of gust
was variable and differ-
ences in peak value of
 $\Delta\alpha$ are not significant.)

Figure 16 COMPARISON OF GUST RESPONSES AS COMPUTED ON THE ANALOG

X-15, t = 90 sec

$$M_{\alpha} = -17.1$$

$$M_{\dot{\theta}} = -.132$$

$$M_{\dot{\alpha}} = -.046$$

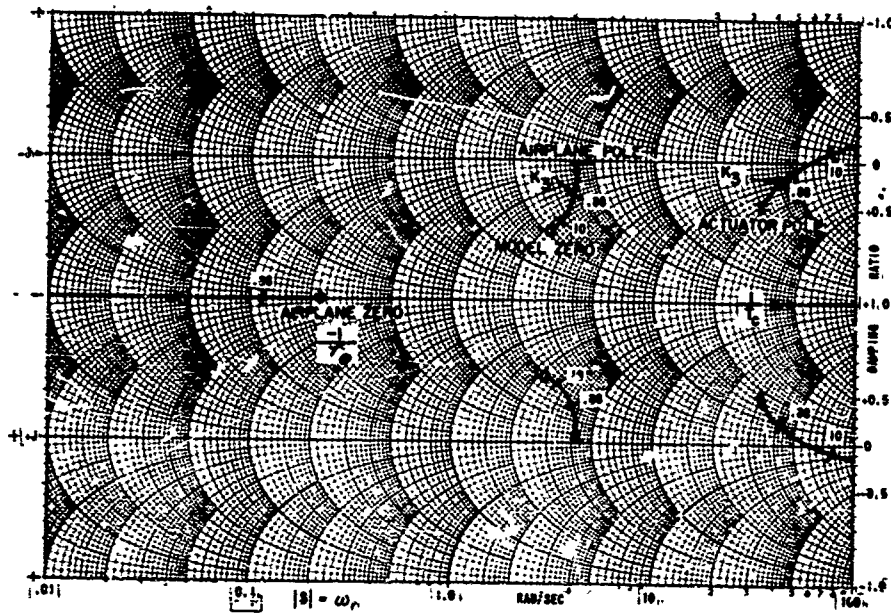
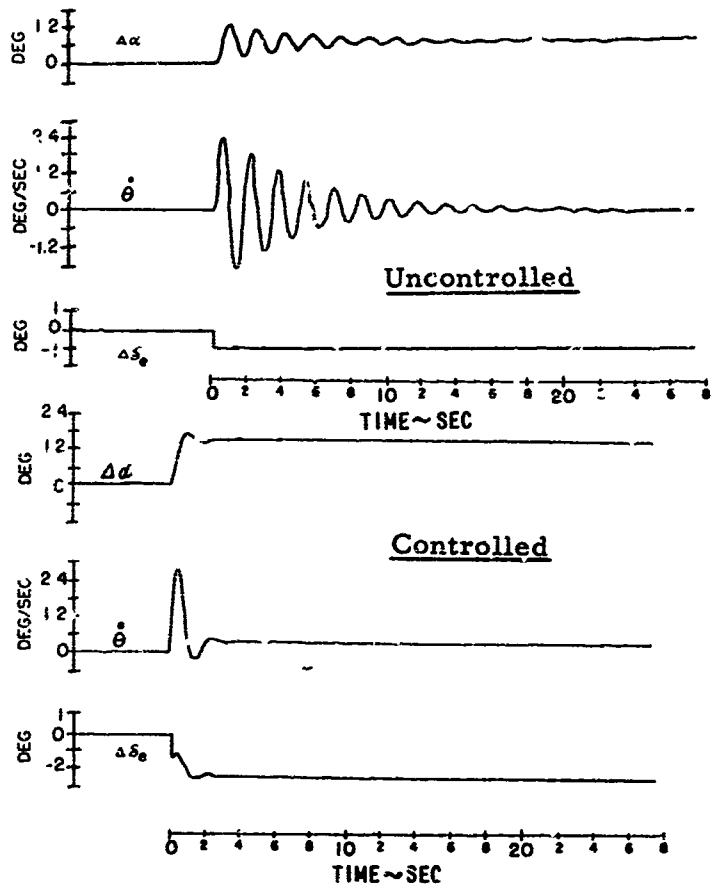
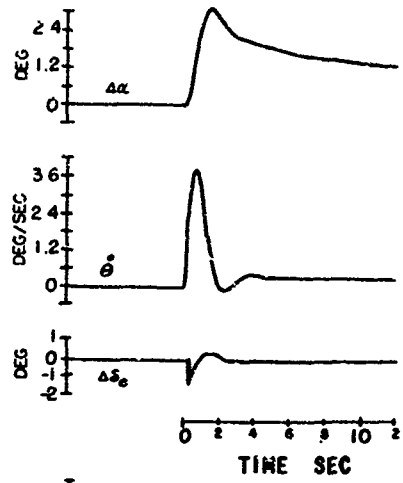


Figure 17 EFFECT OF DESTABILIZING AIRPLANE STATICALLY (M_{α}) AND DYNAMICALLY ($M_{\dot{\theta}}$ AND $M_{\dot{\alpha}}$) PART a NORMAL AIRPLANE

$M_{\alpha} = 0$
 $M_{\dot{\alpha}}$ and $M_{\ddot{\alpha}}$ of Normal Airplane

Controlled



Uncontrolled

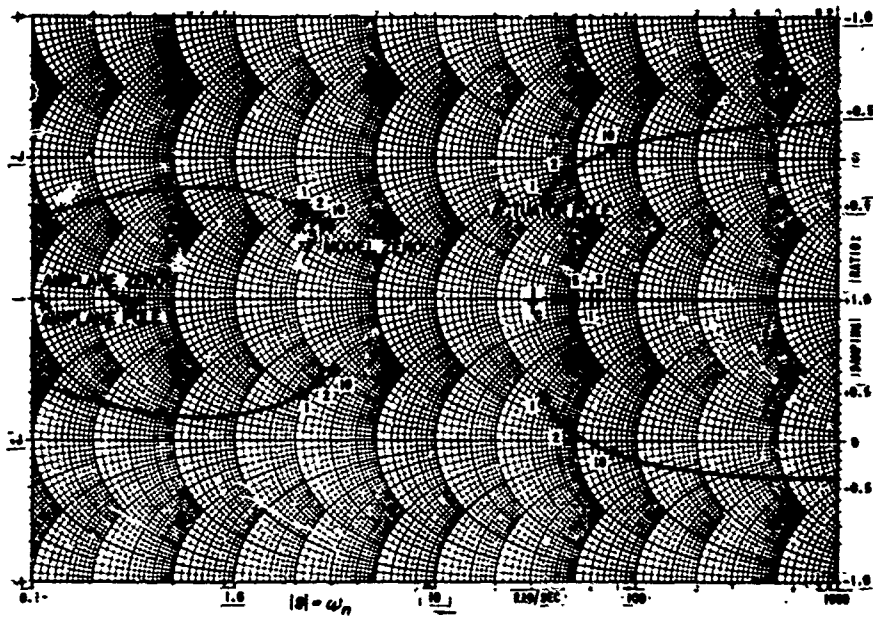
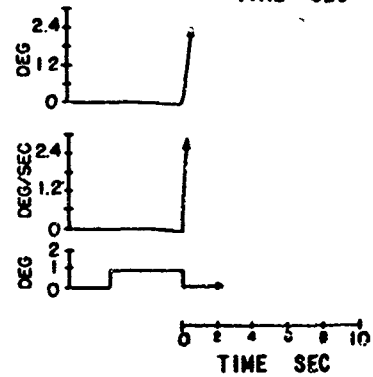


Figure 17 EFFECT OF DESTABILIZING AIRPLANE STATICALLY (M_{α}) AND DYNAMICALLY ($M_{\dot{\alpha}}$ AND $M_{\ddot{\alpha}}$) PART b NEUTRAL STATIC STABILITY

$$M_{\alpha} = +3.64$$

Uncontrolled { More rapid divergence
than for $M_{\alpha} = 0$ case }

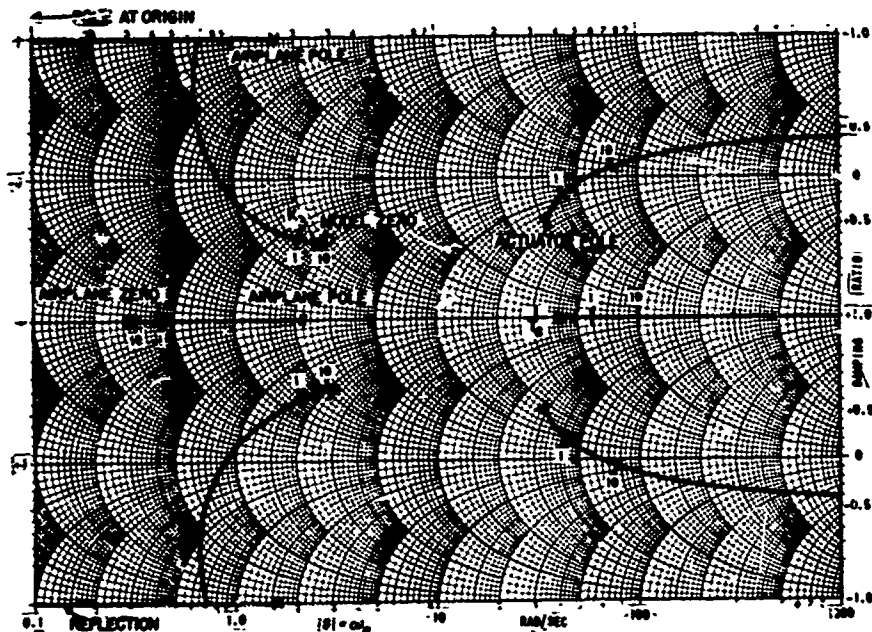
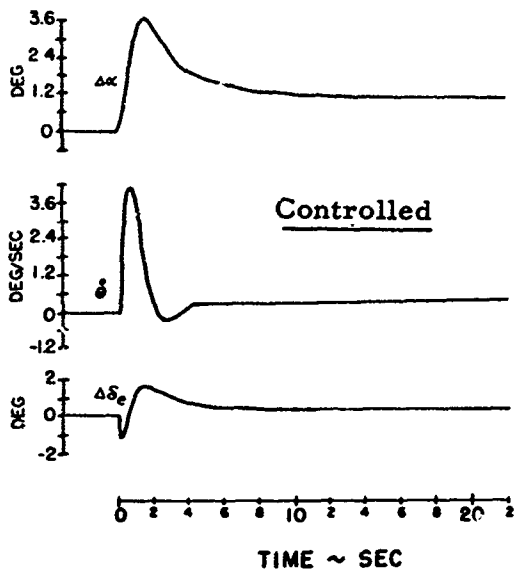


Figure 17 EFFECT OF DESTABILIZING AIRPLANE STATICALLY (M_{α}) AND DYNAMICALLY ($M_{\dot{\alpha}}$ AND $M_{\ddot{\alpha}}$)
PART c STATIC INSTABILITY

$$M_{\alpha} = +7.28$$

Uncontrolled { More rapid divergence }
 { than for $M_{\alpha} = 0$ case }

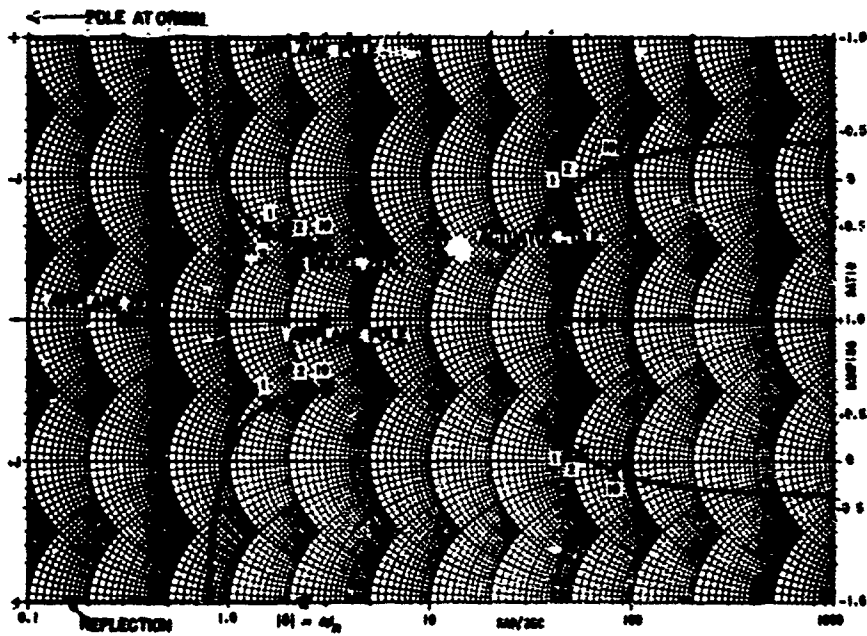
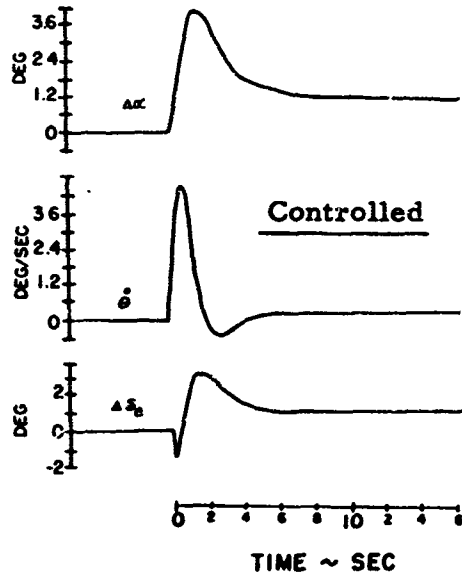


Figure 17 EFFECT OF DESTABILIZING AIRPLANE STATICALLY (M_{α})
 AND DYNAMICALLY (M_{β} AND $M_{\dot{\alpha}}$)
 Part d STRONG STATIC INSTABILITY

$$L_{\alpha} - M_{\dot{\alpha}} - M_{\ddot{\alpha}} \cong 0$$

$$M_{\dot{\alpha}} = +.198$$

$$M_{\ddot{\alpha}} = +.092$$

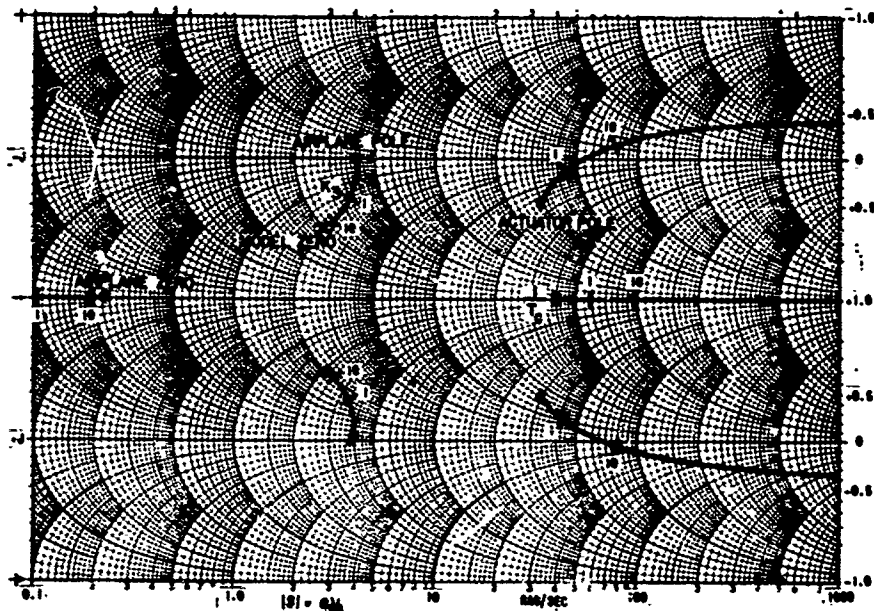
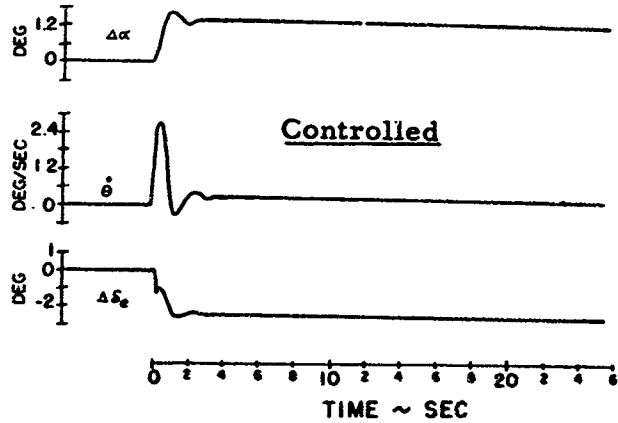
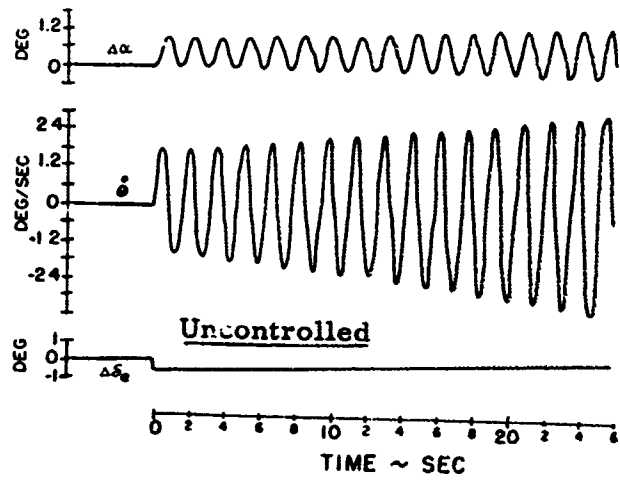


Figure 17 EFFECT OF DESTABILIZING AIRPLANE STATICALLY (M_{α}) AND DYNAMICALLY ($M_{\dot{\alpha}}$ AND $M_{\ddot{\alpha}}$) PART e NEUTRAL DYNAMIC STABILITY

$M_Q = +.529$
 $M_{\dot{\alpha}} = +.194$

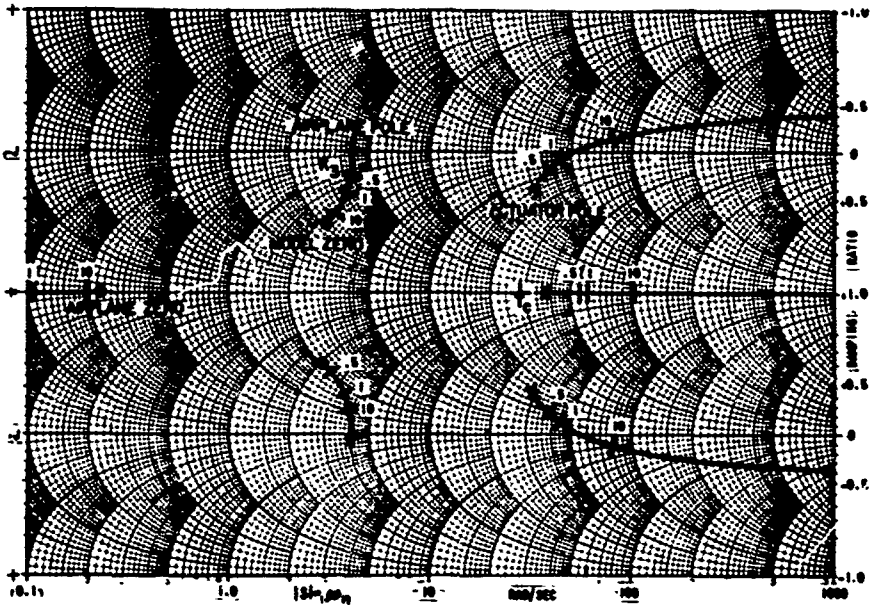
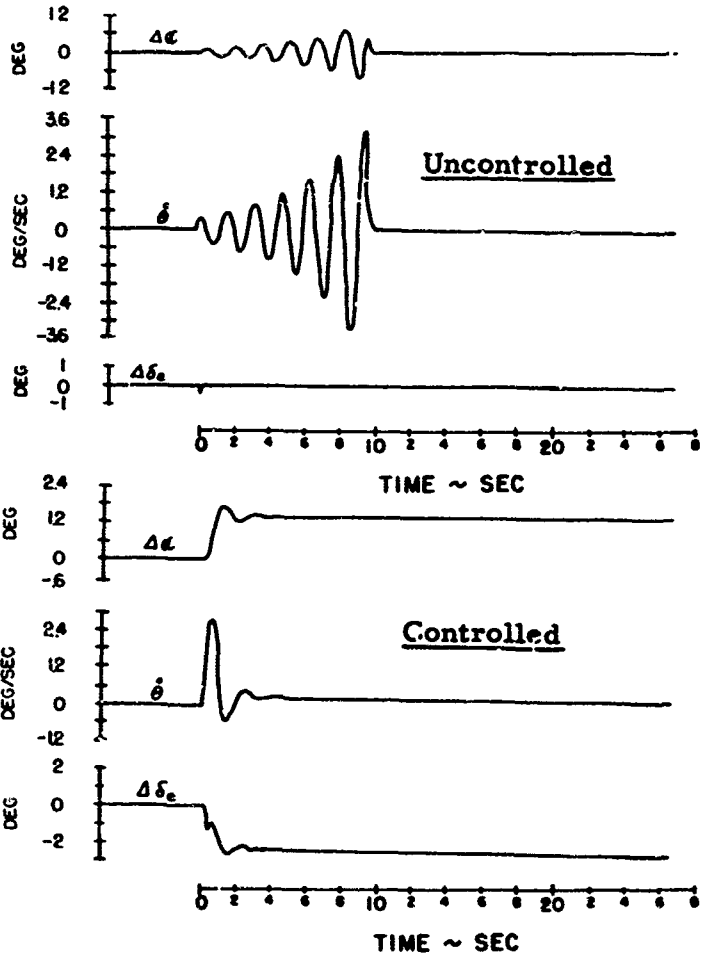


Figure 17 EFFECT OF DESTABILIZING AIRPLANE STATICALLY ($M_{\dot{\alpha}}$) AND DYNAMICALLY (M_Q AND $M_{\dot{\alpha}}$)
 PART I DYNAMIC INSTABILITY

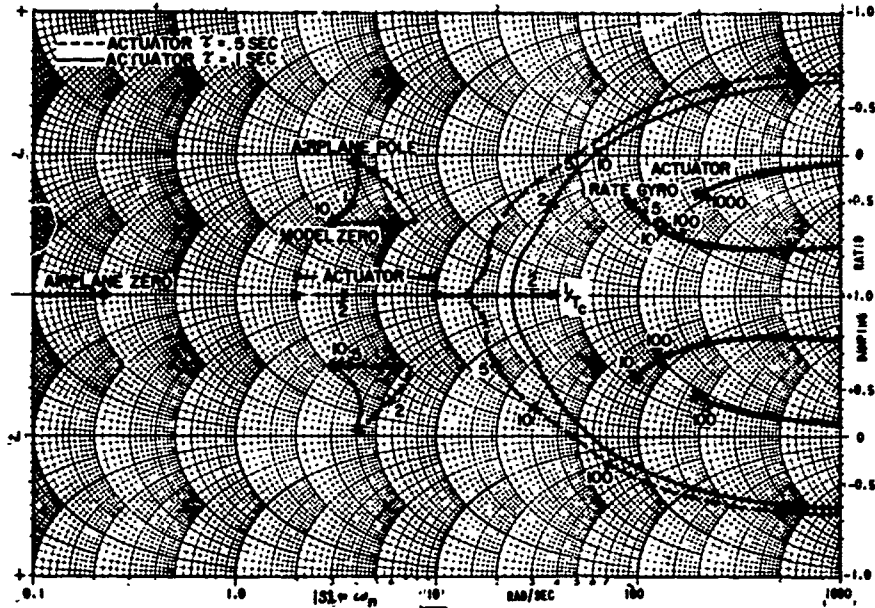


Figure 18 EFFECT OF VARIATIONS IN ACTUATOR TIME CONSTANT

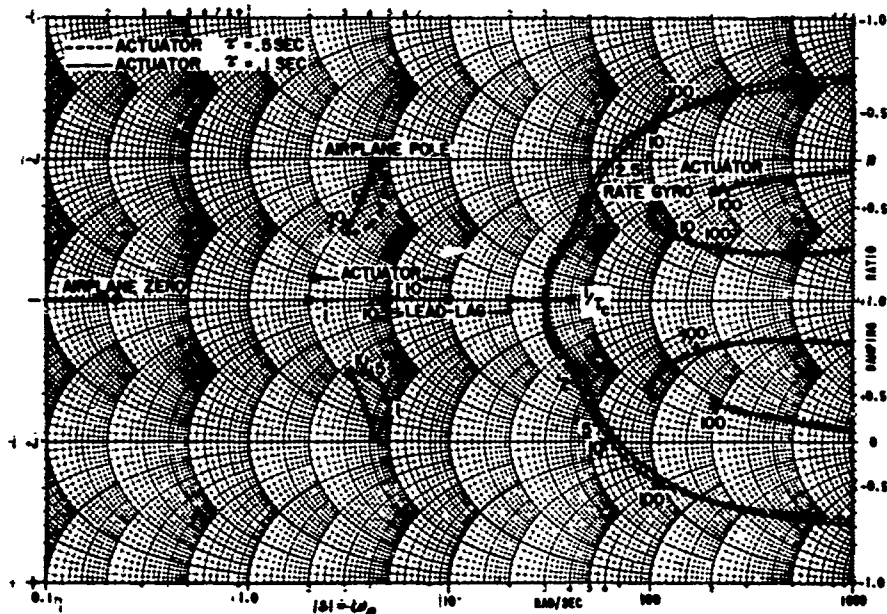


Figure 19 ATTEMPTED COMPENSATION FOR VARIATION IN ACTUATOR TIME CONSTANT

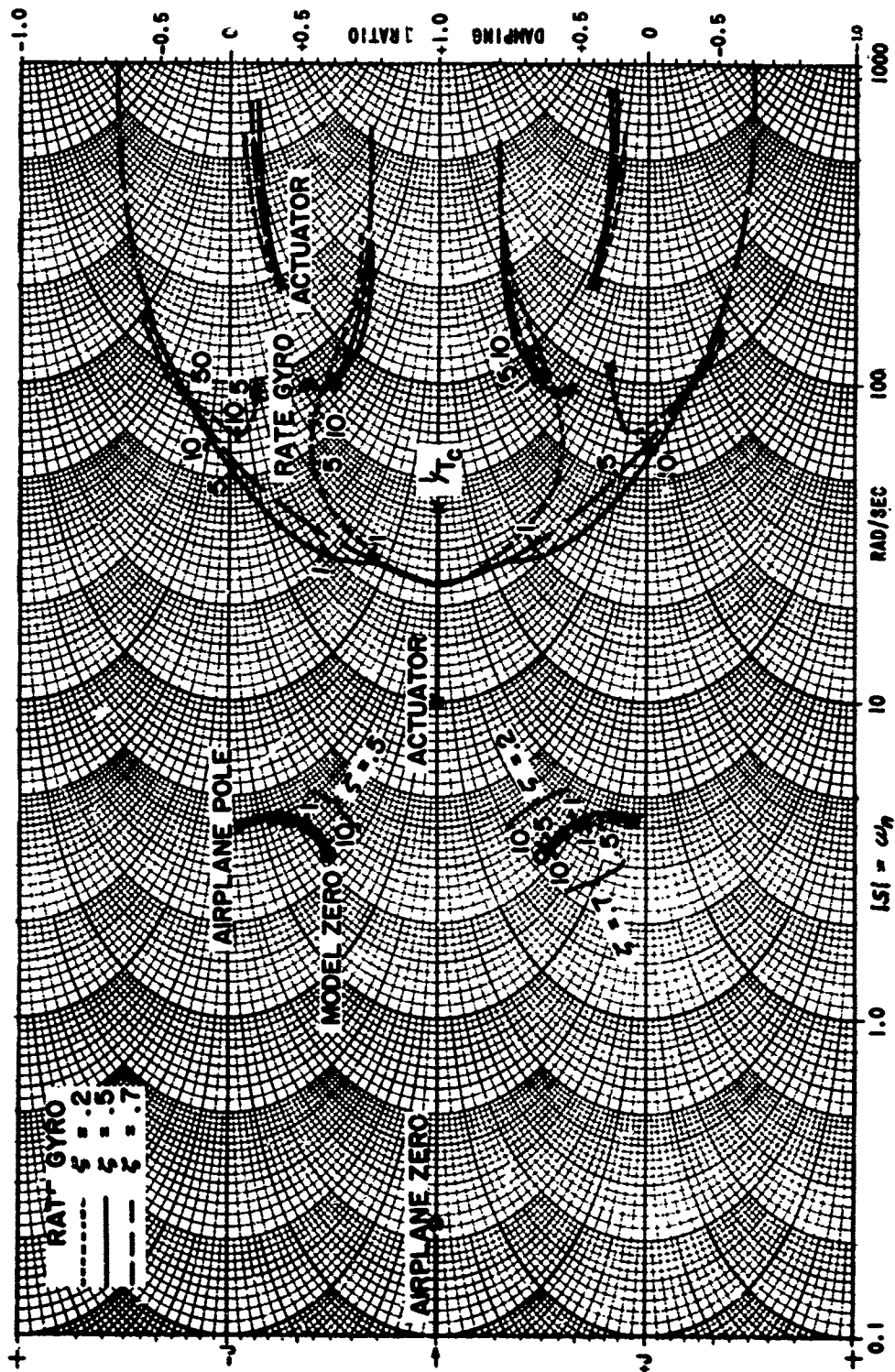
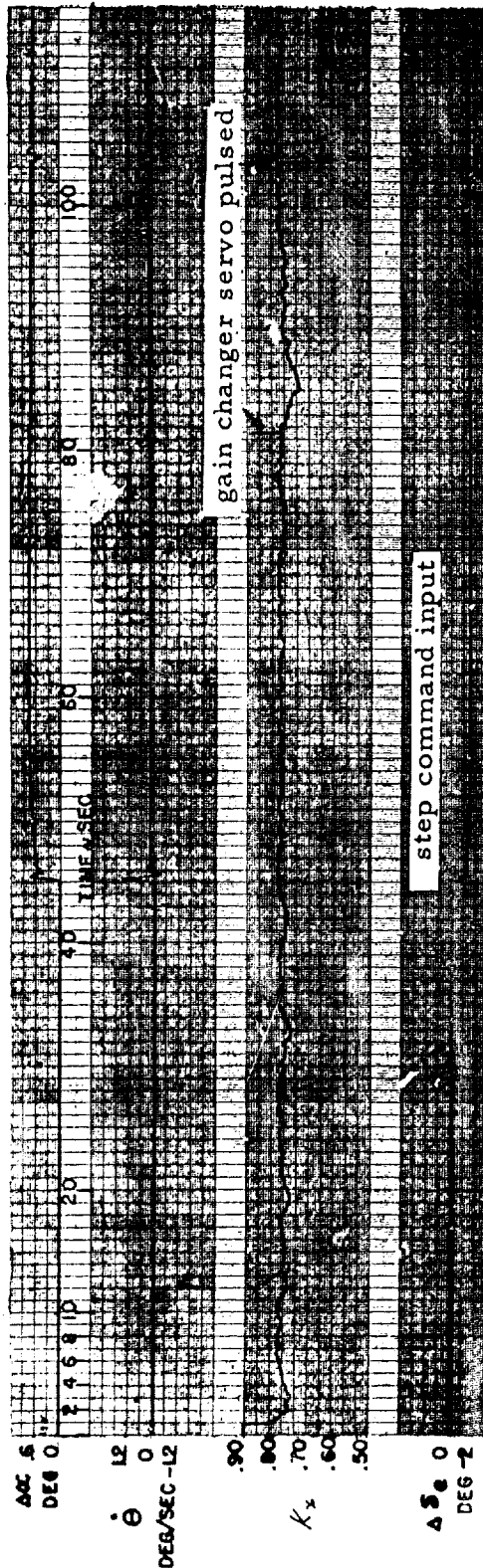
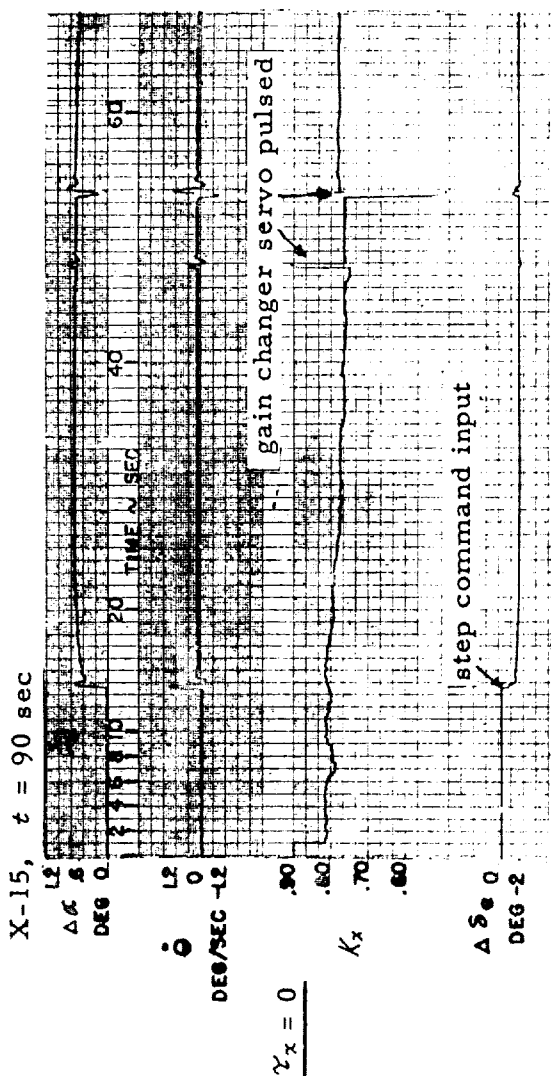


Figure 20 EFFECT OF VARIATION IN RATE GYRO DAMPING



$$\tau_x = .1 \text{ sec}$$

Figure 21 RESPONSE OF ADAPTIVE LOOP TO INITIAL GAIN OFFSET
Part a Positive Gain Offset - High Gain Case

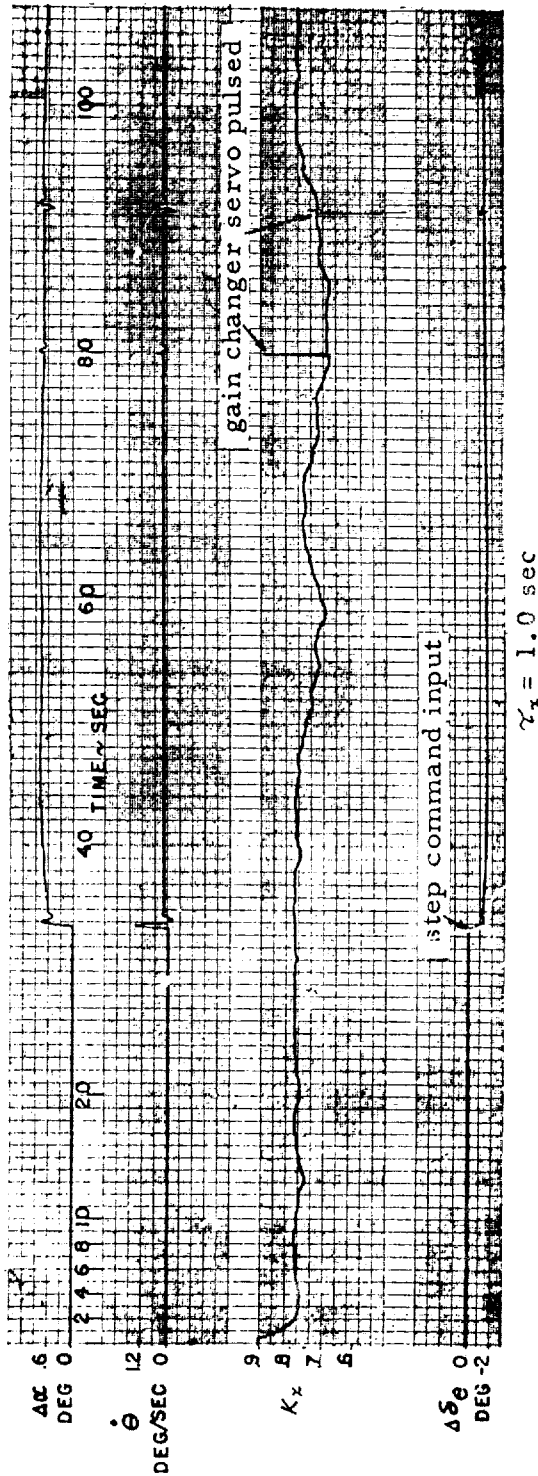
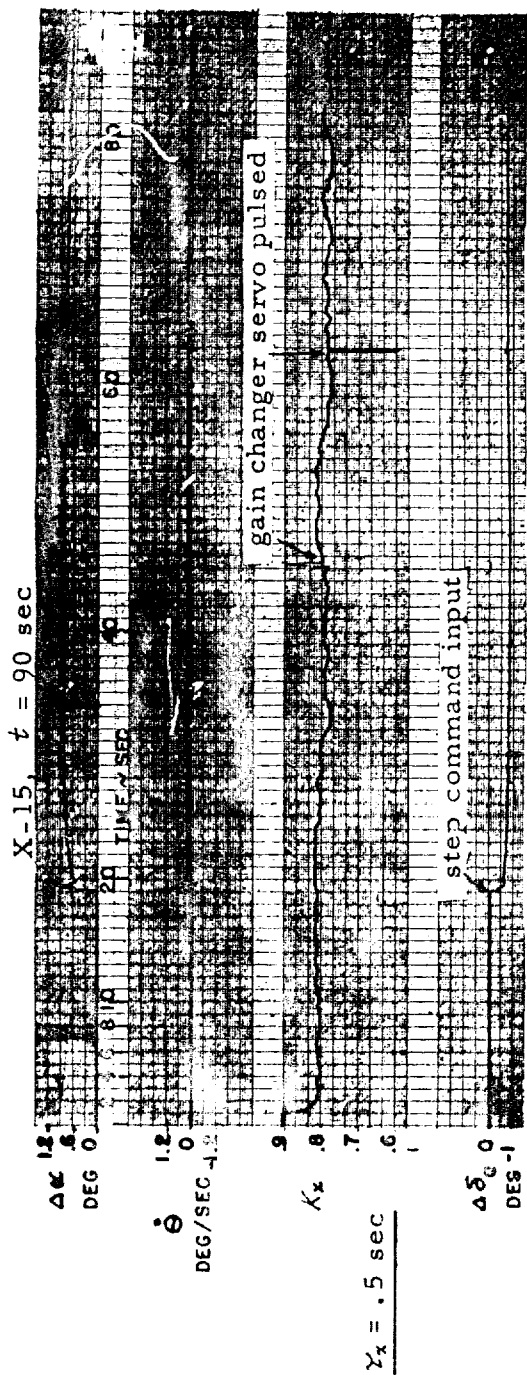


Figure 21 RESPONSE OF ADAPTIVE LOOP TO INITIAL GAIN OFFSET
Part a (continued) Positive Gain Offset - High Gain Case

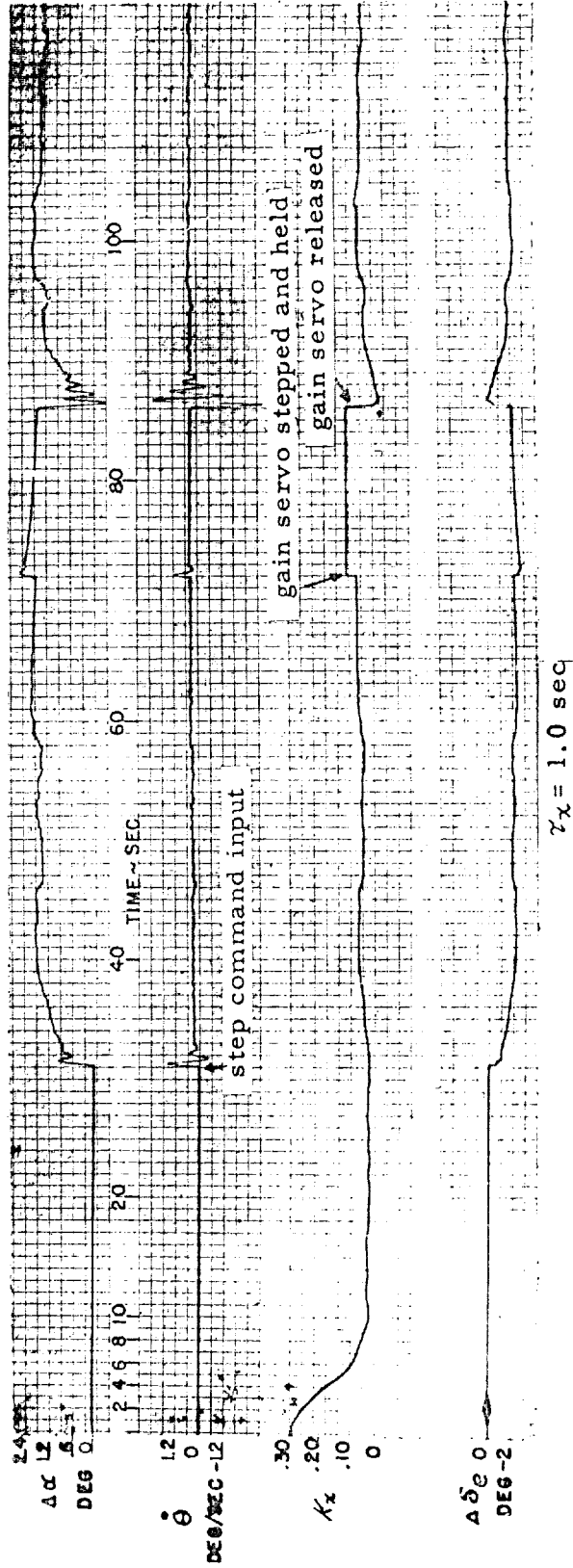
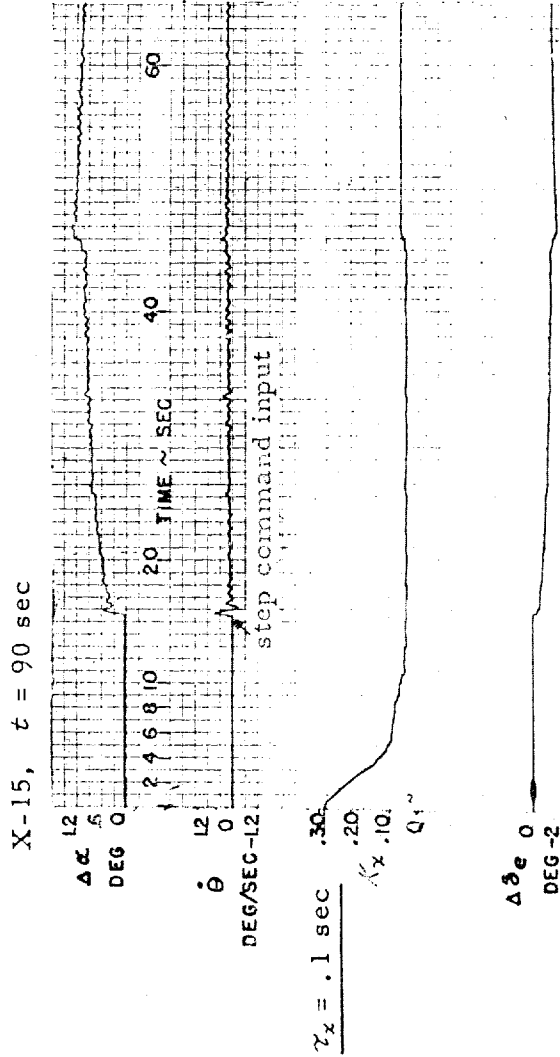


Figure 21 RESPONSE OF ADAPTIVE LOOP TO INITIAL GAIN OFFSET
Part b Positive Gain Offset - Low Gain Case

EASE Analog

X-15, $t = 90 \text{ sec}$

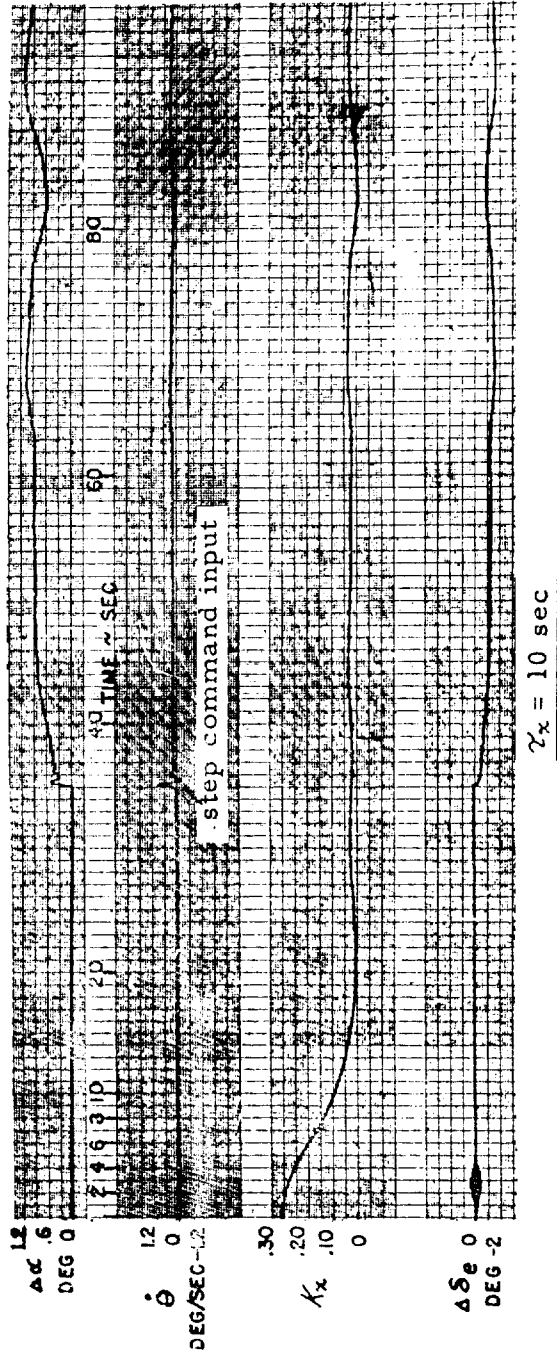


Figure 2i RESPONSE OF ADAPTIVE LOOP TO INITIAL GAIN OFFSET
Part b (continued) Positive Gain Offset - Low Gain Case

EASE Analog
 X-15, $t = 90 \text{ sec}$

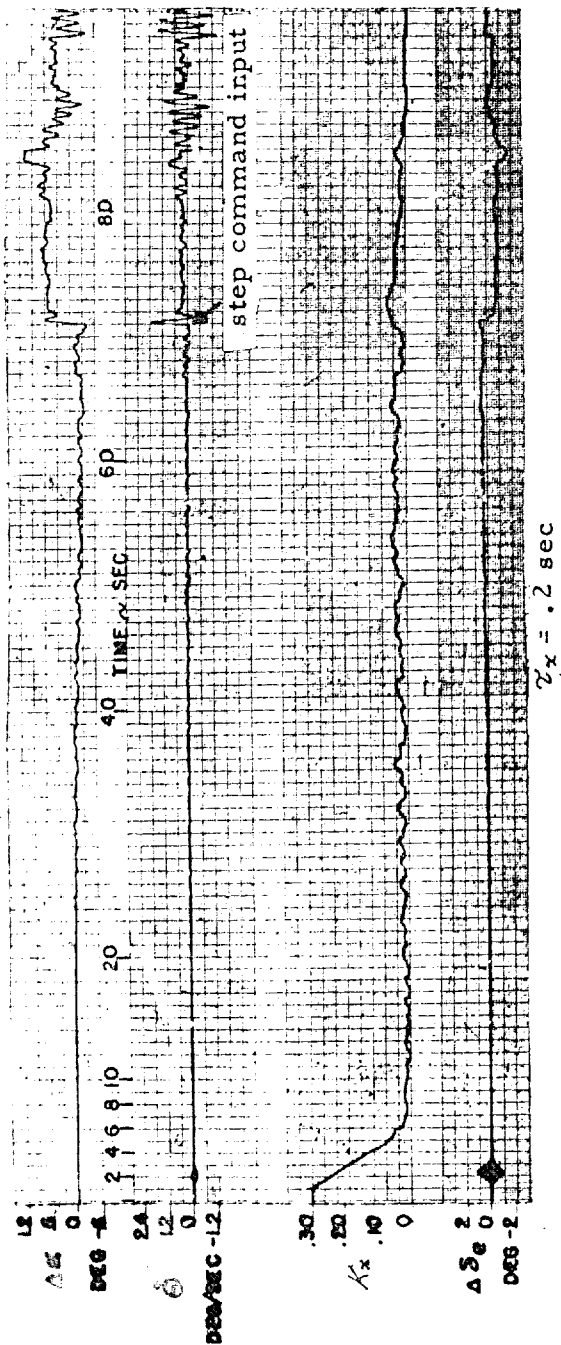


Figure 21 RESPONSE OF ADAPTIVE LOOP TO INITIAL GAIN OFFSET
 Part c Extreme Low Gain Case

EASE Analog

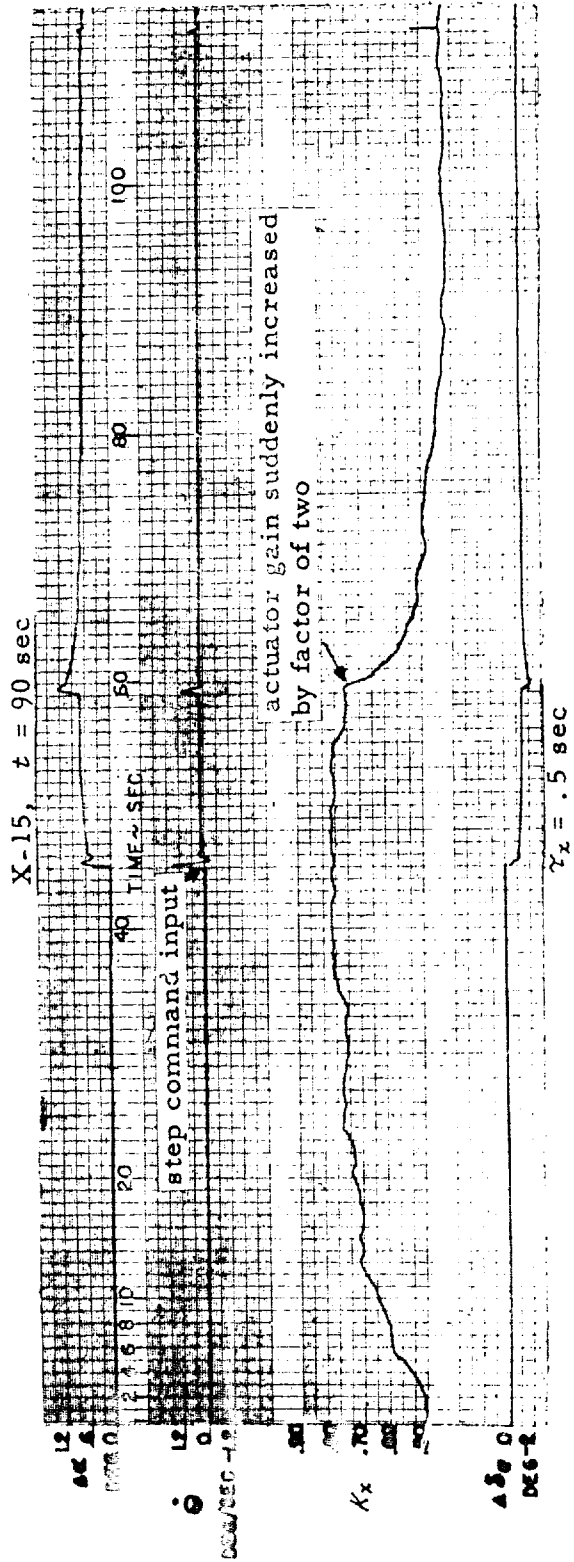


Figure 22 RESPONSE OF ADAPTIVE LOOP TO INITIAL NEGATIVE OFFSET FOLLOWED BY A POSITIVE STEP INCREASE IN ACTUATOR GAIN
High Gain Case

EASE Analog

X-15, $t = 90$ sec

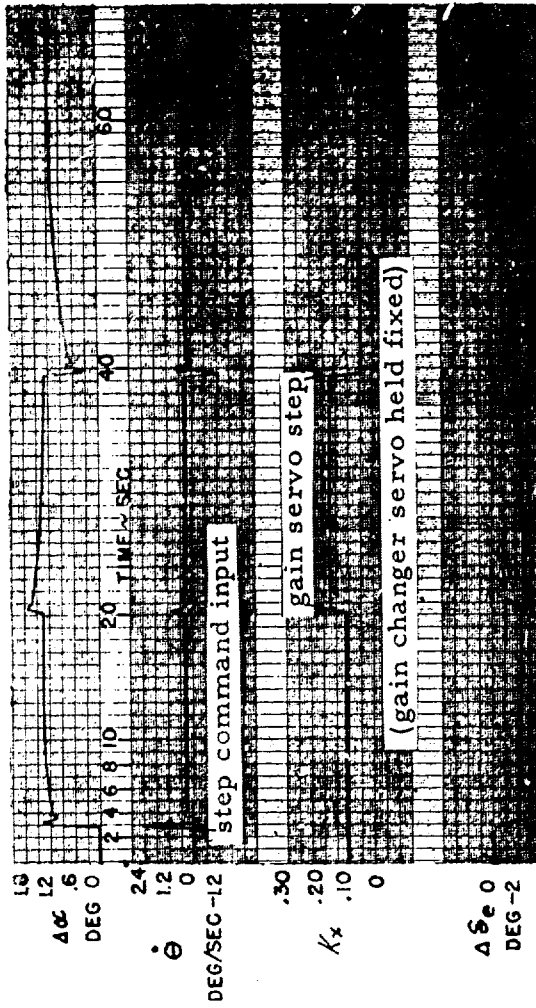
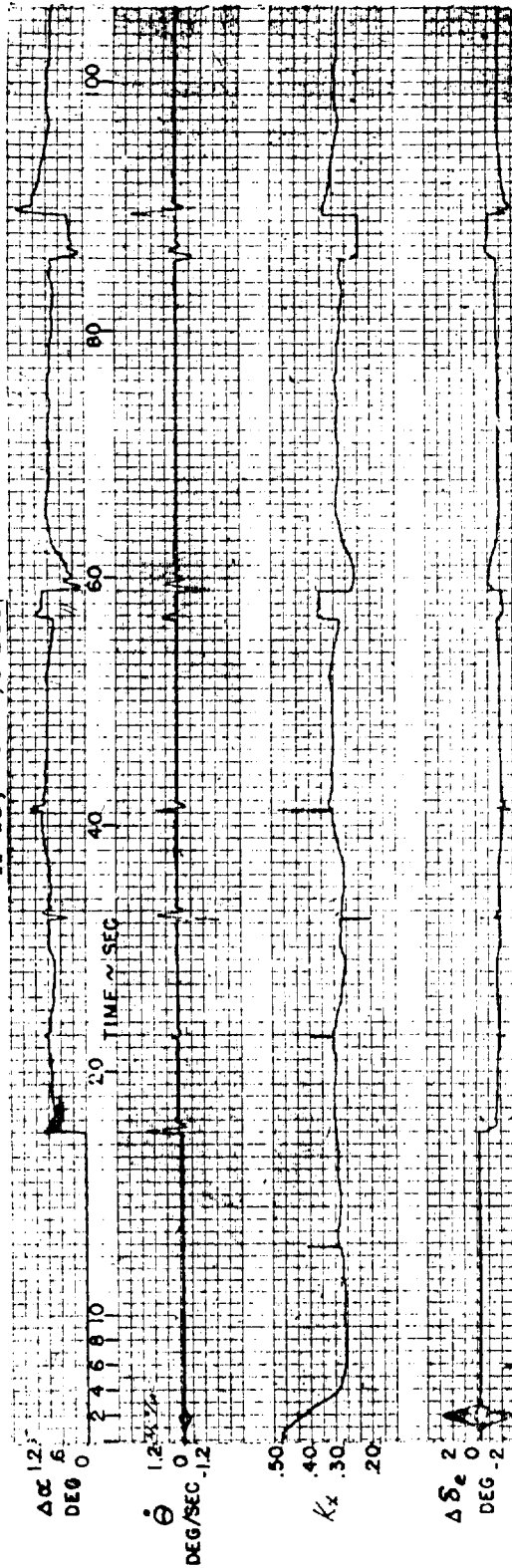


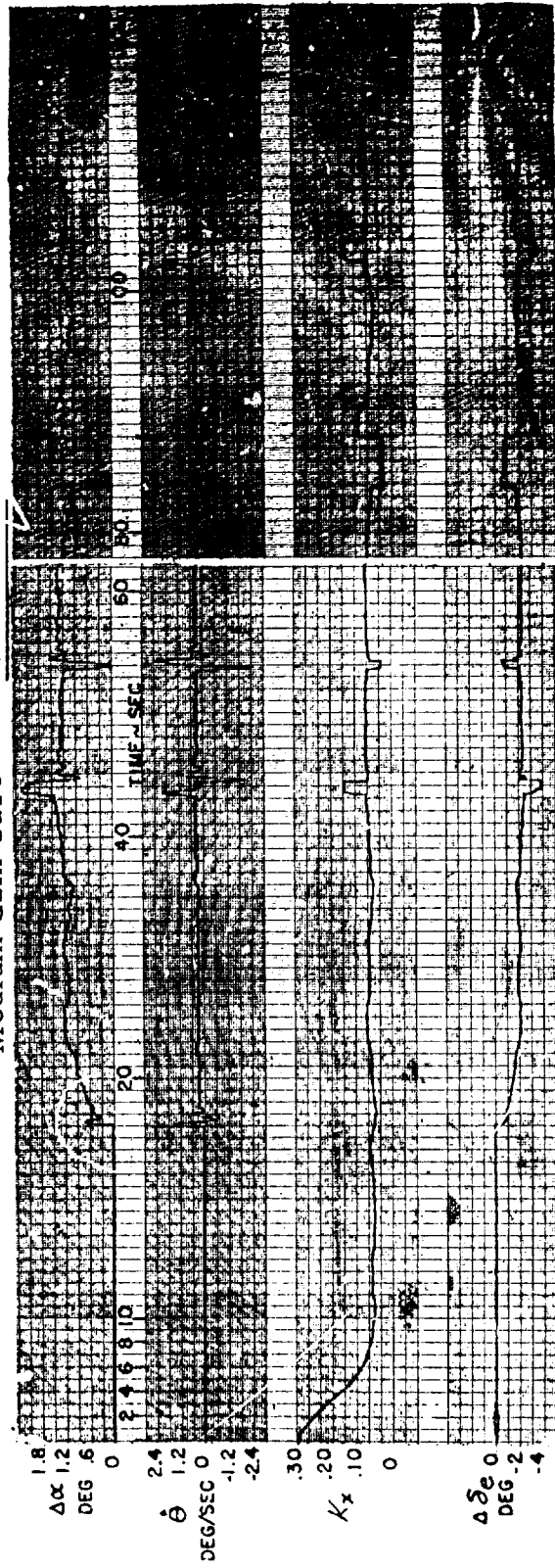
Figure 23 RESPONSE OF AIRPLANE TO STEP CHANGES IN ADAPTIVE GAIN
Part a No Adaptive-Loop Dynamics

EASE Analog

X-15, $t = 90$ sec.



Medium Gain Case $\gamma_x = 1.0$ sec



Low Gain Case $\gamma_x = 1.0$ sec

Figure 23 RESPONSE OF AIRPLANE TO STEP CHANGES IN ADAPTIVE GAIN
Part b Including Adaptive-loop Dynamics

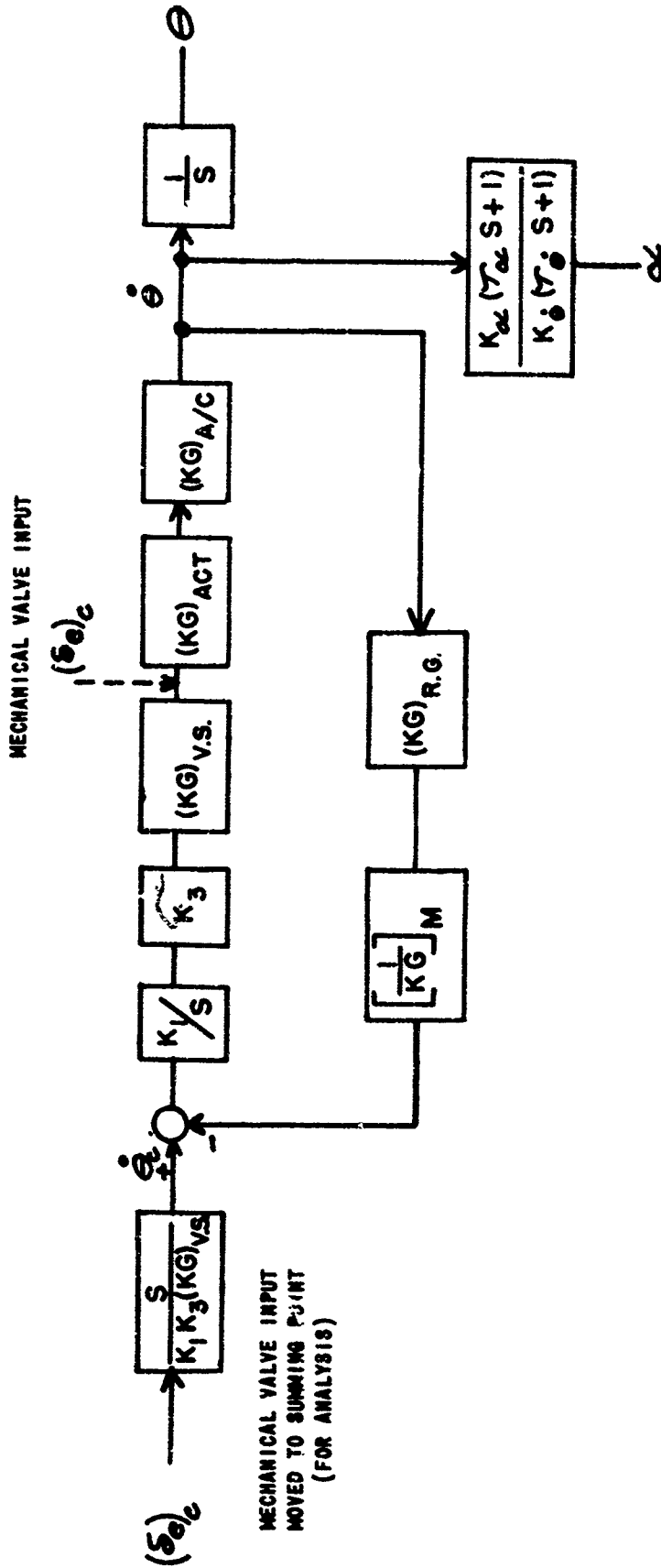


Figure 24 BLOCK DIAGRAM OF THE G.E. SYSTEM WITH PILOT INPUTS AT THE ACTUATOR VALVE

EASE ANALOG

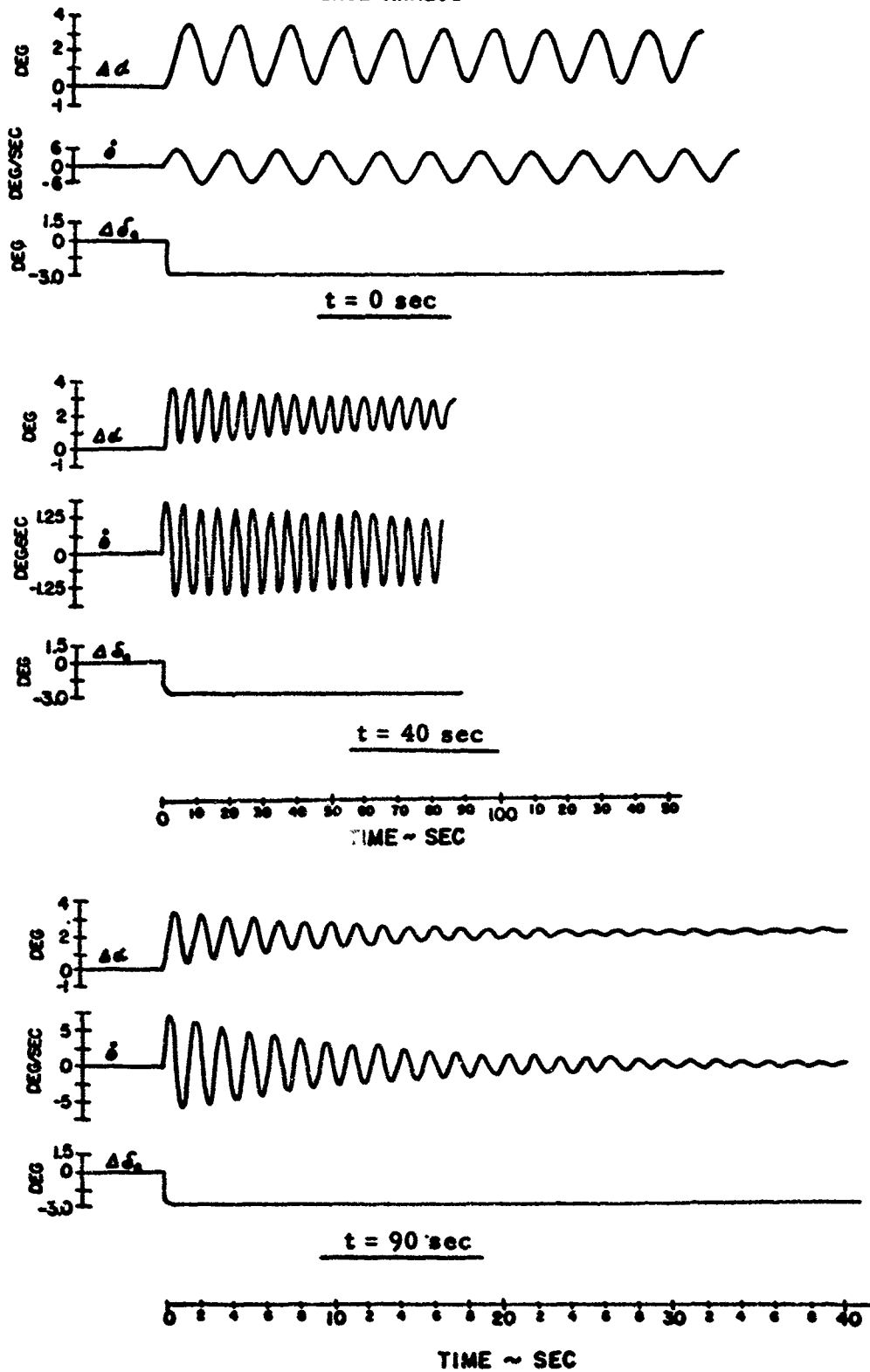
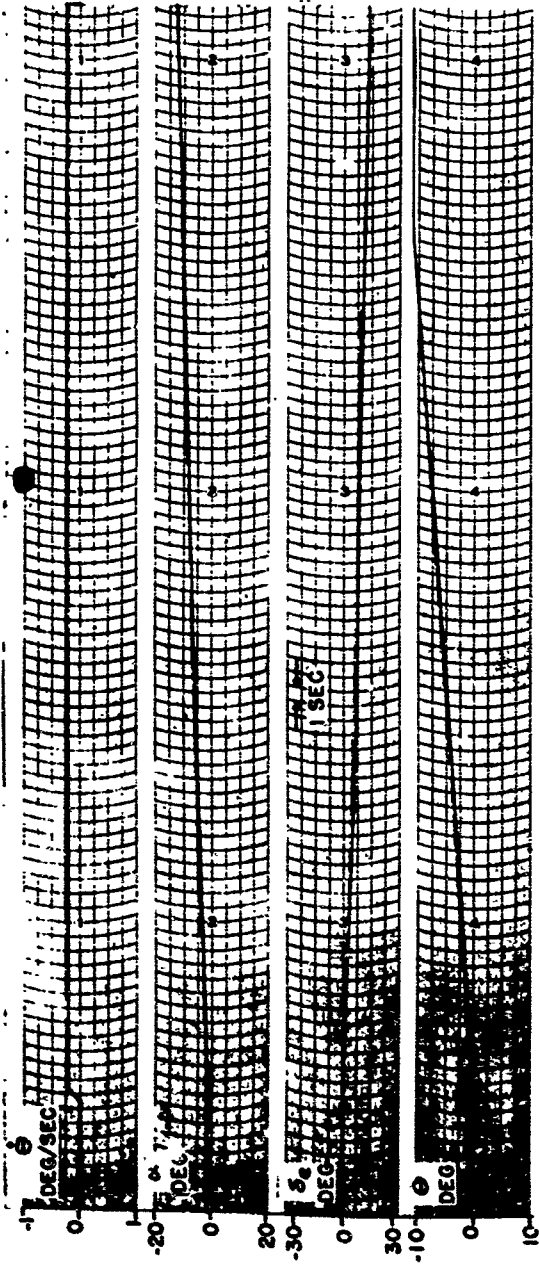
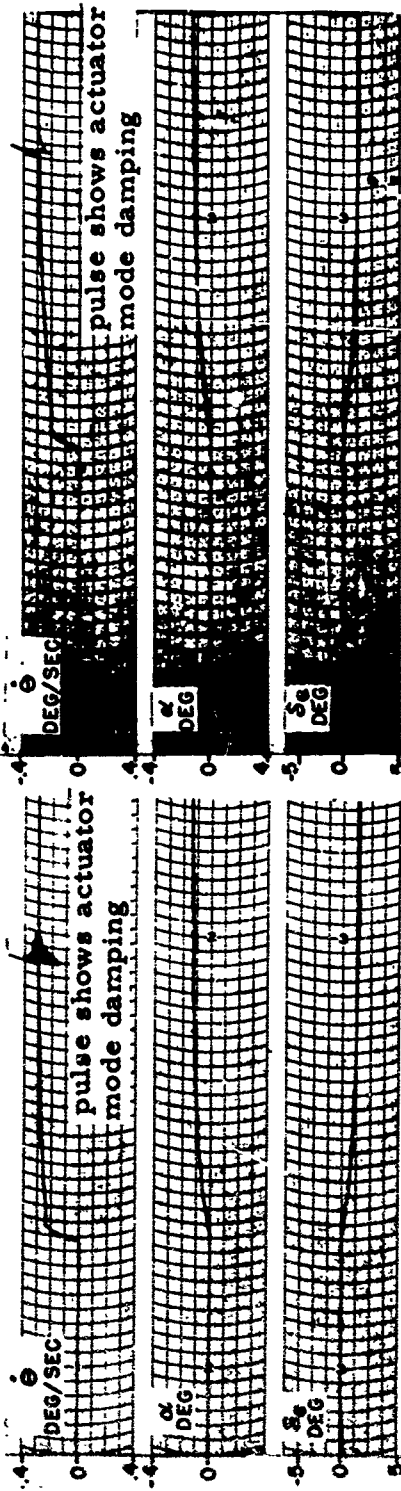


Figure 25 ANALOG RESPONSES OF X-i5 WITH G.E. SYSTEM
PART a RESPONSE TO STEP ELEVATOR COMMAND

REAC ANALOG



Flight Condition:
 $t = 40$
 Actuator - Linear
 $\gamma = 0.1$
 Gain: $K_3 = 30$
 Input: $\dot{\theta}_c = 0.2^\circ/\text{sec}$

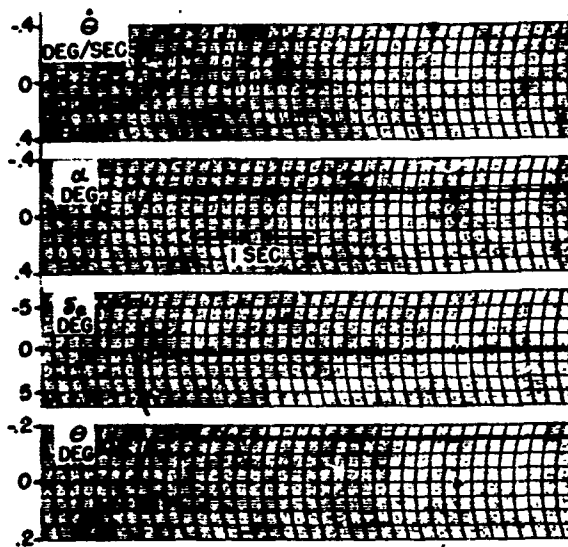


$K_3 = 4$ Flight Condition: $t = 90$ $K_3 = 2$
 Actuator - Linear $\gamma = 0.1$
 Input - $\dot{\theta}_c = 0.3^\circ/\text{sec}$

Figure 25 ANALOG RESPONSES OF X-15 WITH G.E. SYSTEM
 PART b RESPONSE TO PITCH RATE COMMANDS

REAC ANALOG

Flight Condition:
 $t = 0$
 Actuator - Linear
 $\zeta = 0.1$
 Gain: $K_3 = 150$
 Input: Step $\delta_e = 26^\circ$



Flight Condition:
 $t = 0$
 Actuator - Linear
 $\zeta = 0.1$
 Gain: $K_3 = 250$
 Input: Step $\delta_e = 26^\circ$

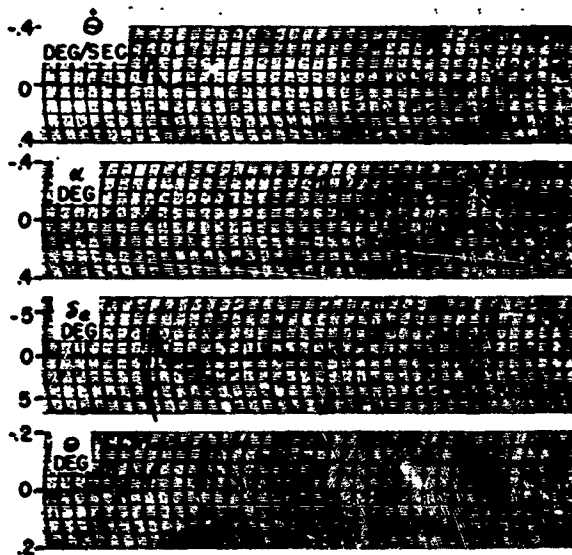
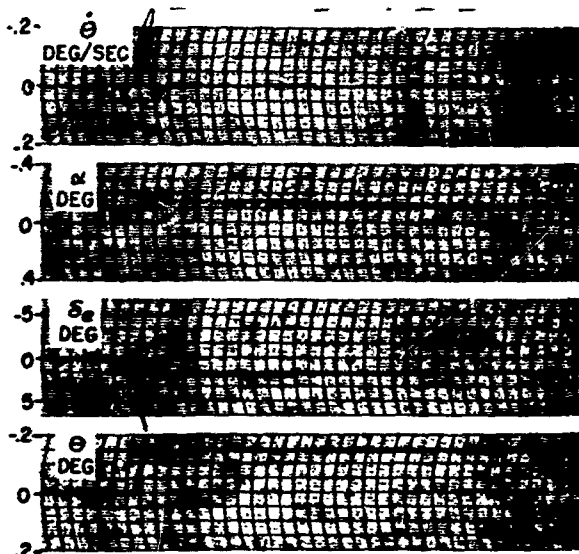


Figure 25 ANALOG RESPONSES OF X-15 WITH G.E. SYSTEM
 PART c RESPONSE TO STEP ELEVATOR COMMANDS, FLIGHT CONDITION $t = 0$

REAC ANALOG

Flight Condition:
 $t = 40$
 Actuator - Linear
 $\gamma = 0.1$
 Gain: $K_3 = 20$
 Input: Step $\delta_e = 3.3^\circ$



Flight Condition:
 $t = 40$
 Actuator - Linear
 $\gamma = 0.1$
 Gain: $K_3 = 36$
 Input: Step $\delta_e = 3.3^\circ$

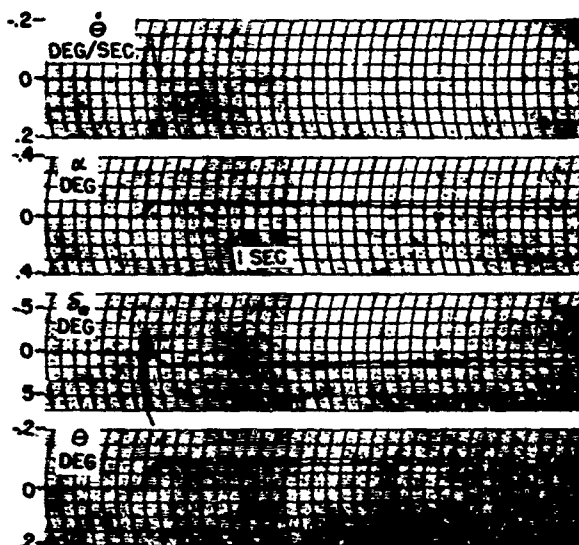
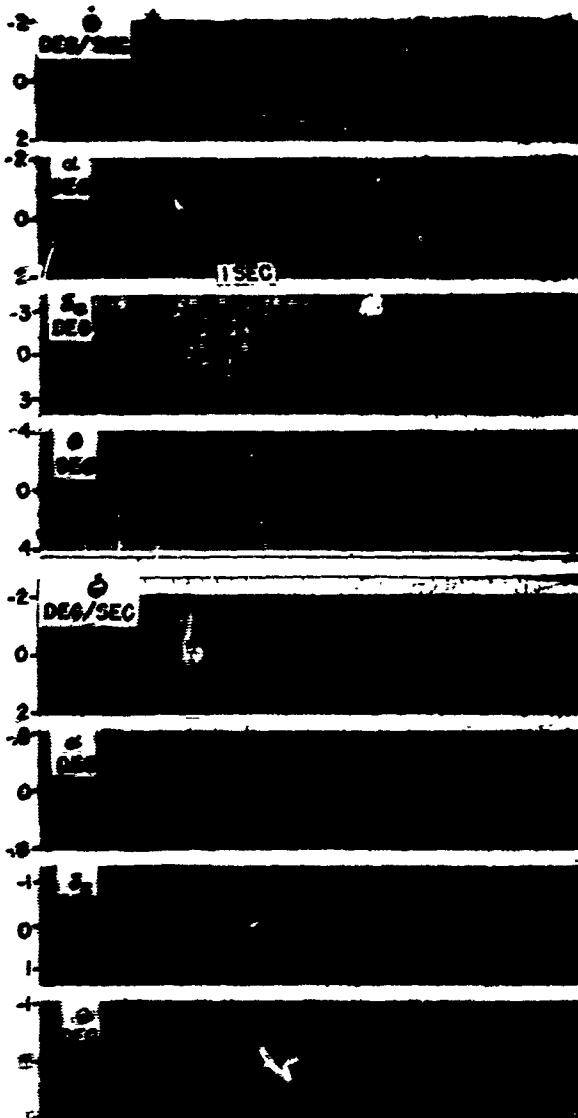


Figure 25 ANALOG RESPONSES OF X-15 WITH G. E. SYSTEM
 PART c (continued) RESPONSE TO STEP ELEVATOR COMMANDS
 FLIGHT CONDITION $t = 40$

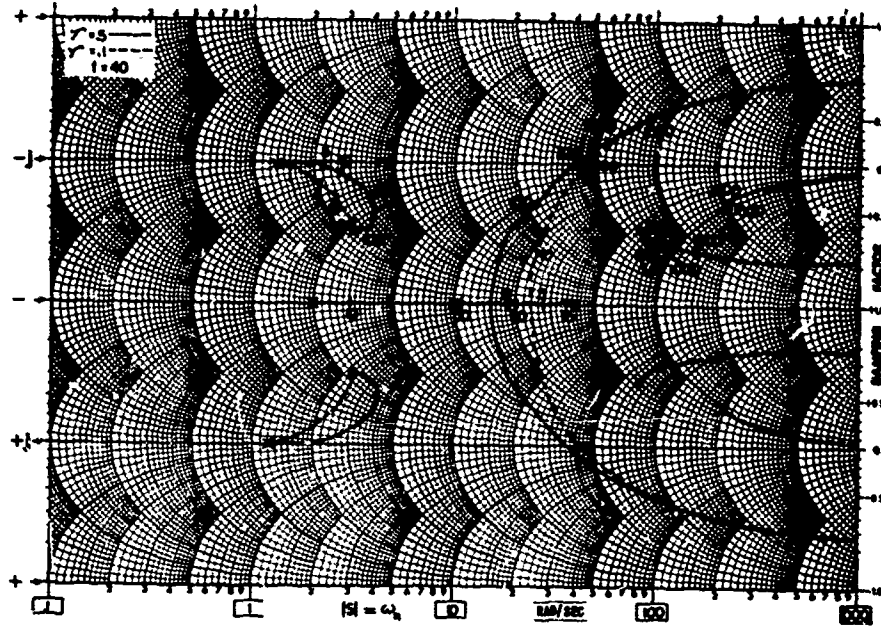
REAC ANALOG

Flight Condition:
 $t = 90$
 Actuator - Linear
 $\gamma = 0.1$
 Gain: $K_3 = 2$
 Input: Step $\delta_e = 4^\circ$

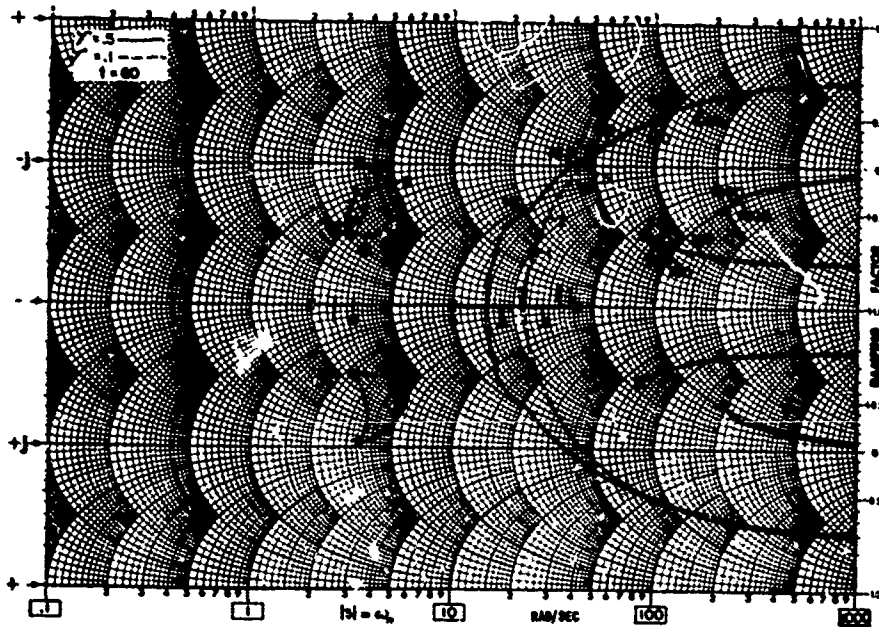


Flight Condition:
 $t = 90$
 Actuator - Linear
 $\gamma = 0.1$
 Gain: $K_3 = 4$
 Input: Step $\delta_e = 4^\circ$

Figure 25 ANALOG RESPONSES OF X-15 WITH G.E. SYSTEM
 PART c (continued) RESPONSE TO STEP ELEVATOR COMMANDS
 FLIGHT CONDITION $t = 90$

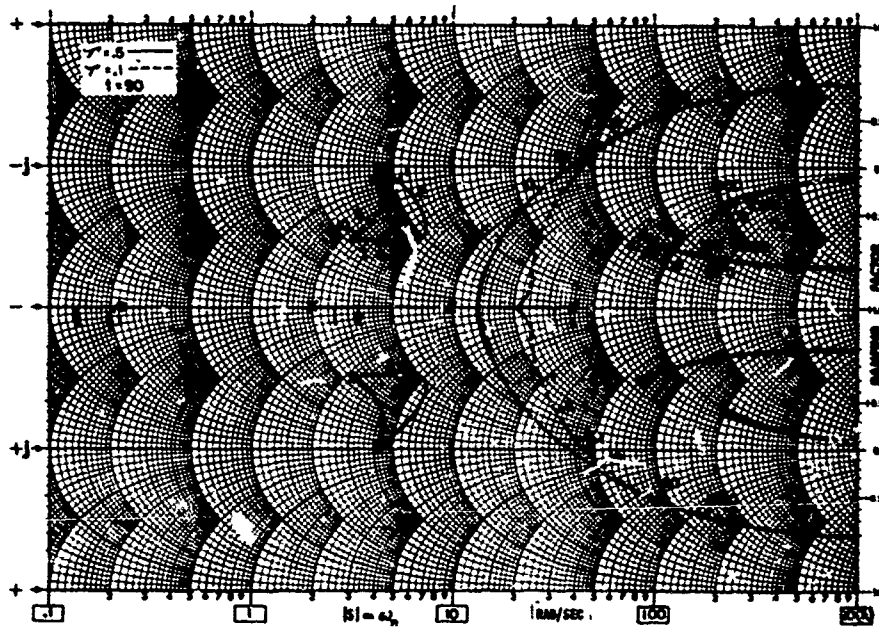
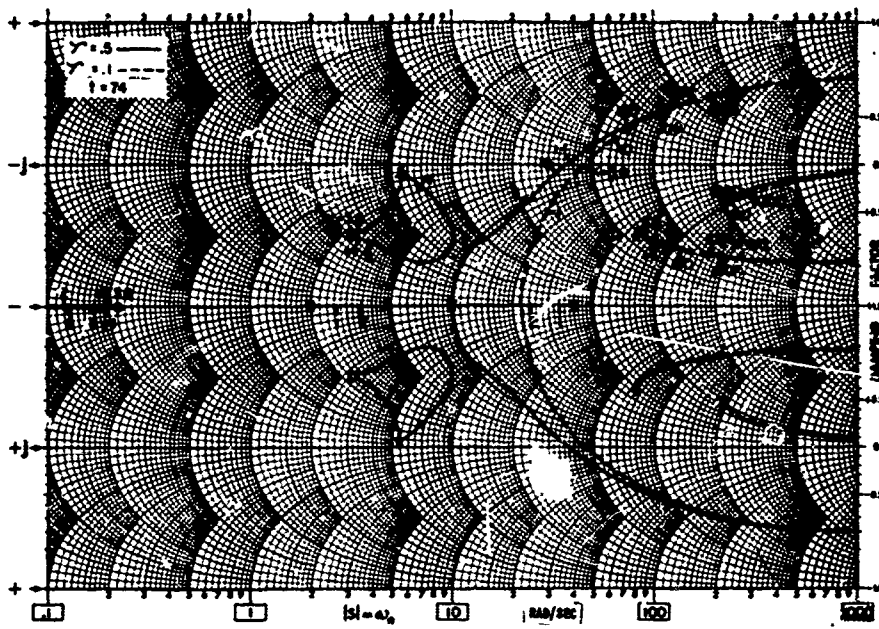


t = 40 SEC



t = 60 SEC

Figure 26 ROOT LOCI FOR X-15 WITH G.E. SYSTEM
PART b FLIGHT CONDITIONS t = 40 AND t = 60



$t = 90 \text{ SEC}$

Figure 26 ROOT LOCI FOR X-15 WITH G.E. SYSTEM
PART c FLIGHT CONDITIONS $t = 74$ AND $t = 90$

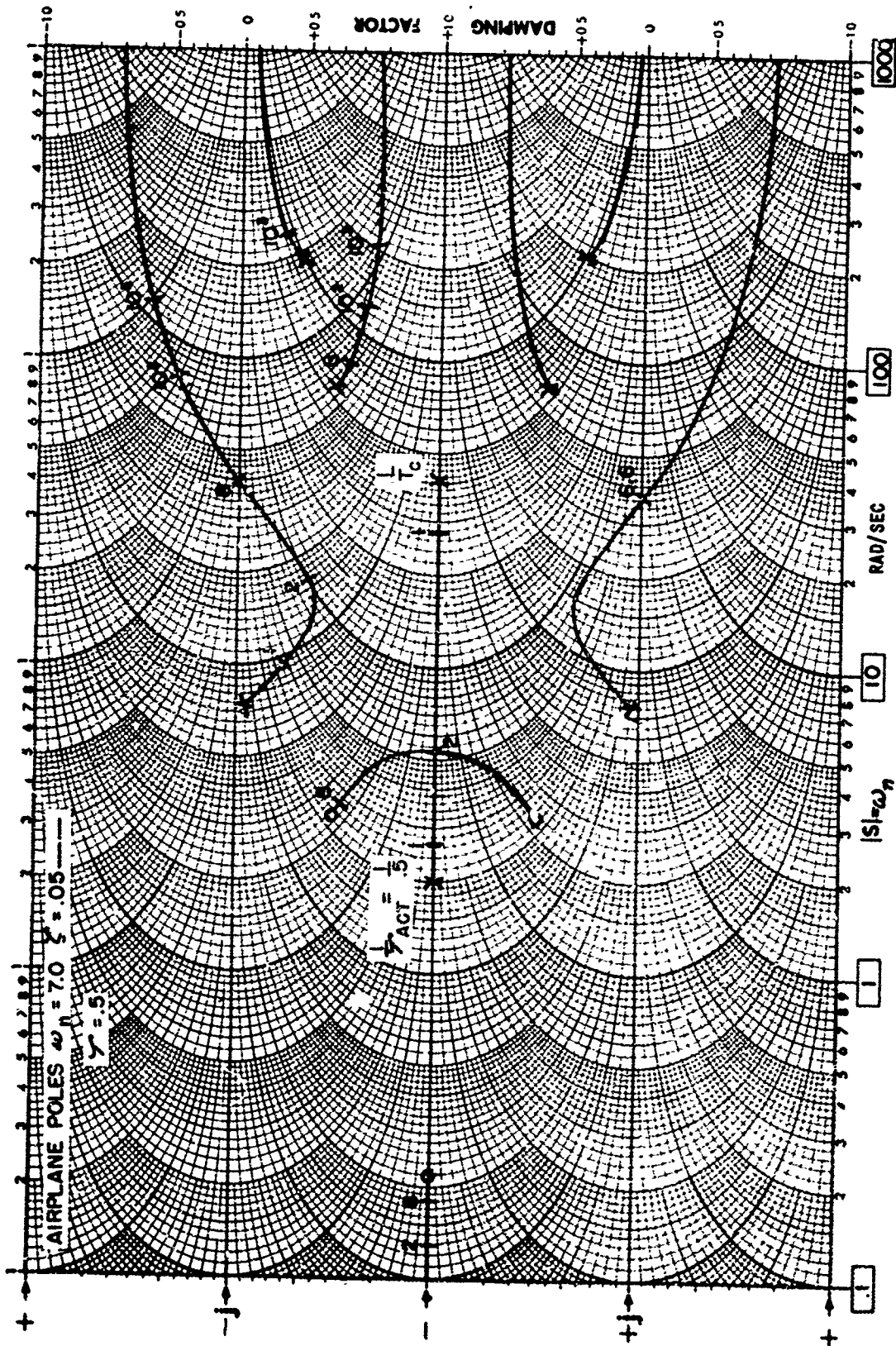


Figure 26d ROOT LOCI FOR X-15 WITH G. E. SYSTEM
PART d FLIGHT CONDITION $t = 74$ WITH
AIRPLANE POLES SHIFTED - SLOW ACTUATOR

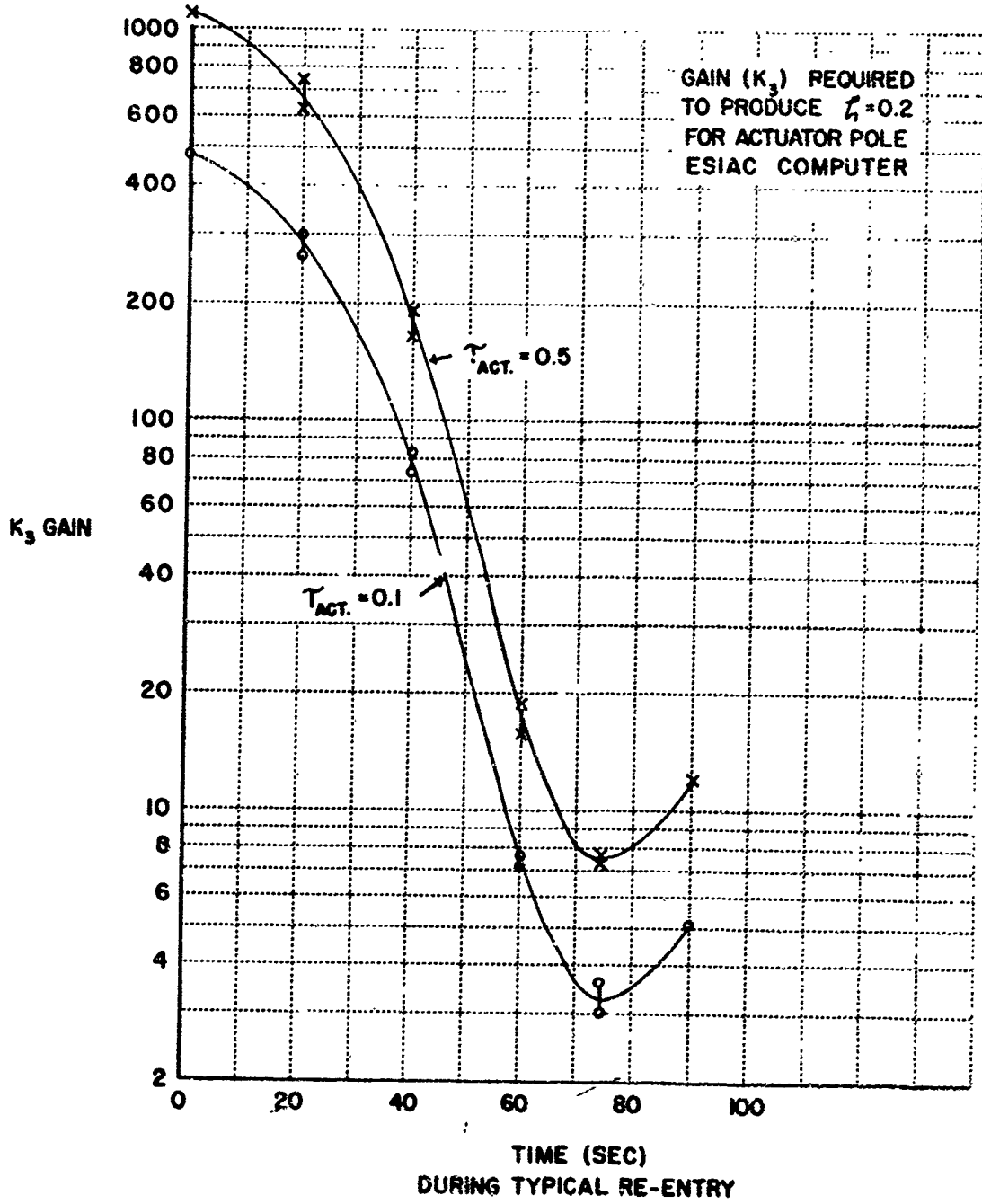


Figure 27 GAIN (K_3) REQUIRED TO PRODUCE $\zeta = 0.02$ FOR THE ACTUATOR POLE FOR TWO ACTUATOR TIME CONSTANTS

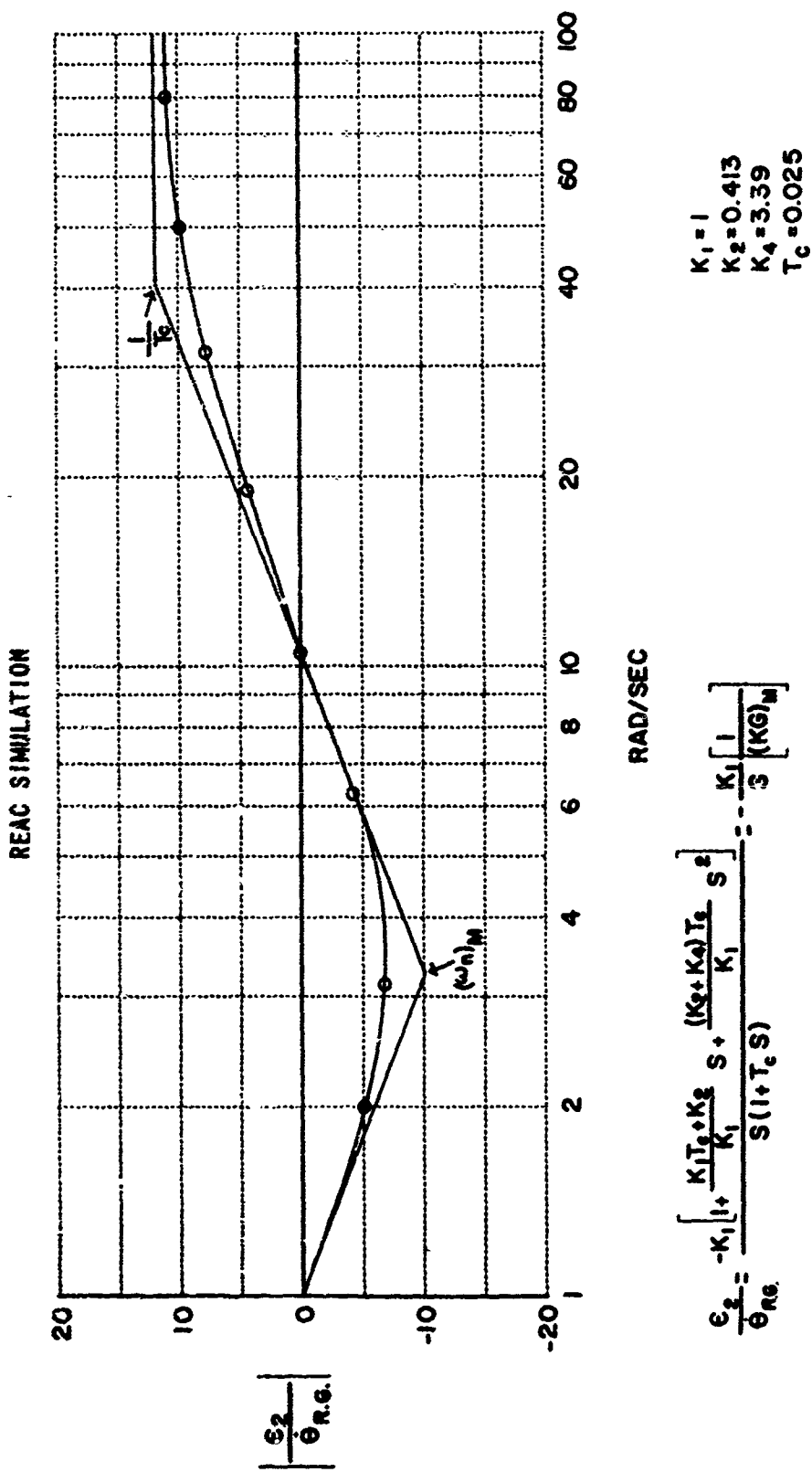


Figure 28 FREQUENCY RESPONSE OF G. E. FEEDBACK

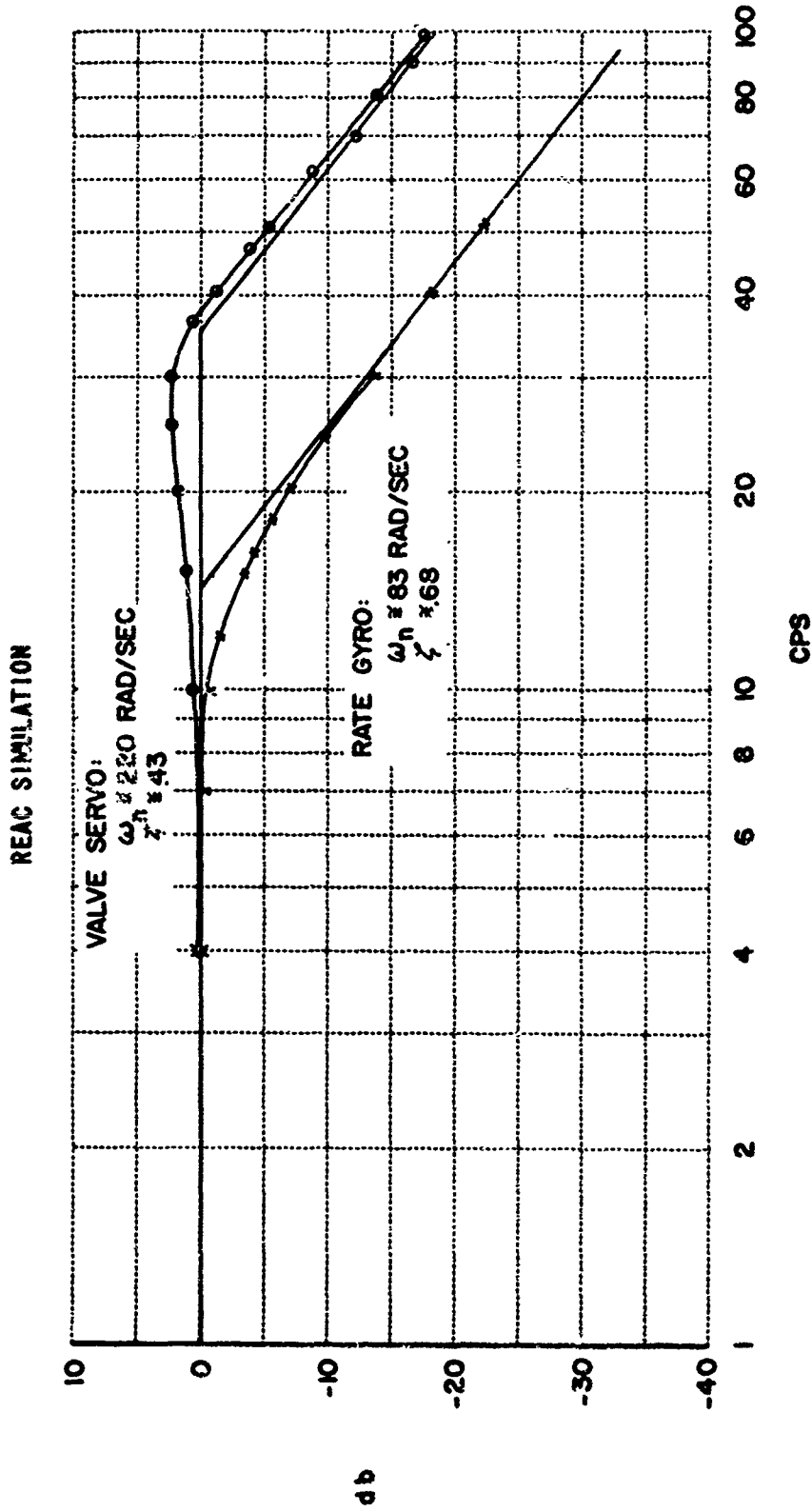


Figure 29 FREQUENCY RESPONSE OF ANALOG SECOND-ORDER SYSTEMS FOR VALVE SERVO AND RATE GYRO

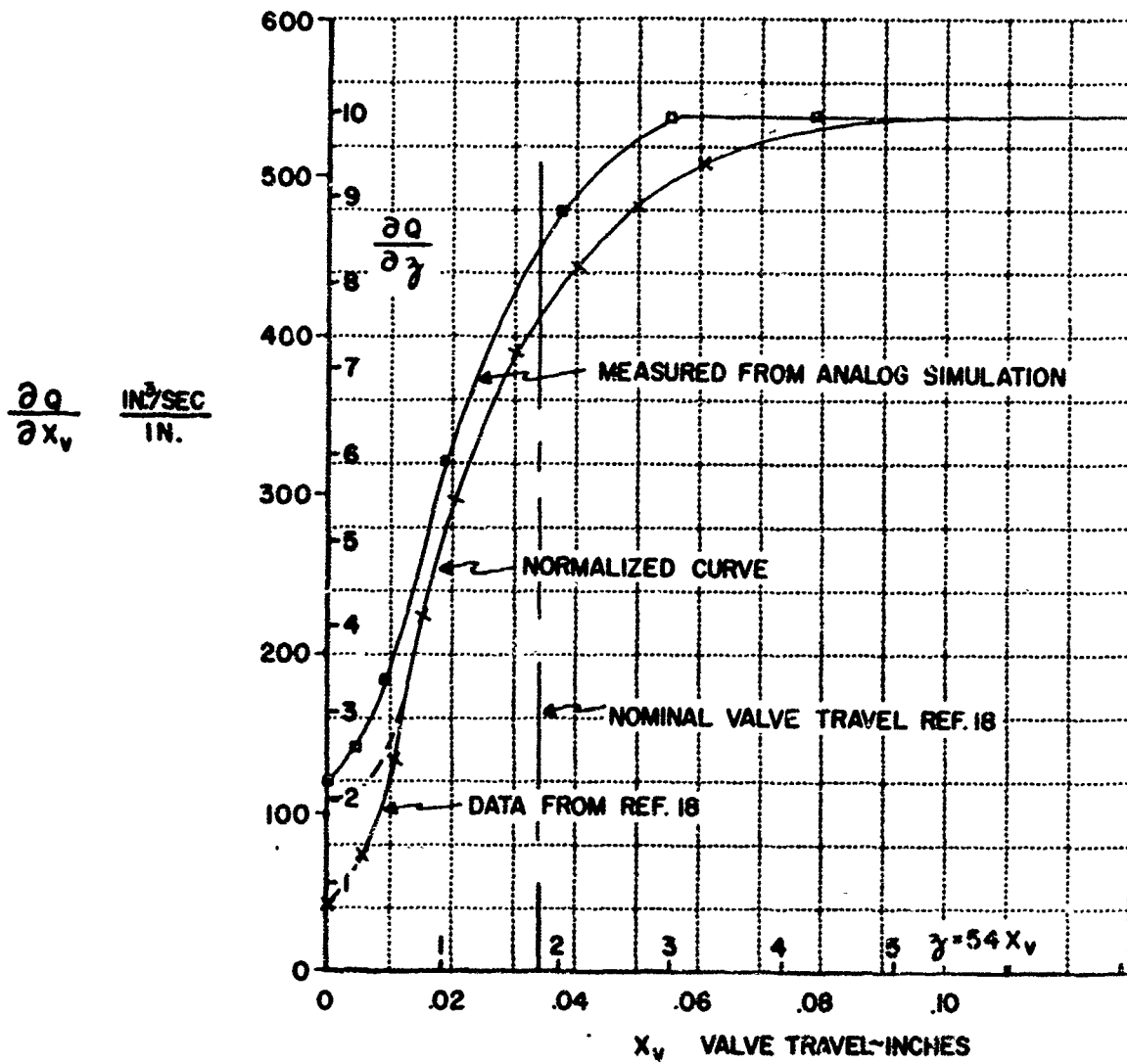


Figure 30 RATE OF CHANGE OF FLOW WITH VALVE DISPLACEMENT FOR NONLINEAR ACTUATOR VALVE

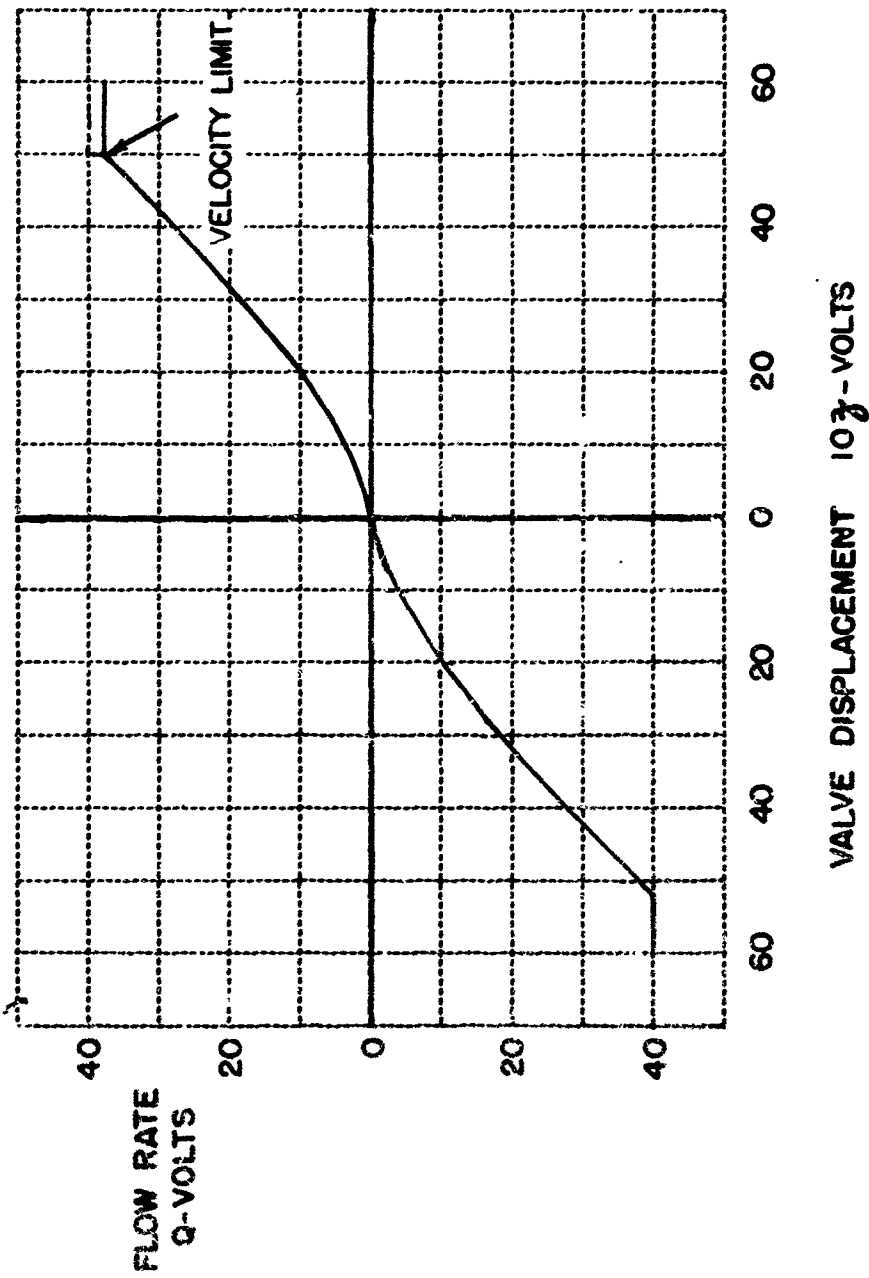


Figure 31 REAC FUNCTION GENERATOR FOR NONLINEAR ACTUATOR VALVE

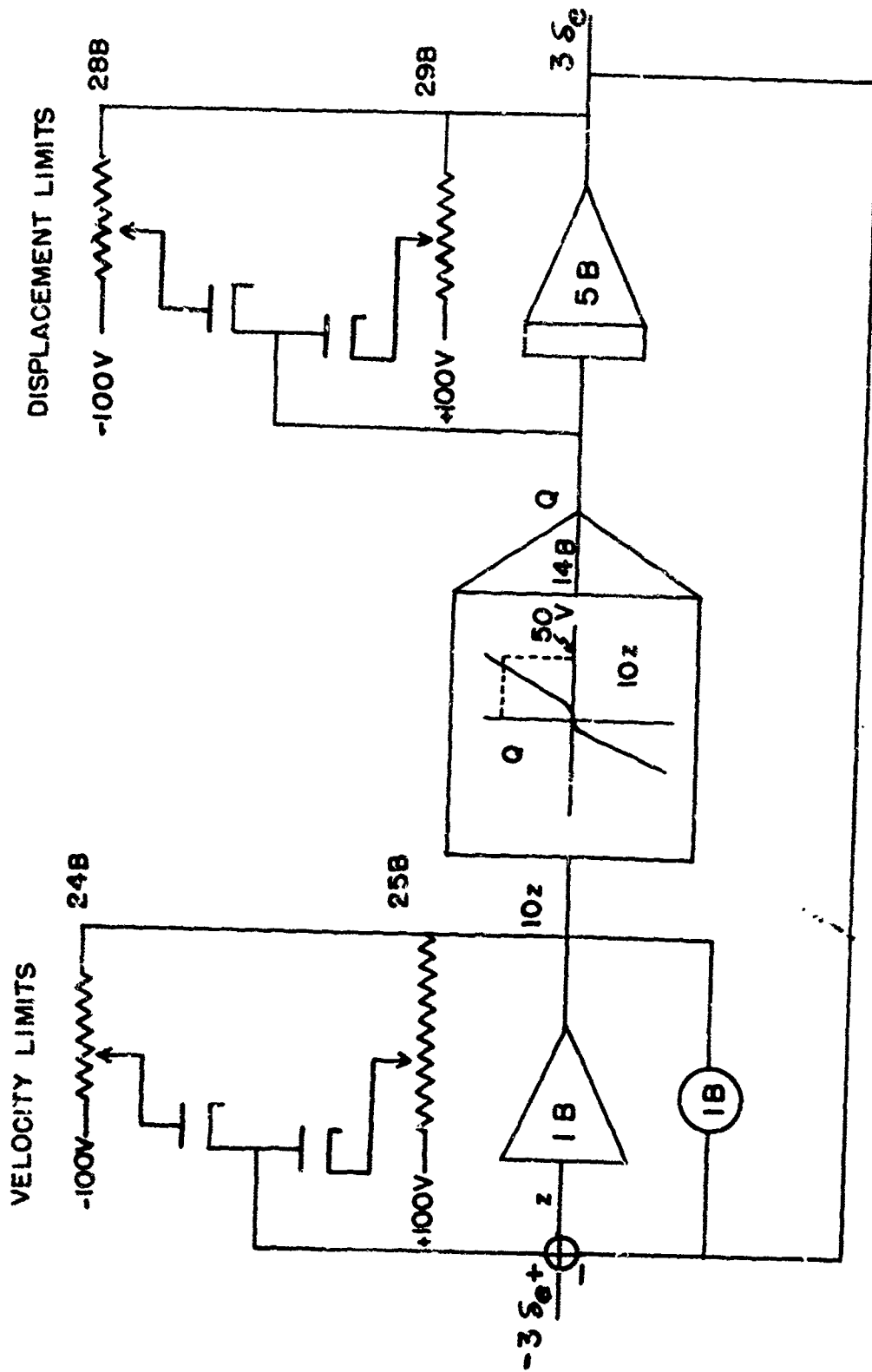


Figure 32 BLOCK SCHEMATIC OF REAC SIMULATION OF NONLINEAR ACTUATOR

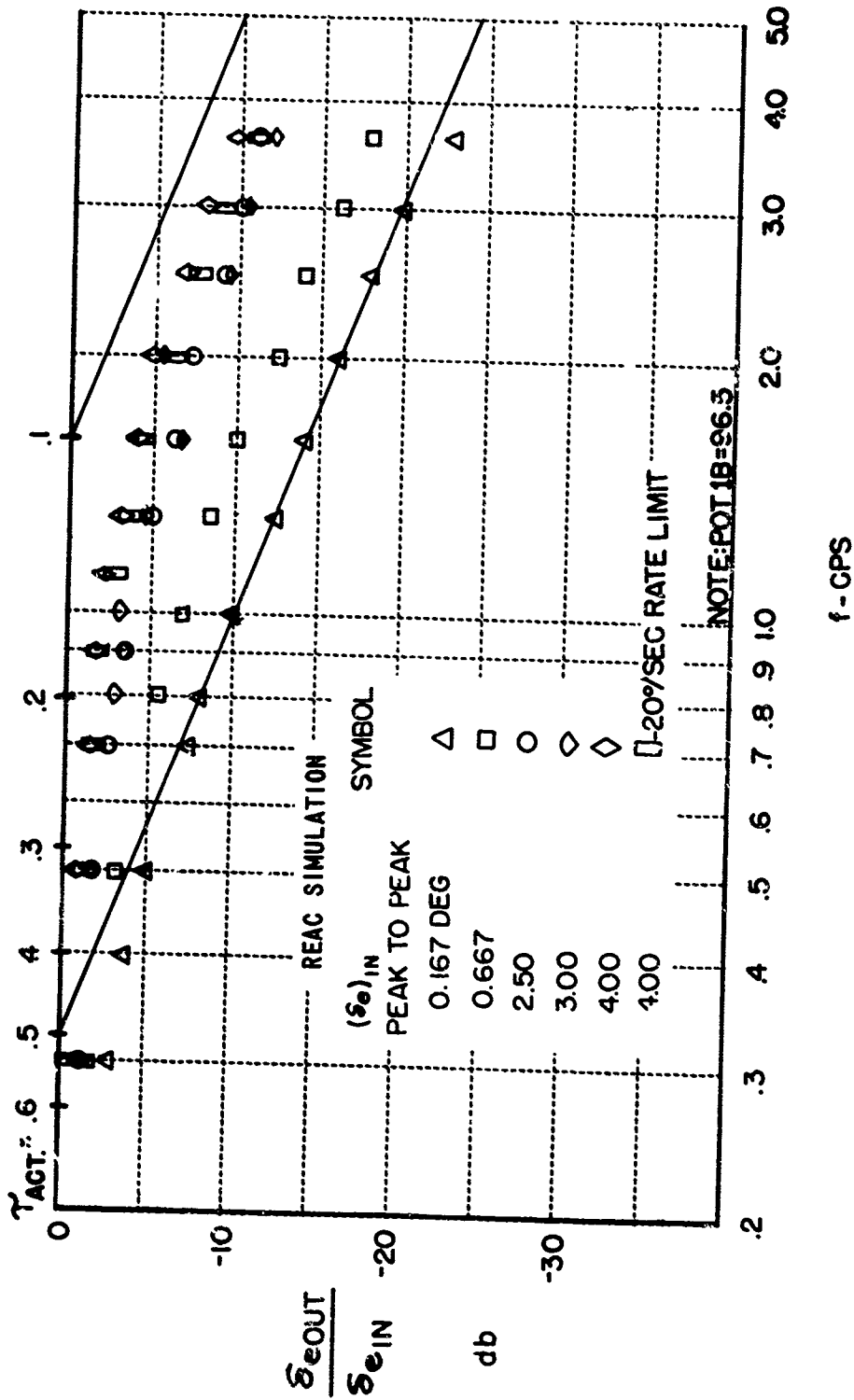


Figure 33 FREQUENCY RESPONSE OF NONLINEAR ACTUATOR

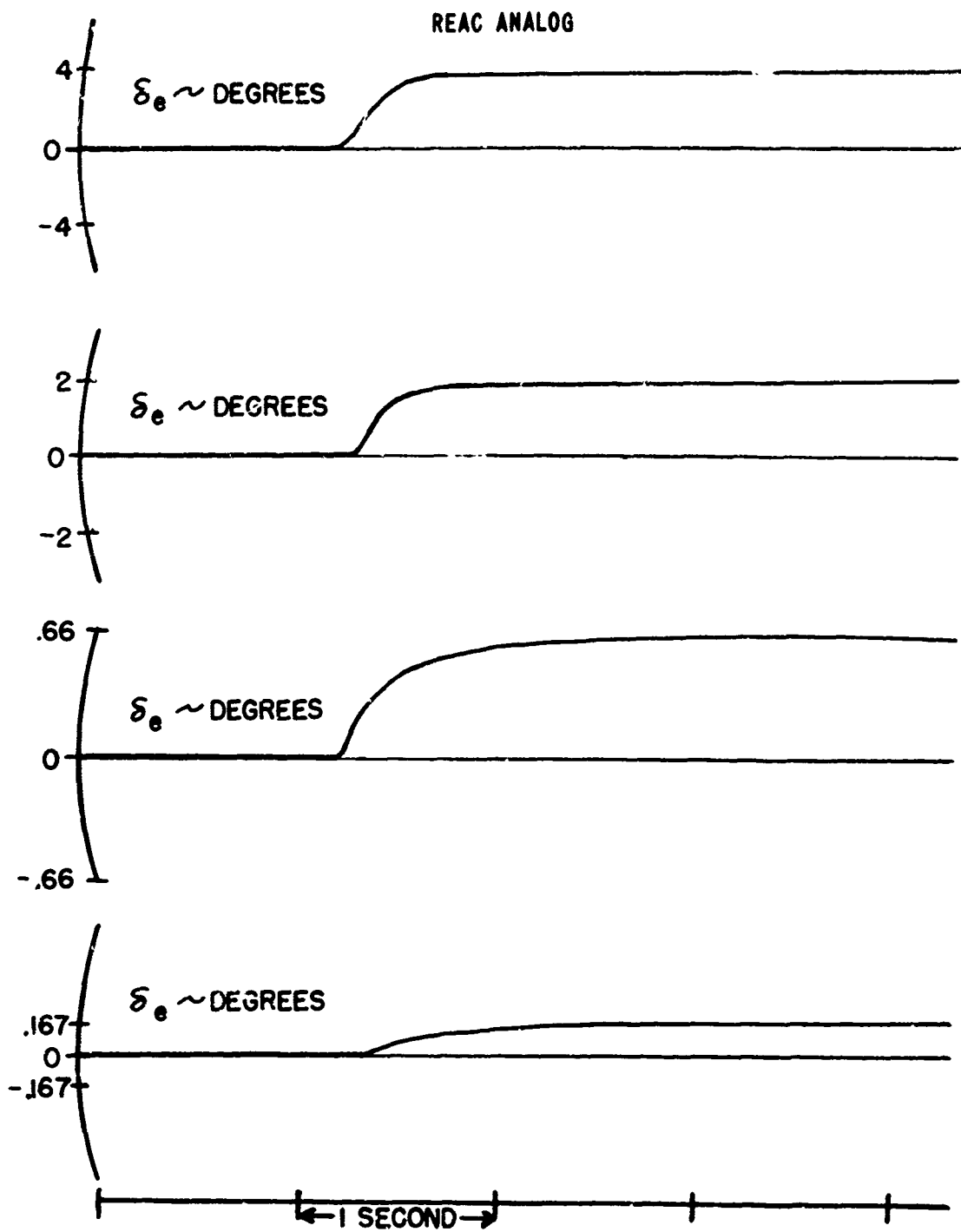
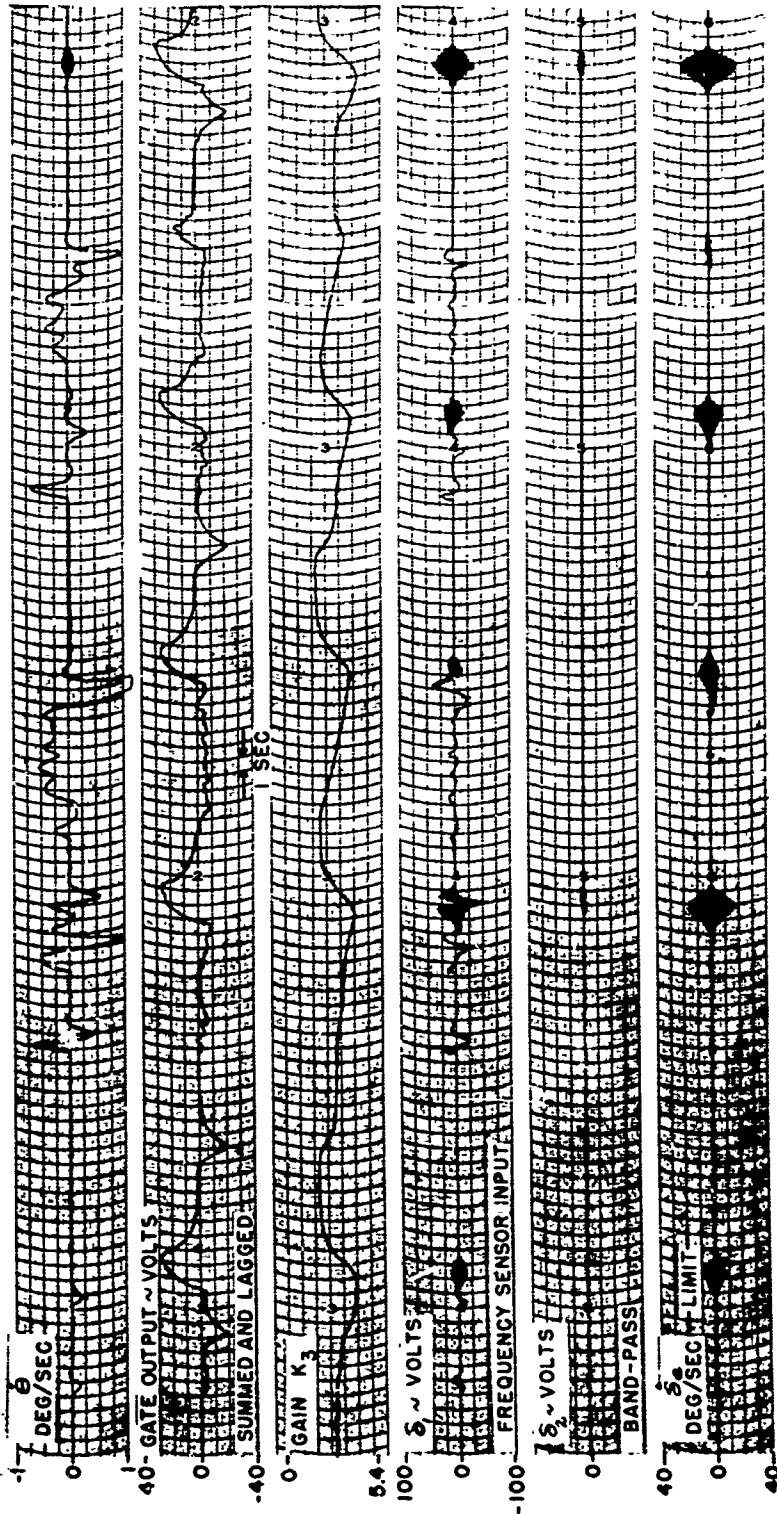


Figure 34 TRANSIENT RESPONSE OF NONLINEAR ACTUATOR

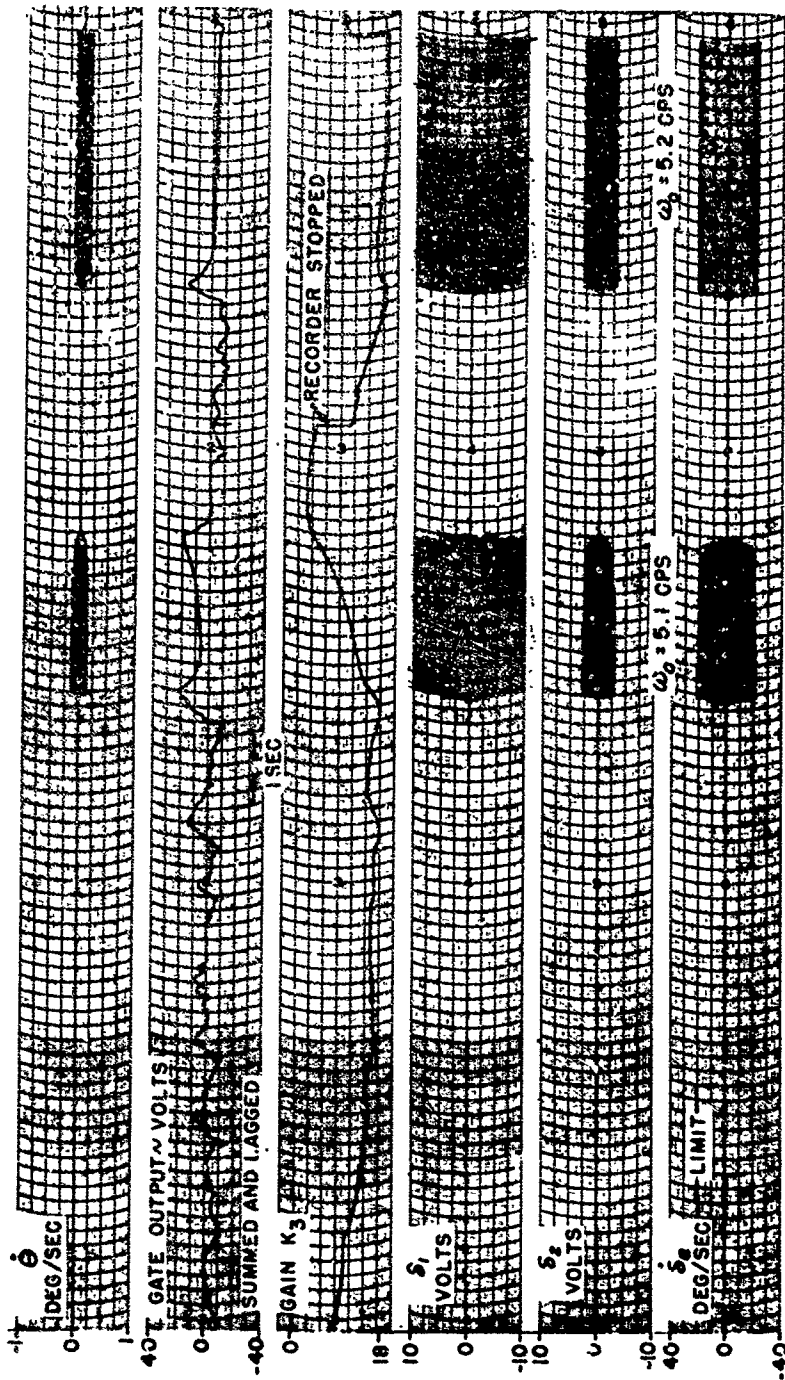
REAC ANALOG



Flight Condition: $\omega_0 = 5.0$ cps
 $t = 90$
 Actuator - Linear
 $\gamma = 0.1$

Figure 35 OPERATION OF FREQUENCY SENSOR WITH LINEAR ACTUATOR

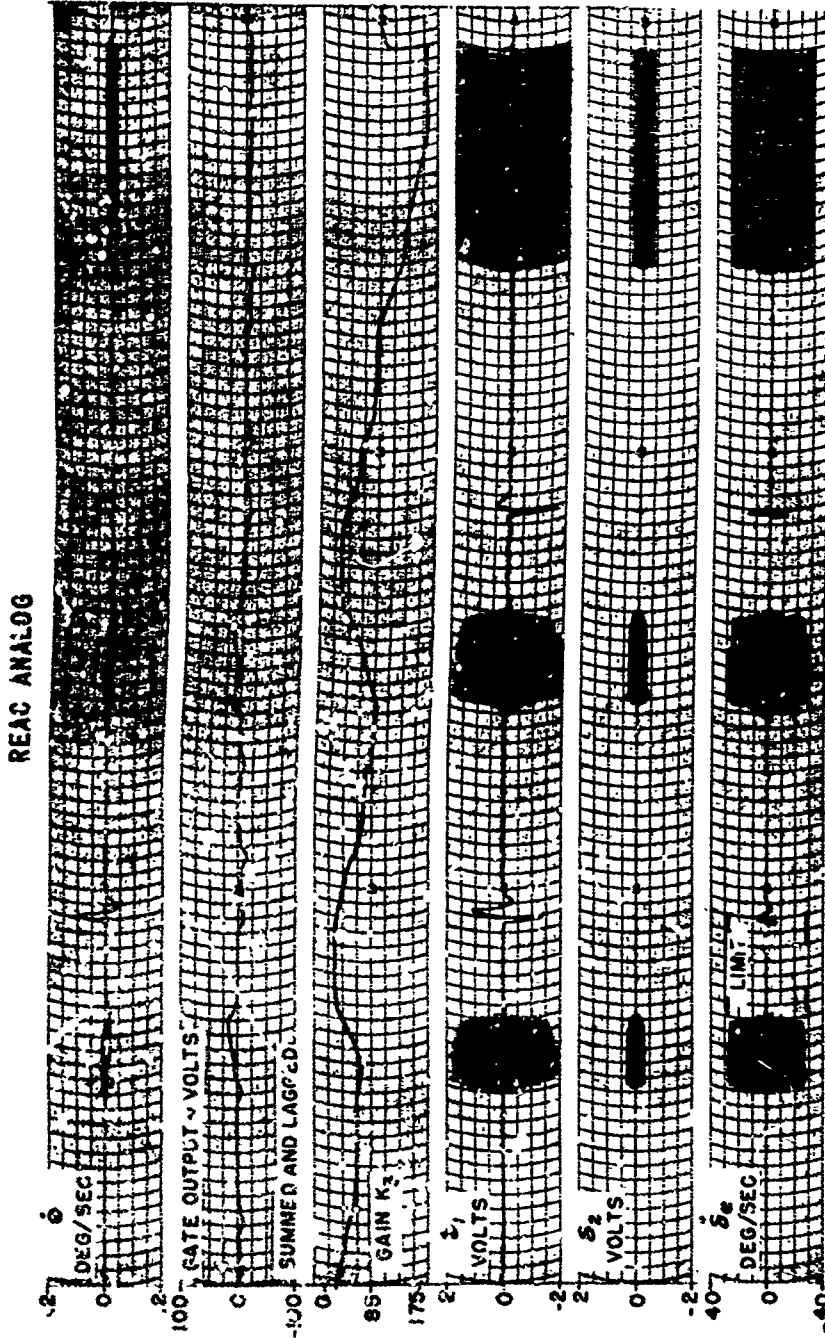
REAC ANALOG



Flight Condition:
t = 90

ACTUATOR - NONLINEAR

Figure 36 OPERATION OF FREQUENCY SENSOR WITH NONLINEAR ACTUATOR
PART a FLIGHT CONDITION t = 90



Flight Condition: $t = 40$ ACTUATOR - NONLINEAR $\omega_0 = 5.3 \text{ cps}$

**Figure 36 OPERATION OF FREQUENCY SENSOR WITH NONLINEAR ACTUATOR
PART b FLIGHT CONDITION $t = 40$**

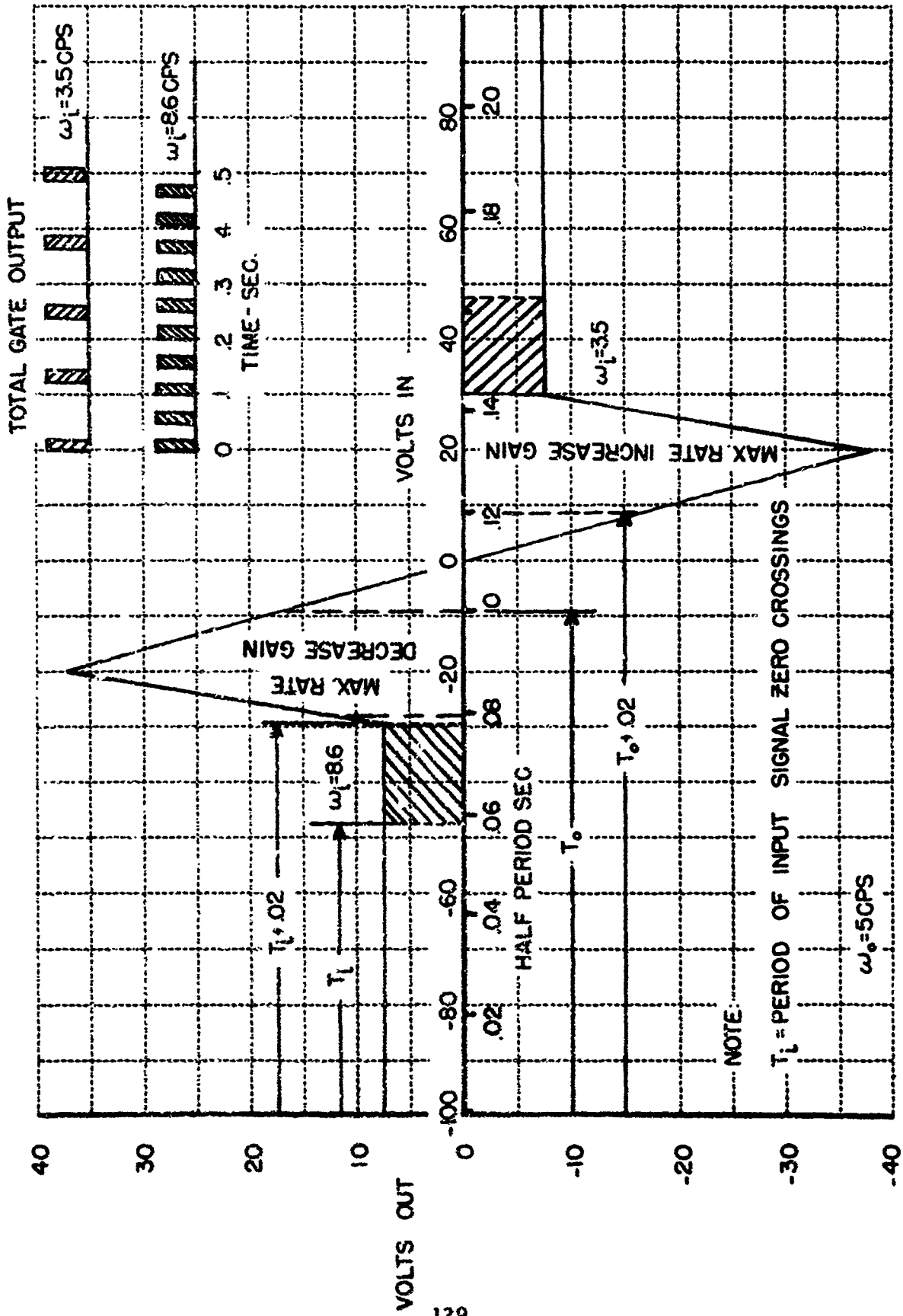


Figure 37 FUNCTION GENERATOR SHAPE AND GATE OUTPUT FOR TWO INPUT FREQUENCIES

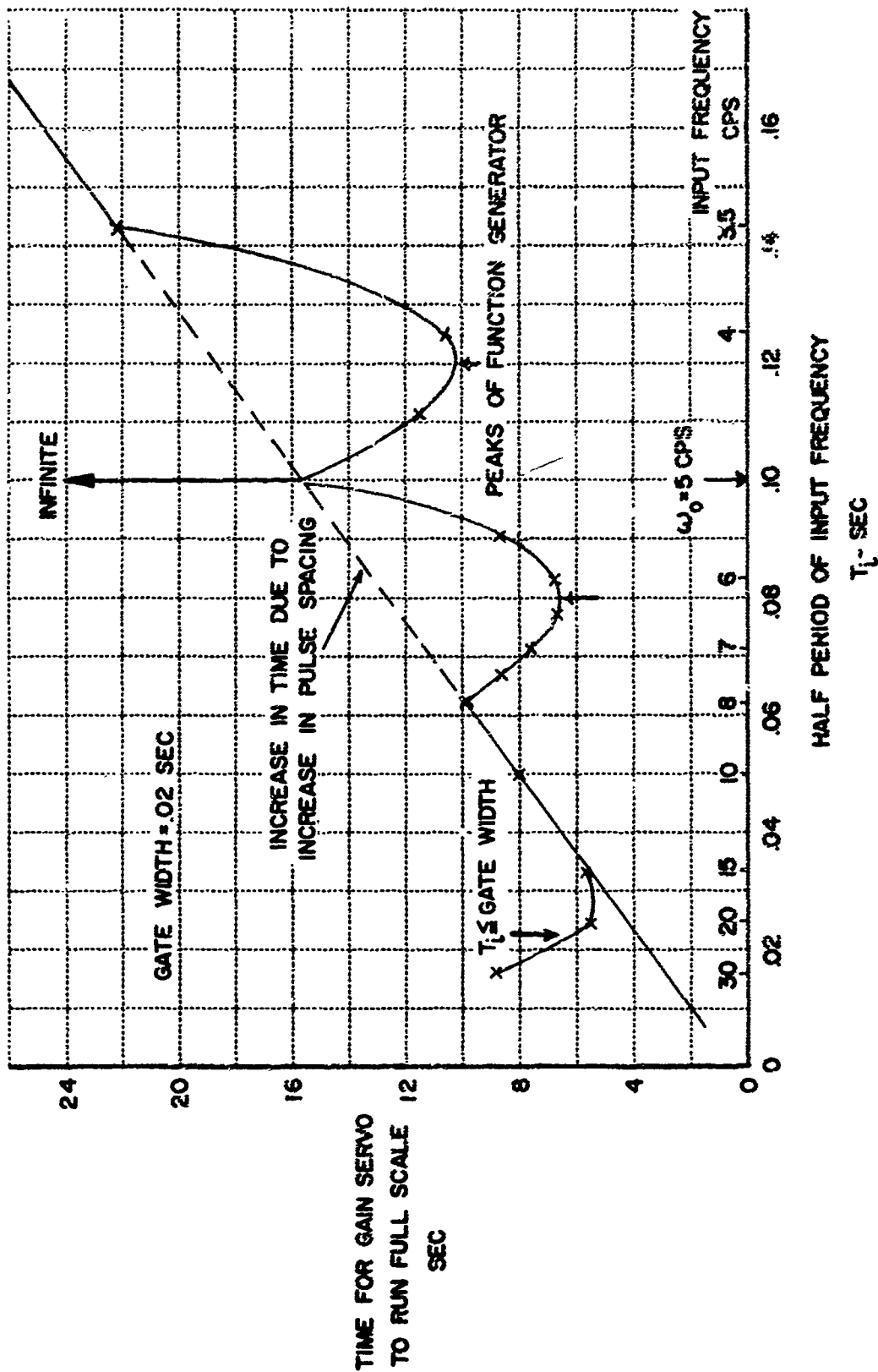


Figure 38 EFFECT OF INPUT FREQUENCY AND FUNCTION GENERATOR ON STEADY-STATE RATE OF GAIN SERVO

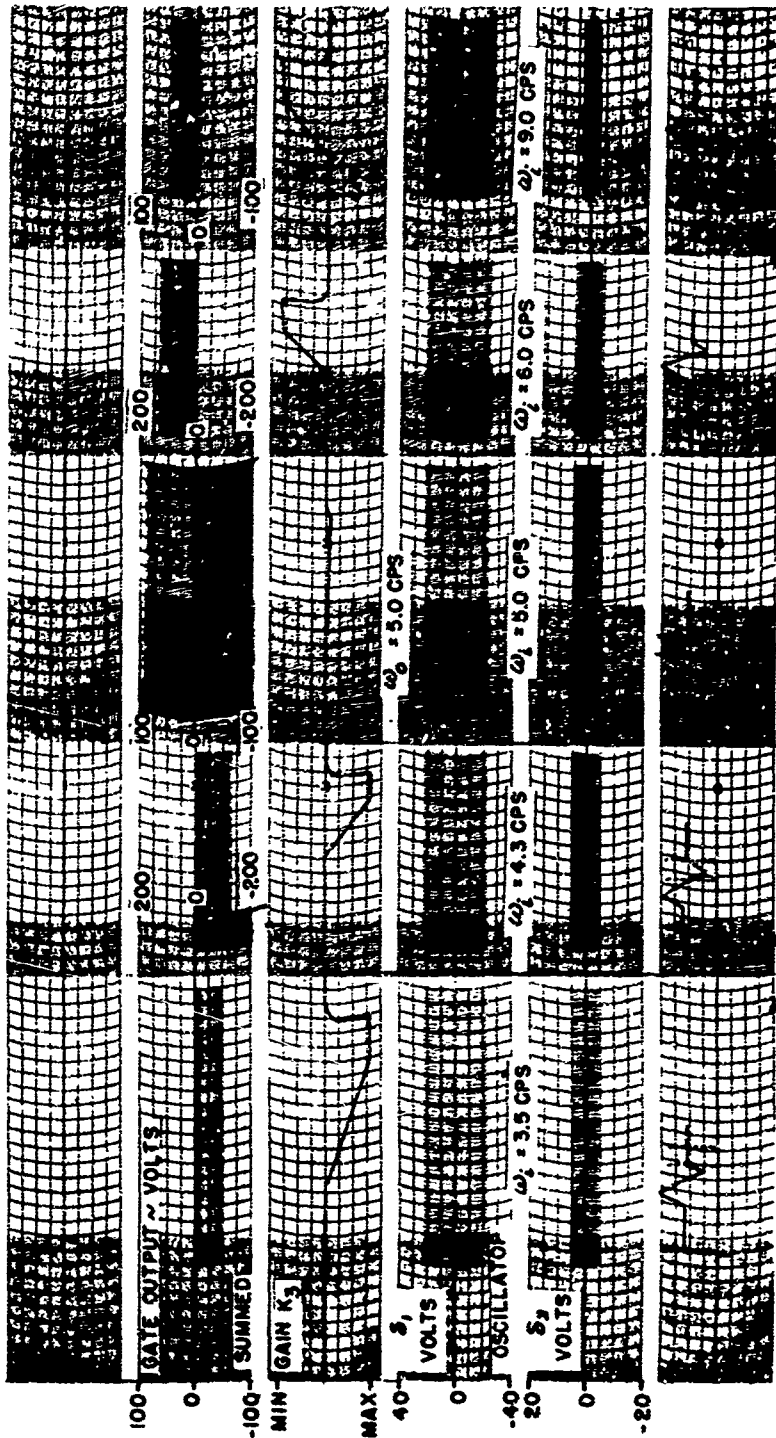


Figure 39 STEADY STATE RATE OF GAIN-SERVO FOR SEVERAL INPUT FREQUENCIES TO THE FREQUENCY SENSOR PART a NO LAG BEFORE INTEGRATOR

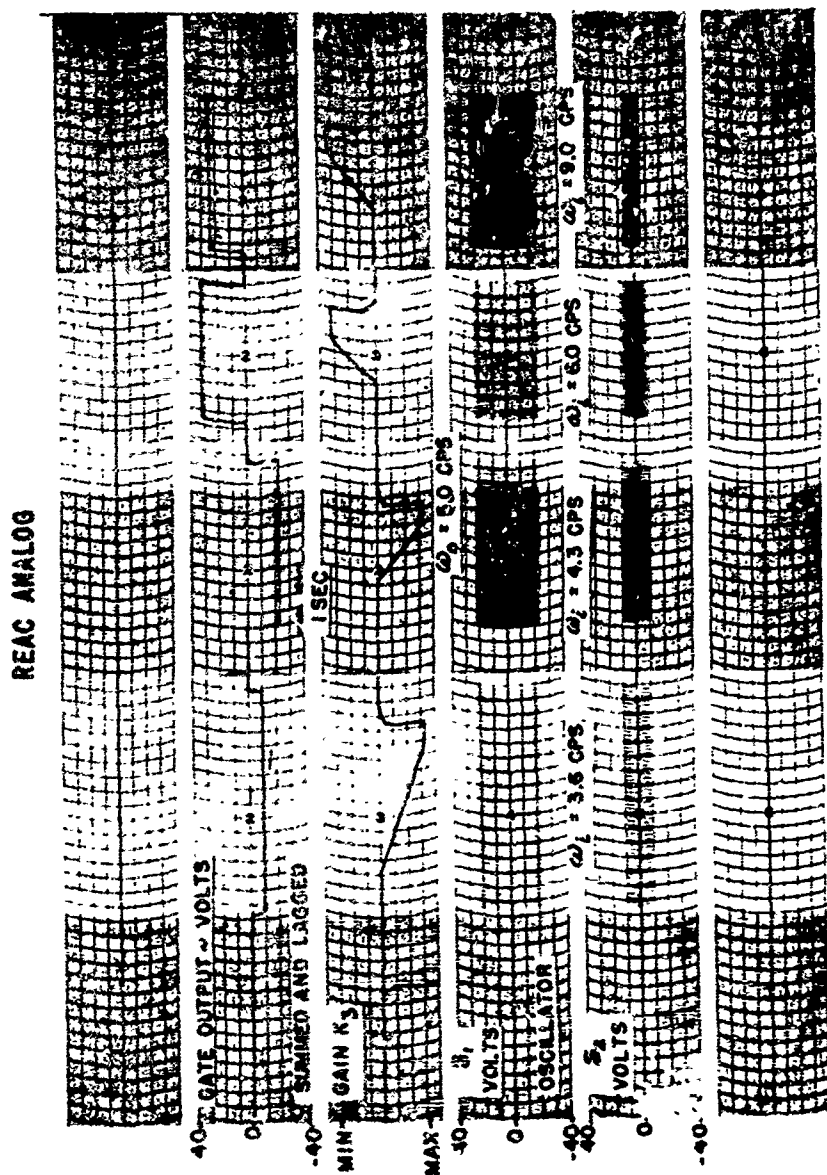


Figure 39 STEADY STATE RATE OF GAIN-SERVO FOR SEVERAL INPUT FREQUENCIES TO THE FREQUENCY SENSOR
PART b ONE-SECOND LAG FILTER BEFORE INTEGRATOR

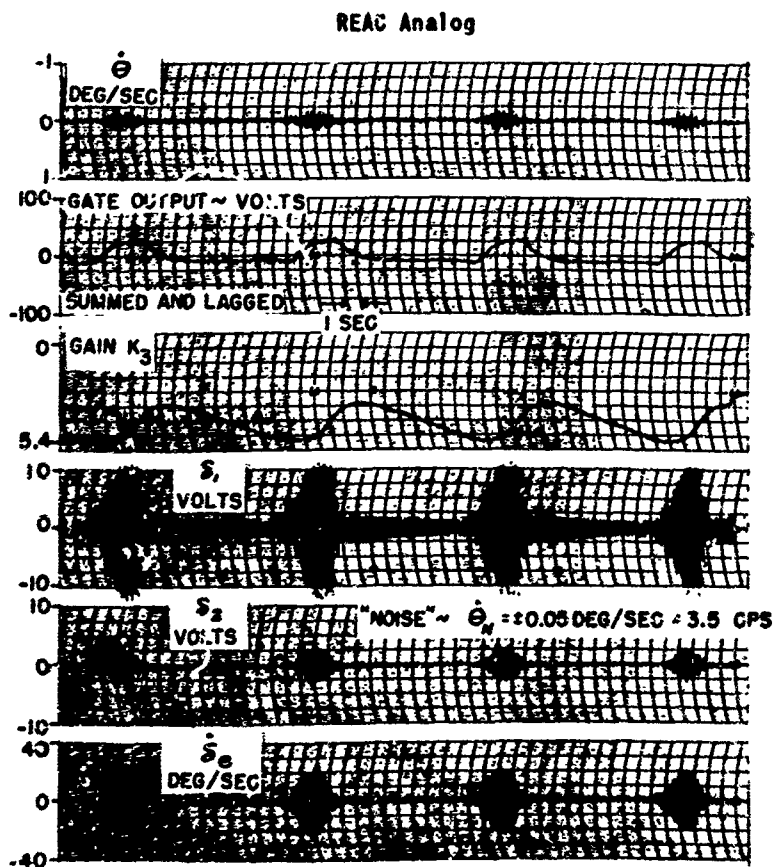
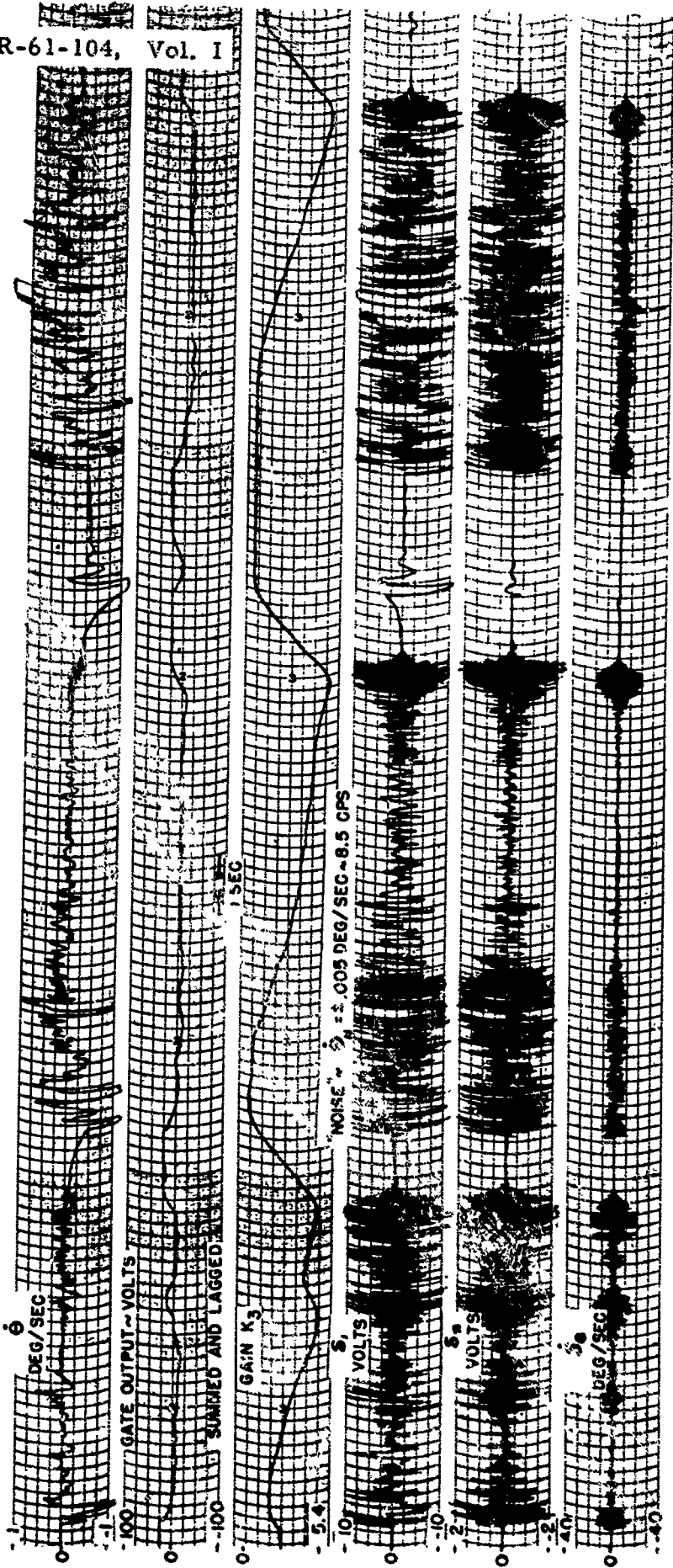


FIGURE 40 EFFECT OF NOISE IN RATE GYRO OUTPUT ON OPERATION OF FREQUENCY SENSOR AND GAIN SERVO

Part a Continuous $\pm 0.05^\circ/\text{sec}$ Sine Wave Input at 3.5 cps

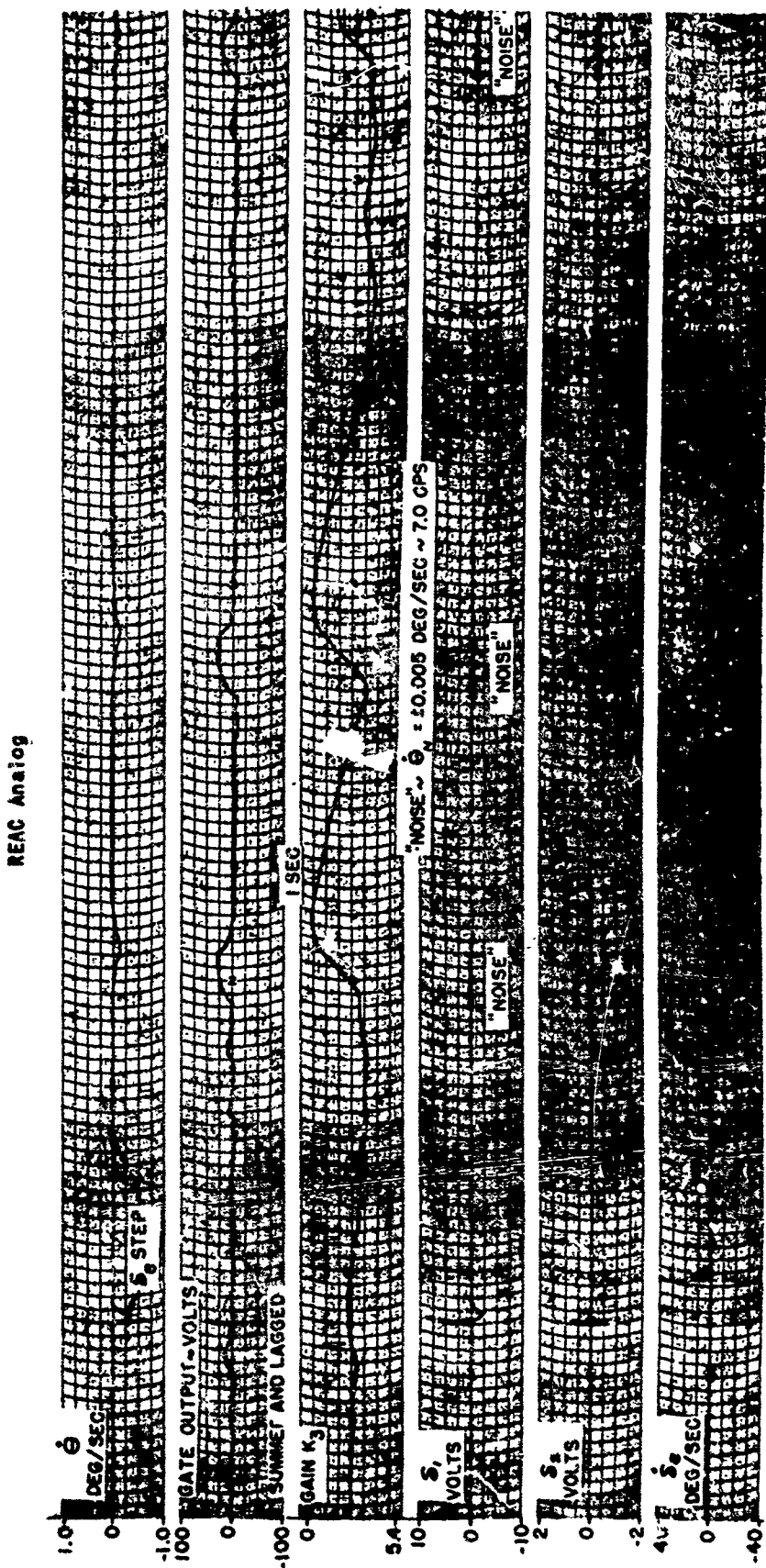
REAC Analog



Flight Condition: $t = 90$ Actuator - Linear $\omega_0 = 5.0$ cps
 $\zeta = 0.1$ sec

FIGURE 40 EFFECT OF NOISE IN RATE GYRO OUTPUT ON OPERATION OF FREQUENCY SENSOR AND GAIN SERVO

Part b Continuous $\pm 0.005^\circ$ /sec Sine Wave Input at 8.5 cps with "Pilot" Disturbances



Flight Condition: $\zeta = 9\%$ Actuator - Linear $\omega_0 = 5.0$ cps
 $\tau = 0.1$ sec

FIGURE 40 EFFECT OF NOISE IN RATE GYRO OUTPUT ON OPERATION OF FREQUENCY SENSOR AND GAIN SERVO

Part c Intermittent $\pm .005^\circ/\text{sec}$ Sine Wave Input at 7.0 cps

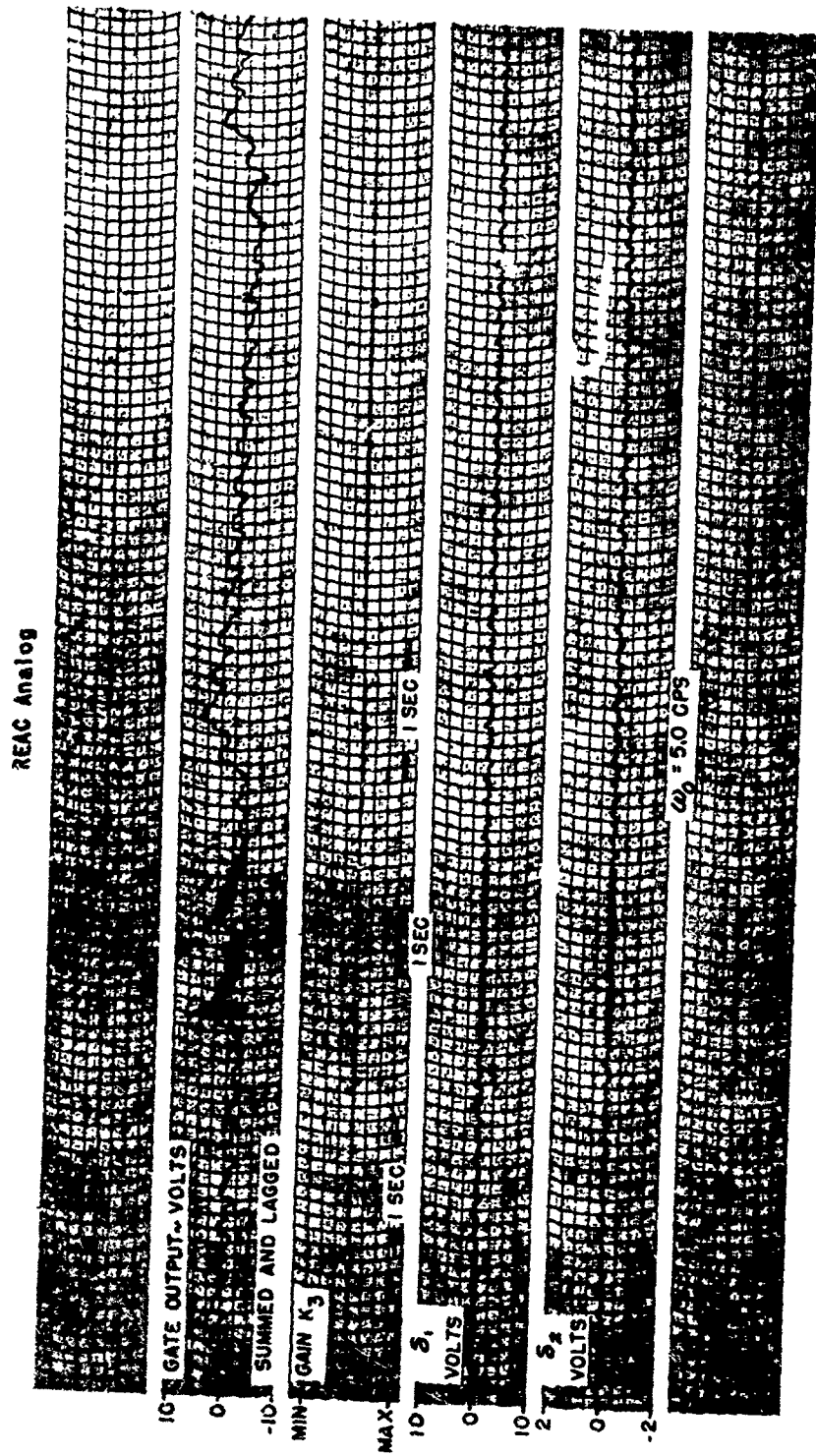


FIGURE 41 RESPONSE OF FREQUENCY SENSOR AND GAIN SERVO TO INPUT SIGNAL COMPOSED OF TWO SINUSOIDS

Part a $\omega_1 = 3.5$ cps at 1.1 volts, $\omega_2 = 8.3$ cps at 1.6 volts

REAC Analog

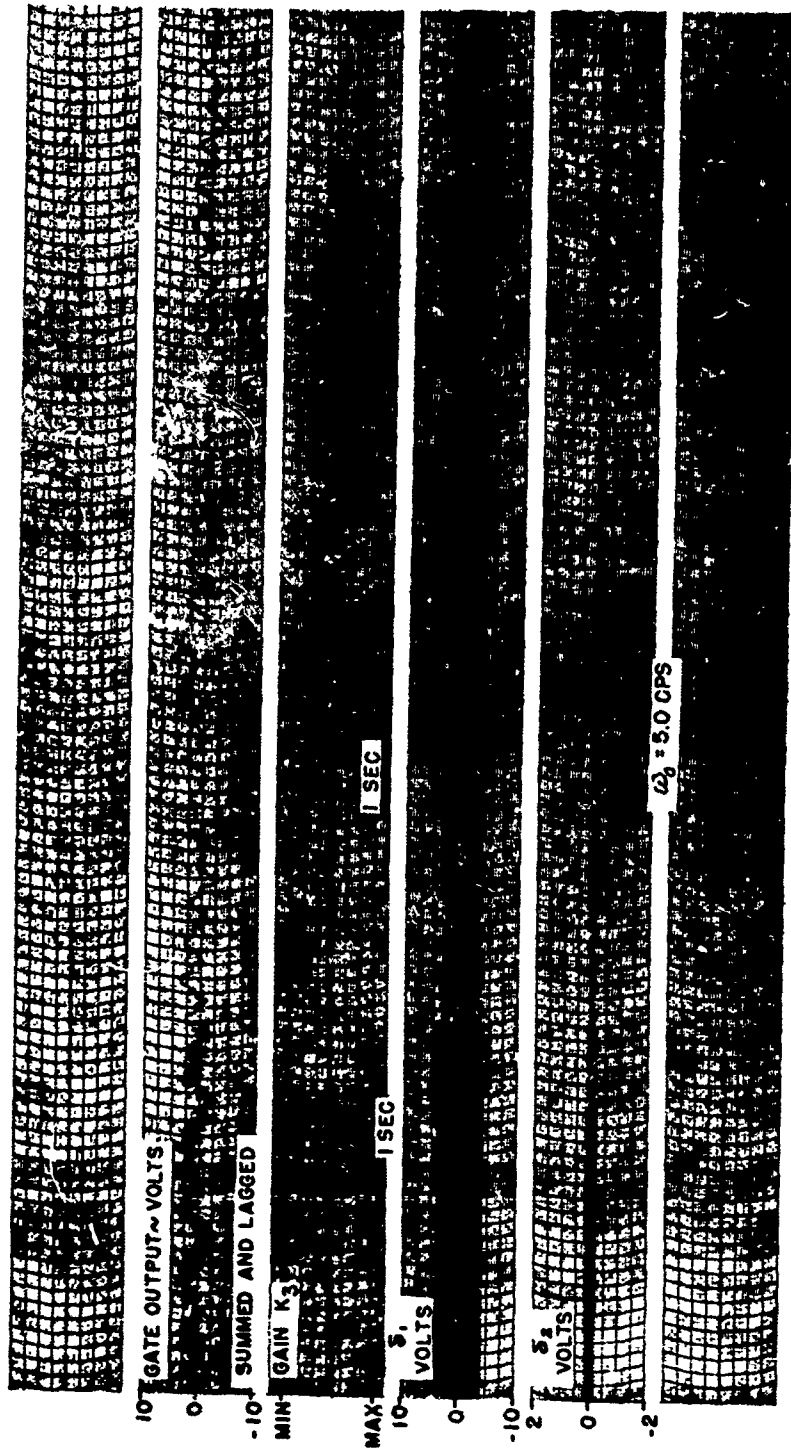


FIGURE 41 RESPONSE OF FREQUENCY SENSOR AND GAIN SERVO TO INPUT SIGNAL COMPOSED OF TWO SINUSOIDS

Part b $\omega_1 = 3.5$ cps at 1.1 volts, $\omega_2 = 20$ cps at 8.6 volts

REAC Analog

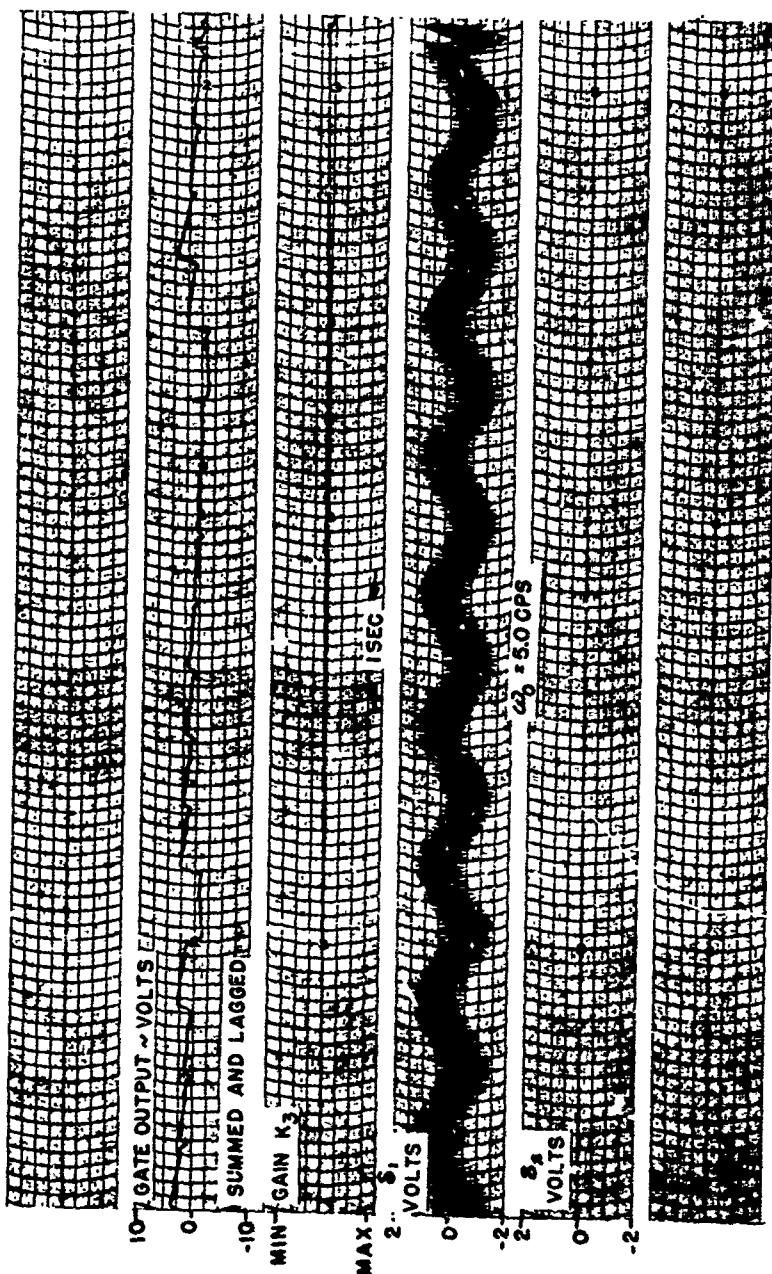


FIGURE 41 RESPONSE OF FREQUENCY SENSOR AND GAIN SERVO TO INPUT SIGNAL COMPOSED OF TWO SINUSOIDS

Part c $\omega_1 = 0.66$ cps at 1.1 volts, $\omega_2 = 20$ cps at 2.1 volts

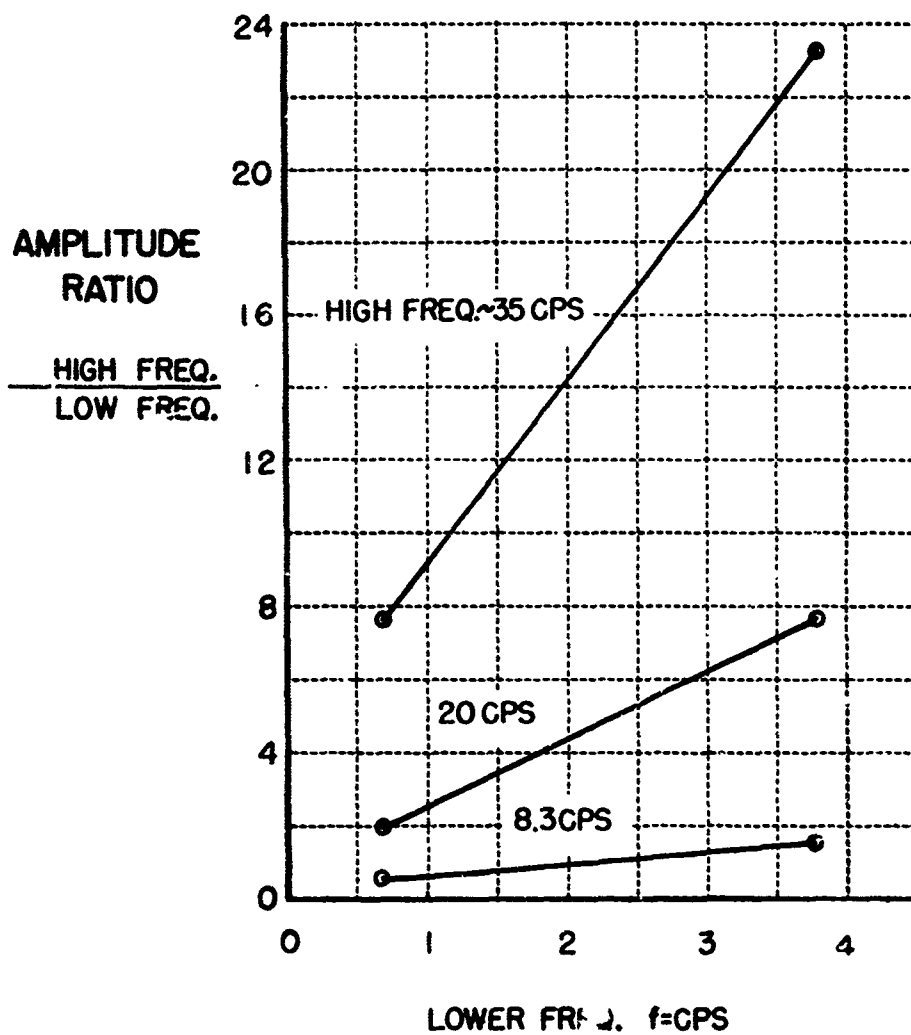


FIGURE 42 RELATIVE AMPLITUDE OF TWO SINE WAVES RESULTING IN NO GAIN CHANGE

APPENDIX A
AIRPLANE EQUATIONS AND PARAMETERS USED IN THE STUDY

The following equations of motion were used to represent the airplane. They assume that there is no speed change, and that the incremental effects of gravity can be neglected.

$$\left. \begin{aligned} \ddot{\Theta} &= M_q \dot{\Theta} + M_{\dot{\alpha}} \dot{\alpha} + M_{\alpha} \alpha + M_{\delta_e} \delta_e \\ \dot{\alpha} &= \dot{\Theta} - L_{\alpha} \dot{\Theta} - L_{\delta_e} \delta_e \\ \dot{\sigma} &= \dot{\Theta} - \dot{\alpha} \end{aligned} \right\} \quad (\text{A-1})$$

The equations imply that the reference axes are stability axes (wind axes if no lateral motions are present) and that the wings are always level so that

$$\dot{\Theta} = q$$

The reference condition for these equations is not equilibrium flight, but is rather a precomputed re-entry flight path. The dependent variables, $(\Theta, \alpha, \delta_e, \text{ and } \sigma)$ are the incremental values from the reference condition.

The following transfer functions arise from Equations (A-1), and are of use in interpreting the analog solutions and root locus plots.

$$\frac{\dot{\Theta}(s)}{\delta_e(s)} = \frac{s(M_{\delta_e} - L_{\delta_e} M_{\dot{\alpha}}) + (M_{\delta_e} L_{\alpha} - M_{\alpha} L_{\delta_e})}{s^2 + s(L_{\alpha} - M_q - M_{\dot{\alpha}}) + (-M_{\alpha} - M_q L_{\alpha})} \quad (\text{A-2})$$

$$\frac{\alpha(s)}{\delta_e(s)} = \frac{s(-L_{\delta_e}) + (M_{\delta_e} + M_q L_{\delta_e})}{s^2 + s(L_{\alpha} - M_q - M_{\dot{\alpha}}) + (-M_{\alpha} - M_q L_{\alpha})} \quad (\text{A-3})$$

$$\frac{\dot{\sigma}(s)}{\delta_e(s)} = \frac{L_{\delta_e} s^2 + s(-L_{\delta_e} M_q - L_{\delta_e} M_{\dot{\alpha}}) + (M_{\delta_e} L_{\alpha} - M_{\alpha} L_{\delta_e})}{s^2 + s(L_{\alpha} - M_q - M_{\dot{\alpha}}) + (-M_{\alpha} - M_q L_{\alpha})} \quad (\text{A-4})$$

The natural frequency and damping in these transfer functions may be expressed as:

$$\omega_H = \sqrt{-M_\alpha - M_g L_\alpha} \quad (\text{A-5})$$

$$\zeta = \frac{L_\alpha - M_g - M_\alpha}{2\omega_H} \quad (\text{A-6})$$

The transfer functions may be written in lumped parameter form as:

$$\frac{\dot{\theta}(s)}{\delta_e(s)} = \frac{K_\theta (\gamma_\theta s + 1)}{\left(\frac{s}{\omega_H}\right)^2 + \frac{2\zeta}{\omega_H} s + 1} \quad (\text{A-7})$$

$$\frac{\alpha(s)}{\delta_e(s)} = \frac{K_\alpha (\gamma_\alpha s + 1)}{\left(\frac{s}{\omega_H}\right)^2 + \frac{2\zeta}{\omega_H} s + 1} \quad (\text{A-8})$$

$$\frac{\dot{\sigma}(s)}{\delta_e(s)} = \frac{K_\sigma (b_\sigma s^2 + a_\sigma s + 1)}{\left(\frac{s}{\omega_H}\right)^2 + \frac{2\zeta}{\omega_H} s + 1} \quad (\text{A-9})$$

$$n_\sigma = \frac{V}{g} \dot{\sigma} \quad (\text{A-10})$$

$$a_\sigma = -V \dot{\sigma} \quad (\text{A-11})$$

where

$$K_\theta = \frac{M_g L_\alpha - M_\alpha L_g}{-M_\alpha - M_g L_\alpha} \quad (\text{A-12})$$

$$K_\alpha = \frac{M_g + M_g L_g}{-M_\alpha - M_g L_\alpha} \quad (\text{A-13})$$

$$\gamma_\theta = \frac{M_g - L_g M_\alpha}{M_g L_\alpha - M_\alpha L_g} \quad (\text{A-14})$$

$$\gamma_\alpha = \frac{-L_g}{M_g + M_g L_g} \quad (\text{A-15})$$

$$K_\sigma = K_\theta \quad (\text{A-16})$$

$$b_{\dot{\theta}} = \frac{L_S}{M_S L_\alpha - M_\alpha L_S} \quad (\text{A-17})$$

$$a_{\dot{\theta}} = \frac{-L_S M_q - L_S M_{\dot{\alpha}}}{M_S L_\alpha - M_\alpha L_S} \quad (\text{A-18})$$

Flight conditions have been selected at various times during a typical X-15 re-entry for the design altitude mission (Reference 8). The flight condition data for this re-entry are given in Table I, the numerical data for the equations of motion in Table II, and the lumped parameters for the $\dot{\theta}/\delta_e$ and the α/δ_e transfer functions in Table III.

APPENDIX B

ESIAC COMPUTER AND ROOT LOCUS COORDINATES

The root locus technique is used in this study as the primary analytical tool for handling linearized problems. The ESIAC computer is used to physically compute and plot these root loci. This computer greatly facilitates this work, but it uses coordinates which are different from those normally used. The purpose of this appendix is to describe these coordinates and show their relation to the normal root locus coordinates.

Description of the ESIAC

The ESIAC solves the equation

$$F = Ks^n \prod_{i=1}^m (1 - \frac{s}{s_i})^{\ell} \quad \ell = +1, -1, +2, -2$$

or

$$F = Ks^n \prod_{i=1}^m (s - s_i)^{\ell}$$

where the s_i are the complex poles (for $\ell = -1, -2$) and zeros (for $\ell = +1, +2$) of the complex polynomial F . K is the gain.

The ESIAC consists of a console with a plotting board at the center, two electrical potential analogy sheets located on either side, and controls as shown on Figure 43. A frame positions moving probes on the potential analogy sheets.

The ESIAC contains two separate analog circuits - one for the magnitude of F , $|F|$, and the other for the angle of F , $\angle F$. In setting up a problem, a pattern of probes is placed in the frame over each sheet at positions corresponding to the s_i 's (the zeros and poles) in the equation. The frames are then moved over the sheets to positions corresponding to values of the complex variable s . The voltage distributions on the sheets are such that the voltage at each probe represents on one sheet the magnitude

and on the other sheet the angle of one of the $(S - s_i)$ or $(1 - S/s_i)$ factors. The exponent ℓ on each factor is established by selecting the value of an electric coupling element in the clamp which attaches the probe to the frame. Dials on the panel provide for setting the values of F , K , and S , and for selecting the sign of K , the value of the exponent n , and the form of the general factor $(S - s_i)$ or $(1 - S/s_i)$.

When the controls representing all the parameters in the equation are adjusted to any combination of values for which the two sides of the equation are equal, a pair of electrical null indicators, one for the magnitude and one for the angle, show the condition of equality. After the values of all given or assumed parameters have been set, the equation is solved simply by adjusting the value of the unknown until null balances are obtained.

For root finding or root locus plotting, the motion of the probe assembly is directly coupled to the stylus on the plotting board. For automatic plotting, the probe assembly is moved to scan values of S , and whenever a magnitude or angle balance is passed, the stylus automatically marks the position on the plotting board. A line joining the marks for magnitude balance is the solution of the magnitude equation, and similarly a line joining the marks for angle balance is the solution of the angle equation. The value of S at each intersection of these lines is therefore a root of the complex equation.

To use the ESIAC for frequency response plotting, the position of the probe assembly in the coordinate representing $\angle S$ is fixed at 90° , and its motion in the $|S|$ direction is coupled to the plotting assembly in the horizontal direction. The vertical motion of the plotting stylus is coupled to the $|F|$ dial for gain plotting or to the $\angle F$ dial for phase plotting. When the circuit is balanced at various values of $|S|$, the stylus plots the log gain or phase angle versus log frequency.

Since the plotting stylus is directly coupled to the dials, it is not necessary to read the dials while making these plots. The stylus is simply

moved about over the plotting paper and the automatic marking circuit plots the curves.

Coordinates for Root Locus Plots

The polar coordinates are the magnitude, $|S|$, and angle, $\angle S$, of the complex variable S . The ESIAC coordinates for the root locus plots are a transformation of the polar coordinates of the $S = \sigma + j\omega$ plane. The transformation is shown in the accompanying three-step diagram, Figure 44. The horizontal scale, ω_n , is logarithmic. The vertical scale is in degrees with corresponding damping ratios at $\cos^{-1}0.1$, $\cos^{-1}0.2$, ... etc.

On Figure 45 are root locus plots of the function,

$$-1 = K \frac{(1 - \frac{S}{-0.2})(1 - \frac{S}{-1.0})}{(1 - \frac{S}{0.22 + 0.20j})(1 - \frac{S}{0.22 - 0.20j})}$$

in both polar and ESIAC coordinates. Note that the pole at the origin is not shown on ESIAC coordinates; however, the information is programmed in the computer electronically.

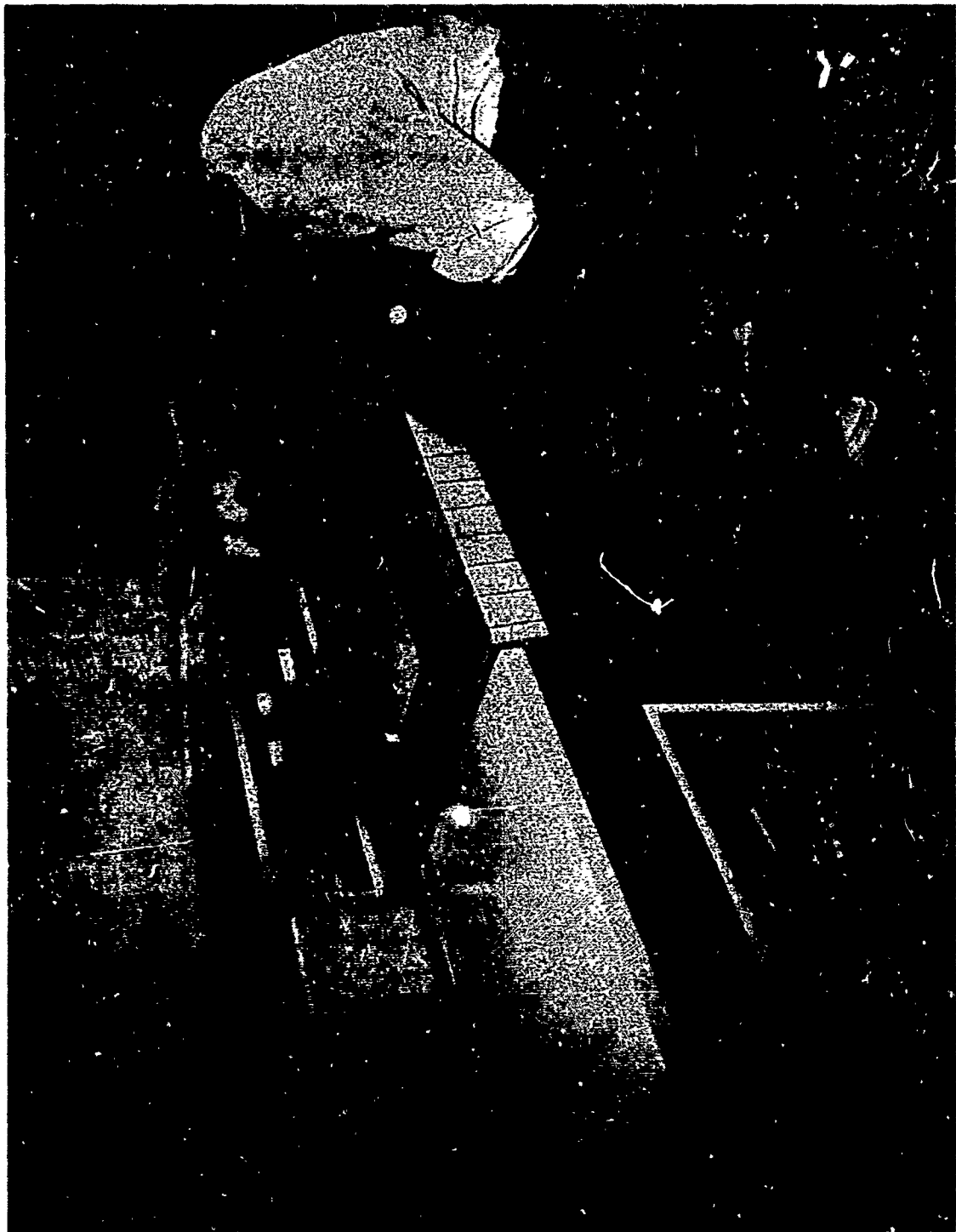
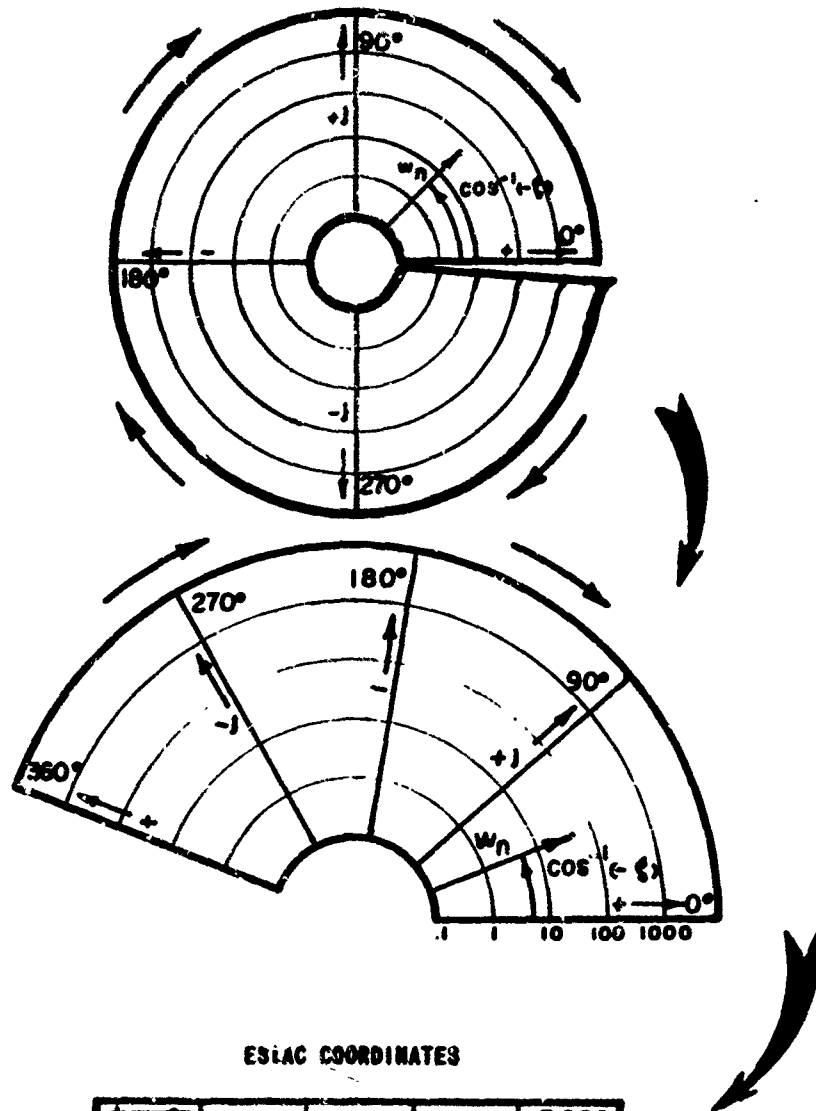


FIGURE 43 THE FLIGHT RESEARCH DEPARTMENT ESIAC

146

ASD-TR-61-104, Vol. I

POLAR IMAGINARY COORDINATES



ESLAC COORDINATES

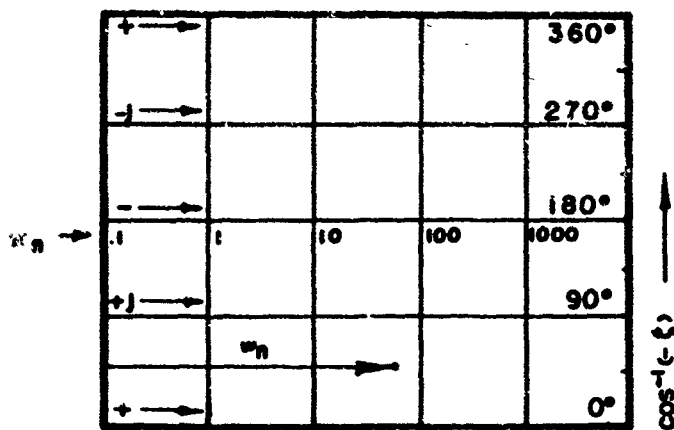


FIGURE 44 ROOT LOCUS COORDINATES

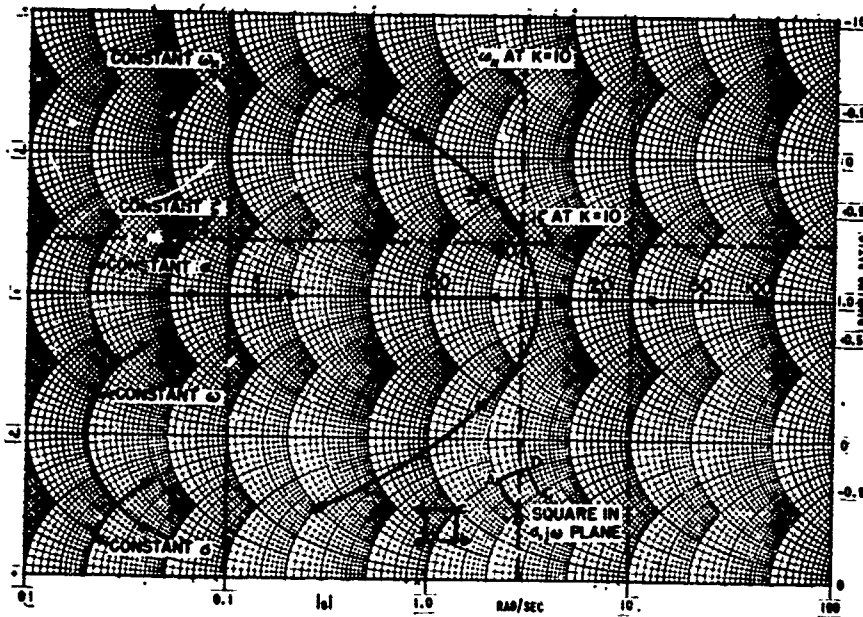
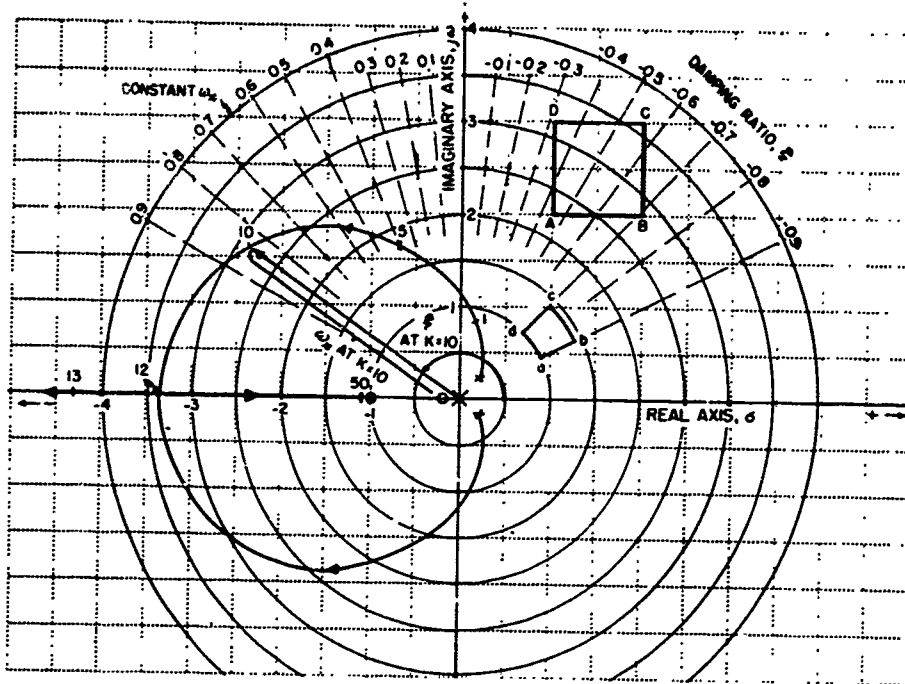


Figure 45 ROOT LOCUS PLOT OF THE FUNCTION

$$-1 = K \frac{(1 - \frac{s}{0.2})(1 - \frac{s}{-1.0})}{(s - \frac{0.22 + 0.20j})(s - \frac{0.22 - 0.20j})}$$

ASD-TR-61-104, Vol. I

APPENDIX C
EASE ANALOG COMPUTER SCHEMATIC DIAGRAMS

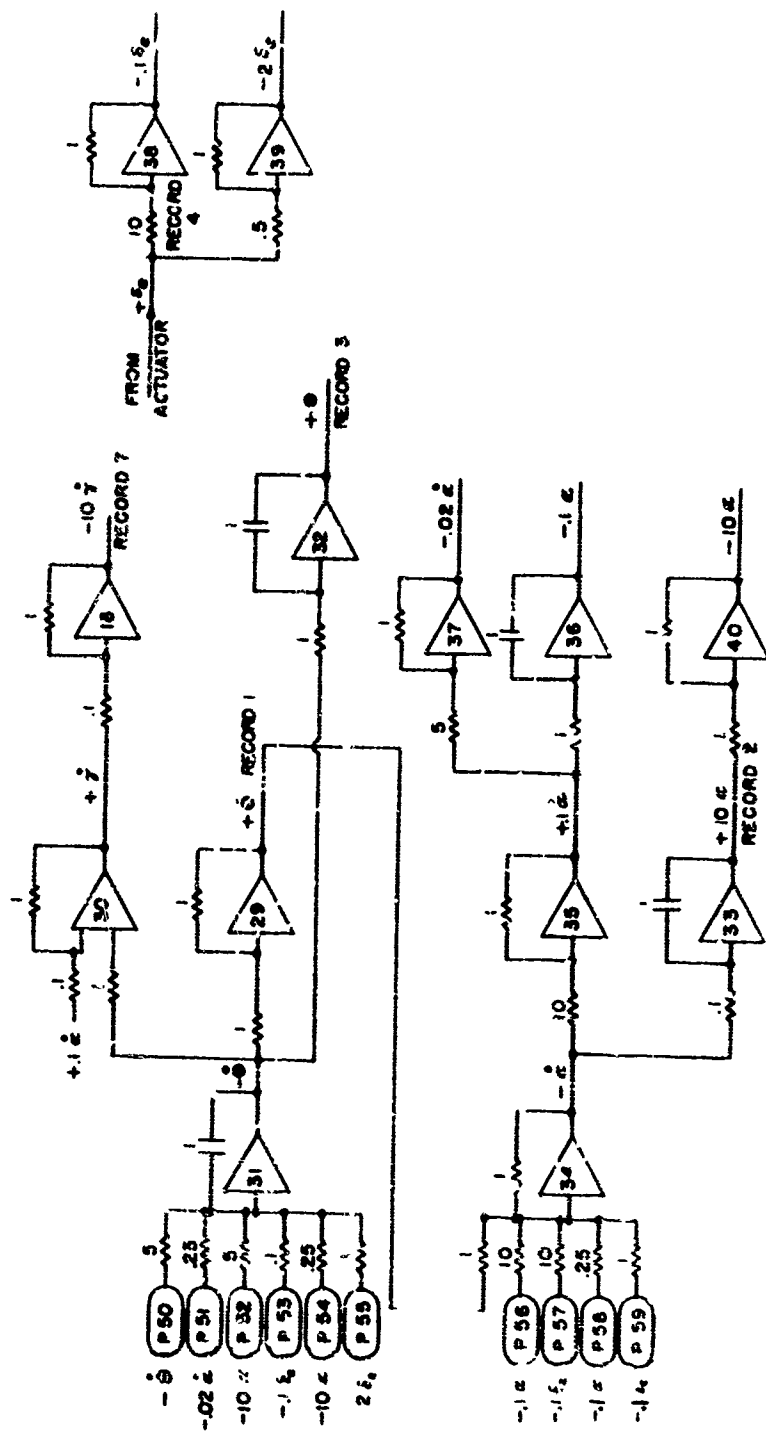


FIGURE 46 ANALOG SCHEMATIC - AIRCRAFT

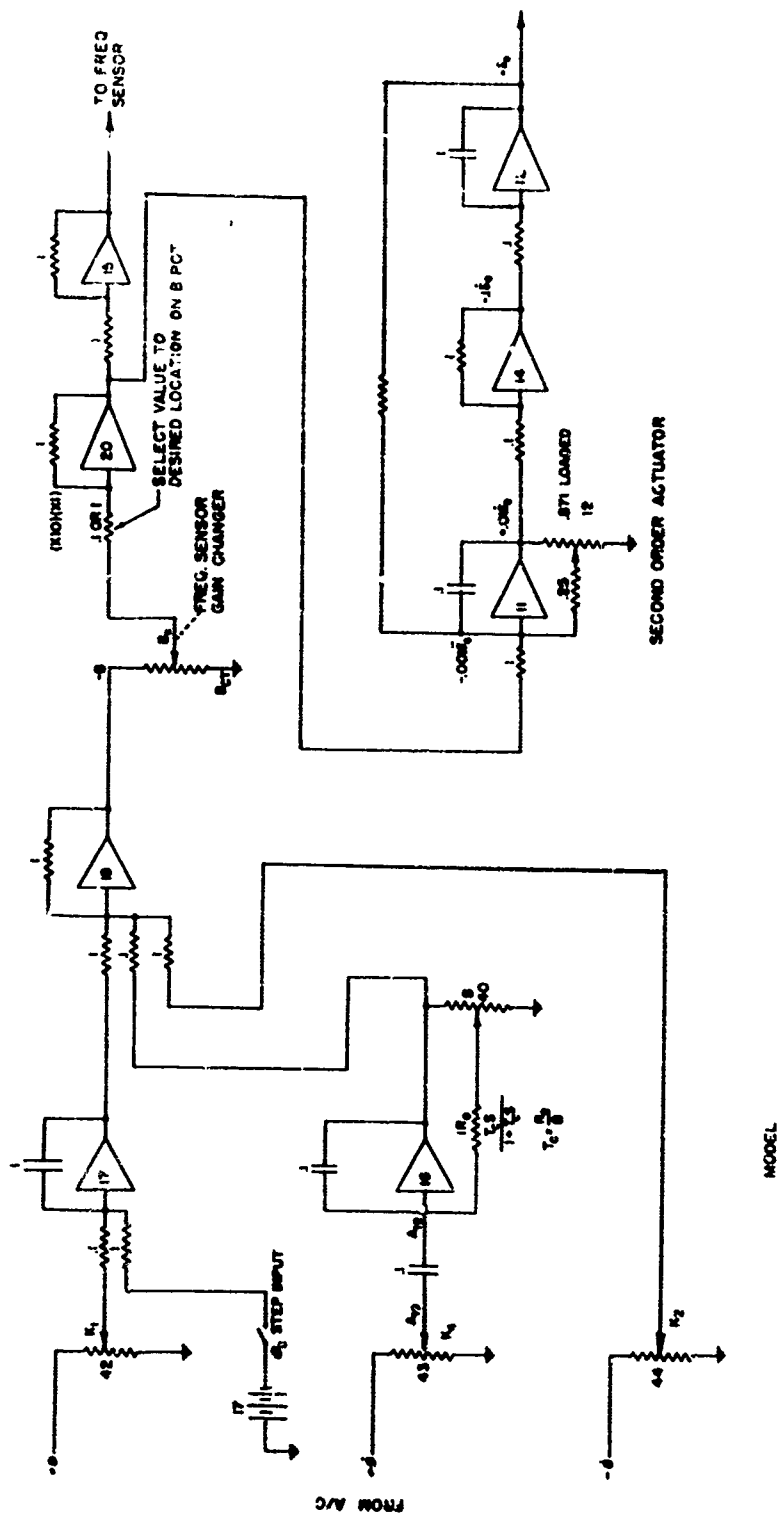


FIGURE 47 ANALOG SCHEMATIC - CONTROL SYSTEM

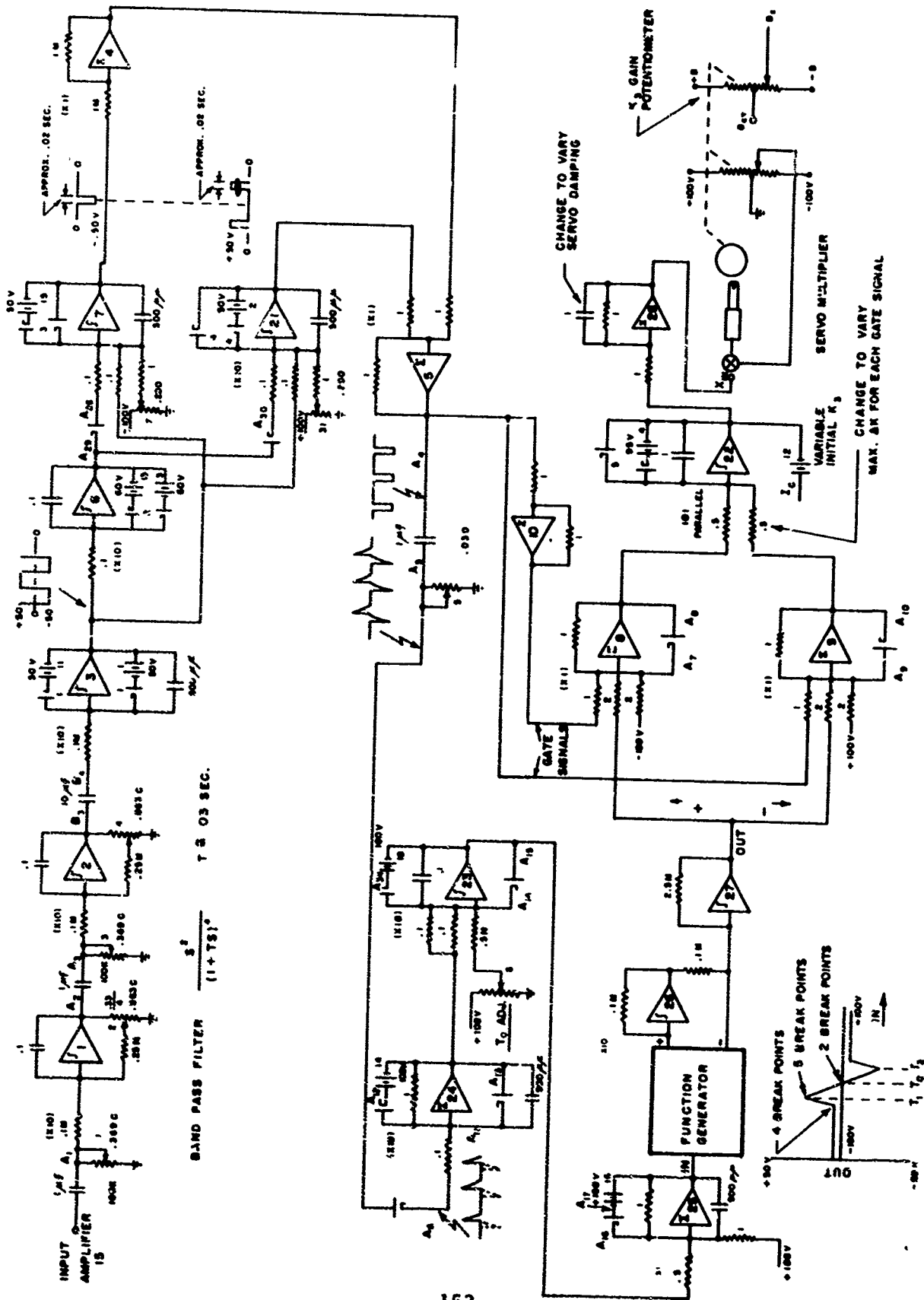


Figure 48 ANALOG SCHEMATIC - FREQUENCY SENSOR

TABLE VI

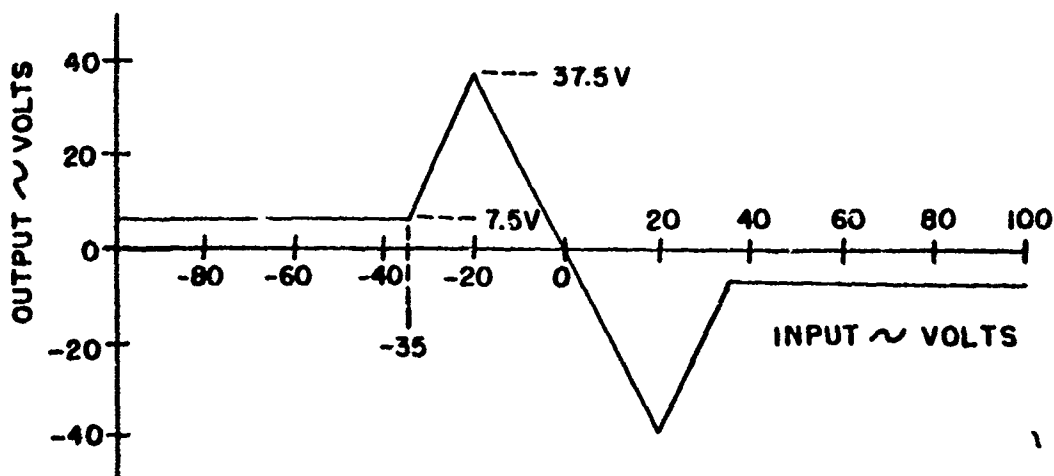
COEFFICIENT POTENTIOMETER SETTINGS FOR
ANALOG SIMULATION OF X-15

These potentiometer settings are for the analog simulation shown in Figure 10, and correspond to the data of Table I.

	t = 0		t = 20		t = 40		t = 60		t = 74		t = 90		Load
	U*	L*	U	L	U	L	U	L	U	L	U	L	
P50	.0055	.0055	.010	.010	.039	.039	.298	.299	.771	.774	.661	.664	5M
P51	.005	.005	.009	.009	.034	.035	.260	.280	.674	.727	.579	.633	.25M
P52	.0785	.0785	.159	.159	.754	.757	0	-	0	-	0	-	5M
P53	.113	.126	.232	.278	0	-	0	-	0	-	0	-	.1M
P54	0	-	0	-	0	-	.278	.301	.660	.713	.428	.470	.25M
P55	0	-	0	-	.058	.062	.426	.532	.875	.932	.610	.730	.1M
P56	.160	.160	.340	.340	0	-	0	-	0	-	0	-	10M
P57	.020	.020	.040	.040	.220	.220	0	-	0	-	0	-	10M
P58	0	-	0	-	.036	.037	.280	.303	.699	.750	.692	.744	.25M
P59	0	-	0	-	0	-	.172	.174	.417	.427	.372	.381	1M

*U = Unloaded, *L = Loaded

NUMERICAL DATA FOR FUNCTION GENERATOR
IN THE FREQUENCY SENSOR



APPENDIX D
REAC ANALOG COMPUTER SCHEMATIC DIAGRAMS

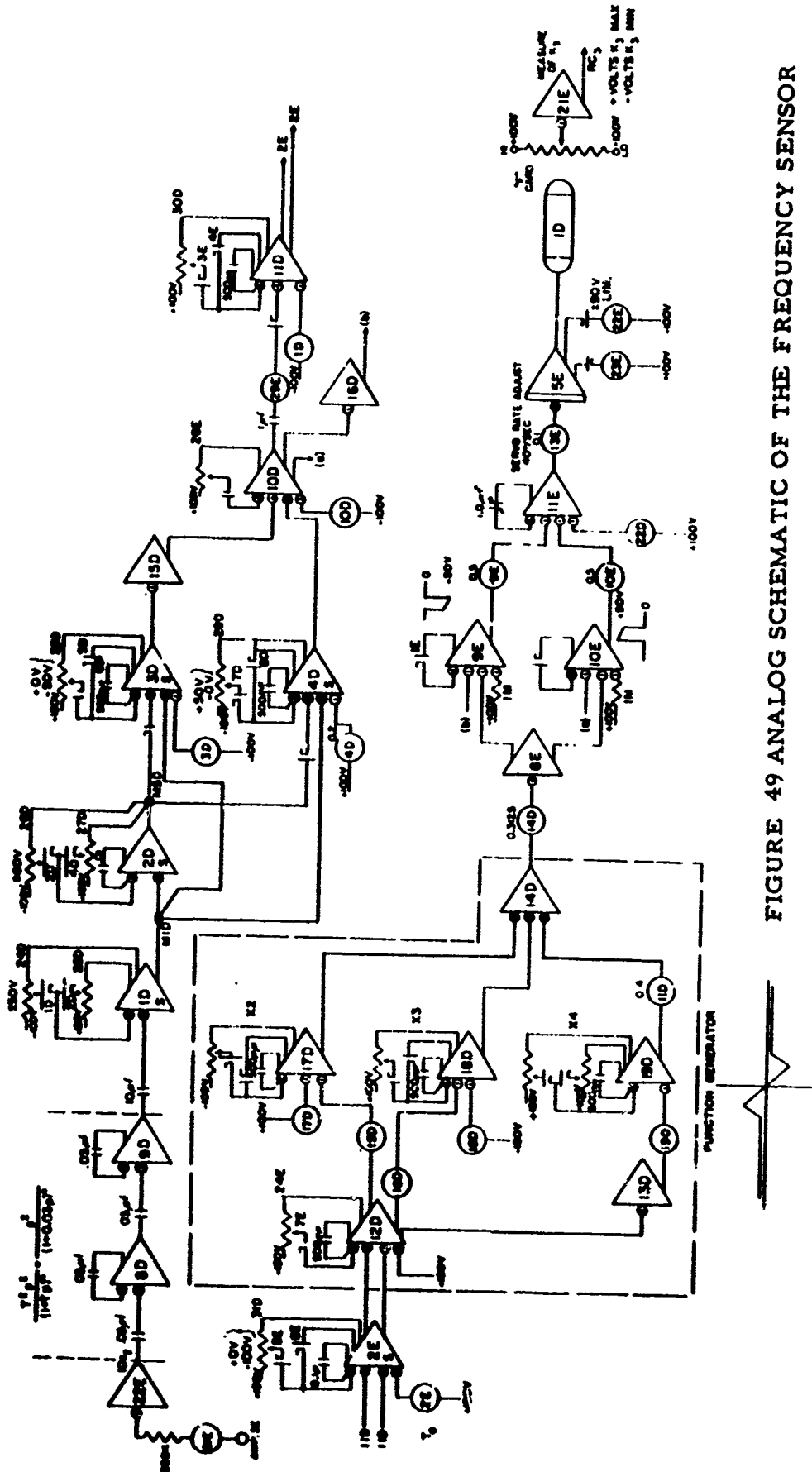


FIGURE 49 ANALOG SCHEMATIC OF THE FREQUENCY SENSOR

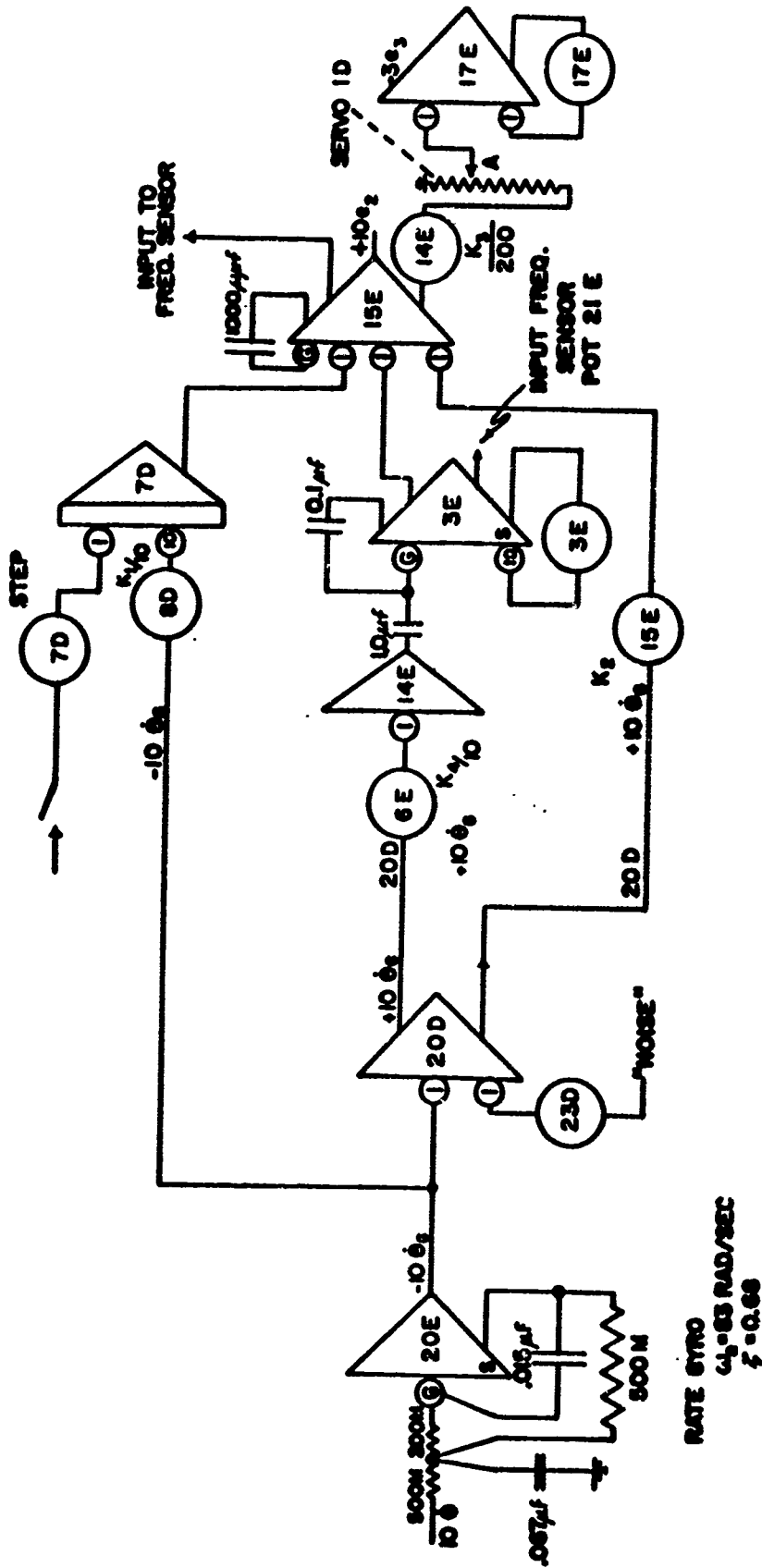
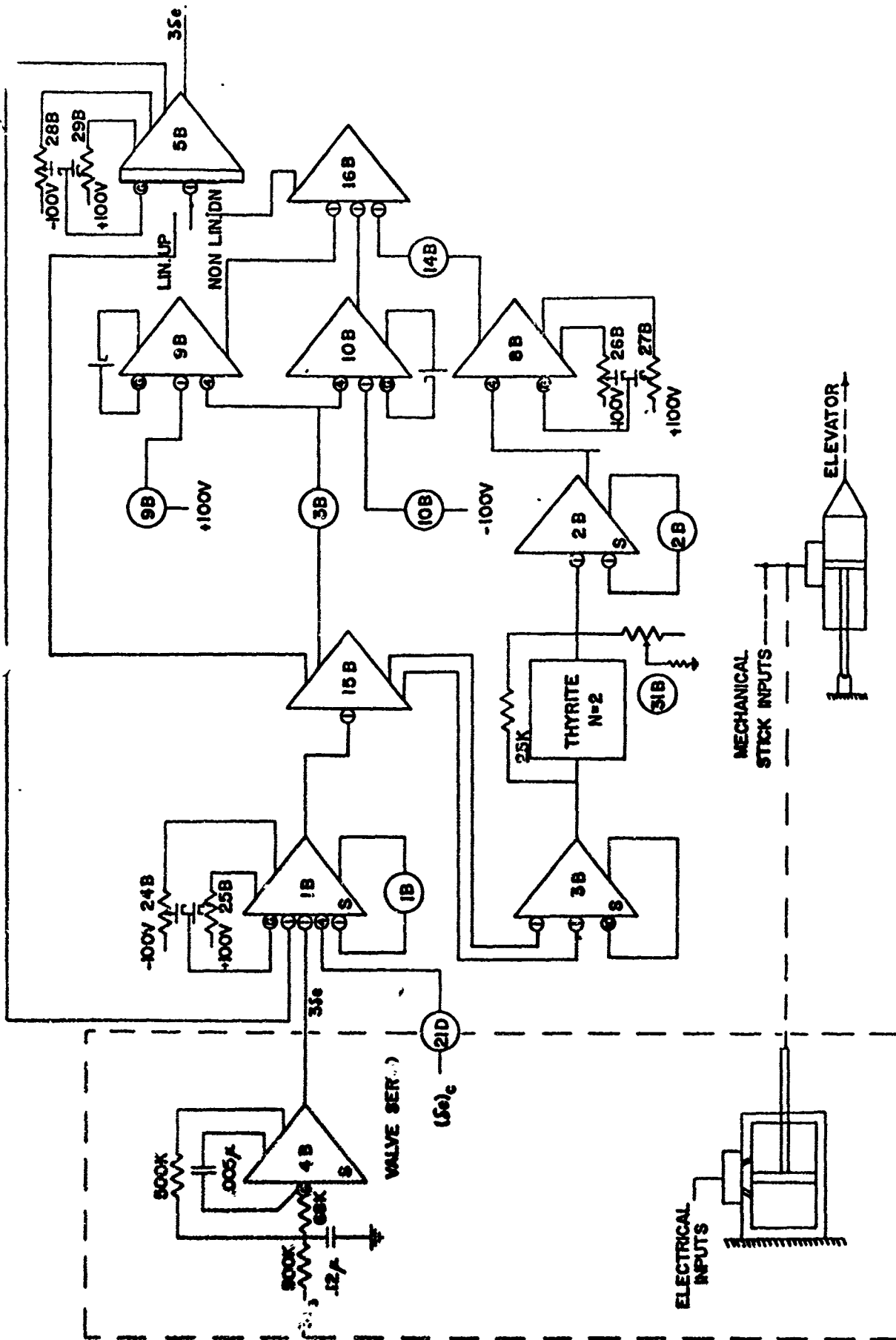


FIGURE 51 ANALOG SCHEMATIC OF G. E. FEEDBACK AND RATE GYRO



VALVE SERVO POWER ACTUATOR
 FIGURE 52 ANALOG SCHEMATIC AND SKETCH OF VALVE SERVO AND ACTUATOR